UNIVERSITY OF SÃO PAULO

POLYTECHNIC SCHOOL

Cátia da Costa e Silva

Geometrically exact shear-rigid shell and rod models

São Paulo

2020

CÁTIA DA COSTA E SILVA

Geometrically exact shear-rigid shell and rod models.

Revised Version

Thesis submitted to Polytechnic School from University of São Paulo in partial fulfillment of the requirements for the degree of Doctor of Science.
Area of concentration: Structural Engineering
Advisor: Prof. Dr. Paulo de Mattos Pimenta

São Paulo
2020

Este exemplar foi revisado e corrigido em relação à versão original, sob responsabilidade única do autor e com a anuência de seu orientador.

São Paulo, _____ de _____ de _____

Assinatura do autor: _____

Assinatura do orientador: _____

Catalogação-na-publicação

Silva, Cátia da Costa e
Geometrically exact shear-rigid shell and rod models / C. C. Silva -- versão corr. -- São Paulo, 2020.
114 p.

Tese (Doutorado) - Escola Politécnica da Universidade de São Paulo. Departamento de Engenharia de Estruturas e Geotécnica.

1.Vigas 2.Cascas I.Universidade de São Paulo. Escola Politécnica. Departamento de Engenharia de Estruturas e Geotécnica II.t.

SILVA, Cátia da Costa e. **Modelo geometricamente exato rígido ao cisalhamento de cascas e barras.** 2020. 114 f. Tese (Doutor em Ciência) – Escola Politécnica – Universidade de São Paulo, São Paulo, 2020.

Resumo

Este trabalho apresenta uma teoria rígida ao cisalhamento, geometricamente exata para formulação de elementos de barra e casca com deslocamentos e rotações finitas. Equações constitutivas elásticas lineares foram consideradas para as barras, e um material Neo-Hookeano foi considerado para as cascas. Tensões e deformações generalizadas energeticamente conjugadas são definidas. Uma configuração de referência reta é considerada para a barra, e plana para a casca. Consequentemente, o uso de sistemas de coordenadas convectivos não cartesianos não é necessário, e apenas componentes ortogonais são aplicados. A parametrização do campo de rotação é realizada pelo tensor de rotações, considerando a fórmula de Rodrigues, o que faz com que a atualização das variáveis rotacionais seja fácil. O método dos elementos finitos foi considerado, e uma continuidade C1 é alcançada no elemento. Tal método é utilizado para discretizar potenciais em um domínio computacional em termos de graus de liberdade. Partindo do princípio que o potencial é não linear, um esquema de iteração de Newton-Raphson é escolhido para resolver o problema. Um conjunto de exemplos de referência ilustra a utilidade da formulação e sua implementação numérica. Esses problemas foram computados e apresentaram resultados satisfatórios. Portanto, pode-se concluir que esta formulação mostra grandes promessas a serem amplamente utilizadas para problemas 3D gerais, em estruturas esbeltas. Teorias rígidas ao cisalhamento podem ser extensamente aplicadas em problemas de engenharia, como em hastes de perfuração de petróleo, braços de robô e para cascas reforçadas com nervuras, comuns na indústria aeroespacial e de automóveis.

Palavras-chave: Casca. Rigidez ao cisalhamento. Barra. Geometricamente Exata.

SILVA, Cátia da Costa e. **Geometrically exact shear-rigid shell and rod models.** 2020. 114 f. Thesis (Doctor of Science) – Polytechnic School – University of São Paulo, São Paulo, 2020.

Abstract

This work presents geometrically exact shear-rigid rod and shell formulations. Displacements and rotations are finite. Linear elastic constitutive equations for small strains are considered in the numerical examples for the rods. A Neo-Hookean material is considered for the shell. Energetically conjugated cross-sectional stresses and strains are defined. A straight reference configuration is assumed for the rod, and a flat reference configuration the shell. Consequently, the use of convective non-Cartesian coordinate systems is not necessary, and only components on orthogonal frames are employed. The parameterization of the rotation field is done by the rotation tensor with the Rodrigues formula, which makes the updating of the rotational variables very simple. The usual Finite Element Method was used and C1 continuity is achieved within the element. This method is used to discretize the potentials on a computational domain in terms of the nodal degrees of freedom. Bearing in mind that the potential is nonlinear a Newton-Raphson iteration scheme is chosen to solve this problem. A set of numerical benchmark examples illustrates the usefulness of the formulation and its numerical implementation. These problems were performed and presented satisfying results. Hence, it can be concluded that this formulation shows great promises to be extensively used for general 3D problems for slender structures. Shear-rigid theories can be widely applied on engineering problems. They can be used in oil drilling rods, robot arms and for rib-reinforced shells that are common in aerospace and automobile industry.

Keywords: Shell. Shear-Rigid. Rod. Geometrically Exact.

Summary

1. Introduction

This work presents fully nonlinear shear-rigid rod and shell formulations. The geometrically exact rod formulation developed in Pimenta and Yojo (1993) [41] is now constrained to obey the Bernoulli-Euler assumption. And the geometrically exact shell formulation developed in Campello, Pimenta and Wriggers (2003) [11] is now constrained to obey the Kirchhoff-Love assumption as developed in Viebahn, Pimenta and Schröder (2016) [65].

As in Campello, Pimenta and Wriggers (2003) [11] and Pimenta and Yojo (1993) [41] our approach defines energetically conjugated generalized cross section stresses and strains. Besides their practical importance, cross section quantities make the derivation of equilibrium equations easier, as well as the achievement of the corresponding tangent bilinear form, which is always symmetric for hyper elastic materials and conservative loadings, even far from an equilibrium state.

A straight reference configuration was assumed for the rod and a plane reference configuration is assumed for the shell mid-surface. Initially curved rods and shells can be regarded as a stress-free deformation from this configuration. This approach was already employed in Pimenta (1996) [42], Pimenta and Campello (2009) [43] and is not addressed in this work. The use of straight reference configuration simplifies the comprehension of tensor quantities, since only components on orthogonal systems are employed.

Rods are elements in which one dimension is predominant over the others, which makes it possible to represent them by their axis. The term rod can be substituted by bars or other terms, here it is used to describe any reticulated structure, such as, beams, columns and trusses. Shells are elements were one dimension is much smaller than the others.

There are some fundamental simplifying assumptions on solid mechanics for rods and shells. The continuity hypothesis, where the solids are idealized as continuous, which allows one to describe a solid by its material points, attributing a set of coordinates to it and disregarding the internal micro-structure, that is, all the volume is totally filled with the material. The homogeneity hypothesis, where the mechanical properties are the same at any point in the solid.

The isotropy hypothesis, where mechanical properties are equal in all directions around a point. The proportionality hypothesis, where in a continuous solid the deformations are related in all their points with the strains, in linear and homogeneous terms. The small deformation hypothesis, where the material undergoes small strains when compared with the dimensions of the structures. The first Bernoulli hypothesis, where a plane section remains plane after deformation. The Saint-Venant principle, that states that as the chosen point moves away from the application point of the force the stresses begin to be evenly distributed in the cross section of the element.

The forces acting on a material are described through stress tensors. One of them is the Cauchy tensor, it is called a true tensor to distinguish itself from other tensors, because it is the measure of force per unit of area in the current deformed configuration. When the deformations are small there is no distinction between the deformed and the initial configuration and the Cauchy tensor is the way of describing these stresses, which is used in the linear theory. But, considering finite deformation, there must be a distinction between the deformed and reference configuration. In this case, a nonlinear theory must be used and, there are several possible ways of defining the action of forces, usually, stress tensors do not have a clear physical meaning like the Cauchy stress tensor. One possibility is to use Piola-Kirchhoff's first and second stress tensors. Piola-Kirchhoff's first stress tensor is used in this work.

As described Crisfield (1996) [16], structures are evaluated by their behaviors from structural models. These structural models' simplifications are made to characterize the structural behavior of interest. With these simplifications and the detailing of the structure, numerical models can be created for structural analysis.

Structures are evaluated using geometrically linear and nonlinear theories, linear ones restrict the magnitude of displacements, rotation and strains for simplification, but are widely used in engineering.

In this work, the author intends to analyze structures with large displacements and rotations considering the Bernoulli-Euler assumption which states that the cross sections initially orthogonal to the rod axis, remain orthogonal to it after deformation. And, analogously, the Kirchhoff-Love's assumption for shells. These assumptions are used to describe slim structures, in which bending are preeminent over shear.

According to Borst et al. (2012) [18] most of the initial work related to geometric nonlinearity was concerned about the problem of buckling. Initially, incremental processes were adopted. Unfortunately, the incremental approach can lead to an accumulation of unquantifiable error and, to overcome this problem, the Newton-Raphson iteration was used and is applied in this work. As the processing power of computers has increased the possibility of performing non-linear analyses has shown advantages and increased as well. An advantage is to directly simulate the collapsing behavior of a structure; therefore, the costs of physical experiments are reduced.

The objectives of this work are to present theories for extremely flexible rods and shells as well as their connection, based on geometrically exact formulations. The rod model is developed using the same mathematical framework presented in Pimenta and Yojo (1993) [41]. However, instead of using Timoshenko (shear deformable) beam theory, Bernoulli-Euler (shear rigid) hypotheses are addressed. The shell model is presented using the same mathematical framework presented used in Viebahn, Pimenta and Schröder (2016) [65]. Moreover, Rodrigues parameters are employed for the description of finite rotations. The connection between the two models are also presented.

The geometrically exact Kirchhoff-Love shell formulation from Viebahn, Pimenta and Schröder (2016) [65] is reviewed and extended here. The connection between shell elements is done differently as it will be shown and is also a contribution of this work.

Novel interpolations schemes for the rod model are presented for the rotation field representing the cross section orientation, which is based on Rodrigues parameters and obeys the Bernoulli-Euler constraint. This formulation has continuous displacement degrees of freedom, however the derivatives of the displacements and the rotation can be discontinuous, to address cross sectional or material changes along the rod and also a change in the axial direction. The connection between elements is enforced by the Rodrigues parameter being equal on both connecting ends. The rod element is also connected to the Kirchhoff-Love shell element.

Bernoulli-Euler and Kirchhoff-Love theories assume a priori the absence of transverse shear strains. Although it was the first available rod theory in the linear case, its generalization to the geometrically exact description of the kinematics was not accomplished until recent years like Meier, Popp and Wall (2014) [38] and Pimenta, Almeida Neto and Campello (2016) [44].

Bernoulli-Euler rod theory is the asymptotic behavior of Timoshenko theory for slender rods, as well as, Kirchhoff-Love theory is the limit of the Mindlin-Reissner theory for thin shells. The development of finite elements for such theories is not straightforward because they require C1-continuity for the transversal displacements at current configuration.

This work presents a simple finite element for the geometrically exact Bernoulli-Euler rod theory that accomplishes an adequate C1-continuity for the transversal displacements at current configuration, which is a desirable feature for contact problems when the element topology is employed directly on contact detection schemes. For the displacements, usual cubic and quintic Hermite polynomials are employed and linear, quadratic and cubic interpolation for the torsion rotation parameter are employed as explained later. Warping was not considered and is subject to be explored in future works.

For the shell a consistent plane stress condition is incorporated at the constitutive level of the model and triangular finite element, with a quadratic interpolation for the displacements are applied.

In practical problems, thin rods and shells are commonly employed. Shear rigid theories and the presented finite element implementation can be used in the very thin limit with no numerical problems.

The finite problem approximation is free of shear-locking. Hence, no numerical trick like reduced integration is necessary. A numerical example shows that any order of numerical integration leads to the same results.

The connection of elements is enforced by the assembly of the stiffness matrix as usual in finite elements methods. Other connection methods are possible and are explained forward, but the simplest one is chosen for the examples.

1.1. Notation

Throughout the text, italic Greek or Latin lowercase letters $(a, b, \dots, \alpha, \beta, \dots)$ denote scalars, bold italic Greek or Latin lowercase letters $(\boldsymbol{a},\ \boldsymbol{b},\ \dots, \boldsymbol{\alpha}, \boldsymbol{\beta}, \dots)$ denote vectors, bold italic Greek or Latin capital letters $(\boldsymbol{A},\ \boldsymbol{B},\ \dots)$ represent second-order tensors. Summation convention over

repeated indices is adopted in the entire text, whereby Greek indices range from 1 to 2, while Latin indices range from 1 to 3.

$\|\boldsymbol{v}\| = \sqrt{\boldsymbol{v} \cdot \boldsymbol{v}}$ is the is the norm of vector $\boldsymbol{v}$ where $\cdot$ indicates the scalar product of two vectors. The operator $\otimes$ denotes the dyadic or tensor product of two vectors. For instance, $\boldsymbol{a} \otimes \boldsymbol{b}$ is a second-order tensor such that $(\boldsymbol{a} \otimes \boldsymbol{b})\boldsymbol{c} = (\boldsymbol{b} \cdot \boldsymbol{c})\boldsymbol{a}$ and $(\boldsymbol{a} \otimes \boldsymbol{b})^T = (\boldsymbol{b} \otimes \boldsymbol{a})$, where $(\cdot)^T$denotes the transpose. The operator axial $(\cdot)$ is such that, if $\boldsymbol{v} = \text{axial}(\boldsymbol{V})$, with $\boldsymbol{V}$ skew-symmetric, then $\boldsymbol{V}\boldsymbol{x} = \boldsymbol{v} \times \boldsymbol{x}$, $\forall \boldsymbol{x}$, where $\times$ denotes the cross or vector product of two vectors. If $\boldsymbol{v} = \text{axial}(\boldsymbol{V})$, then $\boldsymbol{V} = \text{Skew}(\boldsymbol{v})$, with $\boldsymbol{V}$ skew-symmetric. From now on the following notation for partial derivatives has been defined $(\cdot)' = \frac{d(\cdot)}{d\zeta}$, $(\cdot)_{,\alpha} = \frac{\partial(\cdot)}{\partial \xi_\alpha}$ and $(\cdot)_{,\alpha\beta} = \frac{\partial(\cdot)}{\partial \xi_{\alpha\beta}}$.

2. Literature Review

This section intends to draw a brief history about rods and shells. Timoshenko (1953) [64] drew a history in the strength of materials starting in the 16th century. Galileo became interested in the works of Euclid and Archimedes and became acquainted with Leonardo da Vinci's discoveries in mechanics. In 1586 Galileo made a hydrostatic balance for measuring the density of various substances and he carried out investigations of centers of gravity and solid bodies. In 1590 the treatise "De Motu Gravium" was prepared and was the beginning of dynamics as known today. In 1594 Galileo produced a treatise that treated problems of static using the notion of the principle of virtual displacements. In 1638 Galileo published a book "Two new Sciences" that part of it dealt with the mechanical properties of structural materials and with the strength of beams, this book constitutes the first publication in the field of strength of materials. The first consistent formulations.

Still in the 17th century, Hobert Hooke established the relation between the magnitude of forces and the deformations that they produce. Hooke's Law, was used as the foundation for further development of the mechanics of elastic bodies. Then, Jacob Bernoulli addressed the shape of the deflection curve of an elastic bar and started an important chapter in the mechanics of elastic bodies. Bernoulli did not contribute to the physical properties of materials, he made calculations of the deflections of the beams. After Mariotte's assumption of the position of a neutral axis, he took the tangent of the boundary of the cross section on the concave side orthogonal to the plane of action of external loads. Jacob Bernoulli assumed a wrong calculation regarding the axis rotation, but in general he was right about the starting curvature of the deflection at each point being proportional to the bending moment at that point, this was used later by other mathematicians. Later John Bernoulli formulated the principle of virtual displacements, which the notion was applied in earlier works. Then much more important contributions to strength of material were made by his son Daniel Bernoulli and his pupil Leonard Euler. Daniel Bernoulli contributed to the theory of elastic curves, he suggested that Euler should apply the variational calculus in deriving the equations of elastic curves, he indicated that he should solve a problem that had $\int ds/r^2$ as a minimum, this integral is known now as the strain energy of a bent bar aside from a constant factor. In 1744 Euler wrote a book that was the first on variational calculus and it also contained the first systematic treatment of elastic curves. Euler does not limit his discussion to small deflections, so upon solving the problem indicated by Bernoulli he found a

complicated term in the expression which made the equation a complicated one. In these early works some mistakes were made, but it was the breaking ground for geometrically non-linear theory for rods with linear elastic material. Euler and Lagrange studied problems regarding the buckling of columns. Lagrange also made important work in variational calculus and introduced the notions of “generalized coordinates” and “generalized forces” and changed the theory of mechanics to have general formulas from which the necessary equations in any particular problem could be derived.

In 1775, Euler expressed the base transformation for a rigid body motion (known today as the rotation tensor) in terms of the direction cosines of the rotation angles. In 1840 the rotation formula was improved by Rodrigues and in 1844 Hamilton introduced the concept of quaternion as the reader can see in Cheng and Gupta (1989) [17]. These improvements were made especially by Rodrigues. The use of a rotation tensor and vector made it possible to work with large rotations in three dimensional bars.

Ericksen and Truesdell (1957) [22] developed further the purely kinematical description of Cosserat continua emphasizing the one- and two-dimensional cases of rods and shells. Ericksen and Truesdell (1957) [22] remarked that the developed model, in one and two dimensions, serves admirably to represent the twisting of rods and shells in addition to their bending.

Reissner (1972) [49] wrote about a one-dimensional finite-strains beam theory on plane problems where the strain-displacement is a system of non-linear relations which is consistent with exact one-dimensional equilibrium equations for forces and moments regarding the principle of virtual work.

Reissner (1973) [50] also wrote about a large-deformation theory of space-curved lines, with the cross sections of the lines acted upon by forces and moments form of the principle of virtual work to obtain a system of strain displacement relations, involving force strains and moment strains in association with the assumed cross-sectional forces and moments. Reissner (1973) [50] suggests experiments for the three-dimensional.

As for the non-linear theory of rods one of the first to describe it geometrically exact way was Antman (1974) [1], he developed this theory by generalizing the theory presented by Kirchhoff in 1859 and it was also a generalization of Whitman and Desilva (1974) [68] who addressed the problem only for a special set of linear constitutive equations of hyper elastic type, but

Antman (1974) [1] did not present consistency in terms of mechanics of deformable solid in a clear and concise way.

Reissner (1981) [48] expanded on the manner of derivation and showed an application of large-displacement finite-strain theory of space-curved beams.

Argyris (1982) [3] developed an exploration of the matrix formulation of finite rotations in three-dimensional space using a consistent parametrization for large rotations. He pointed out that, for finite rotations, the vector identity cannot be assigned as it is for infinitesimal rotations, because of its commutative properties which is not true for two or more finite rotations. Another point Argyris (1982) [3] made was that the components of the matrix for finite rotations cannot be interpreted as component rotations about the Cartesian axis as they can in infinitesimal rotations.

Then Simo (1985) [53] evolved on geometrically exact rod theories, which means that he made no geometrical approximations, by considering in his work a continuum basis relevant to the numerical formulation of the rod theory with finite strains. He discussed an approach generalized to the fully dynamic three-dimensional case with the formulation originally developed by Reissner for the static plane problem, he did it consistently with the motion equations of equilibrium. He treats his approach as a convenient parameterization of a three-dimensional extension of what he considers the classic Kirchhoff-Love rod model. The process used was to limit the three-dimensional theory with the introduction of the kinematics assumption. The cross section doesn't stay normal to the axis due to shear, but he introduces the kinematics assumption in terms of a three-dimensional orthogonal moving cross section defined so that one of its vectors remains perpendicular to a typical cross section in any configuration. A rotation tensor was introduced as a measure of the finite three-dimensional rotation of the cross section, the resulting geometric stiffness matrix was non-symmetric away from equilibrium and it was symmetric in an equilibrium configuration.

Simo and Vu-Quoc (1986) [60] continued the work of Simo (1985) [53]. They present the variational and computational aspects of a three-dimensional finite-strain rod model. The nonlinear equations of static equilibrium, for three-dimensional Timoshenko rod model, were deduced and further detailing the derivation of the tangent operator. Rotations are orthogonal, generally non-commutative, transformations. A parameterization is employed that circumvents the singularity typically associated with the use of Euler angles. As in the classic Kirchhoff-

Love model for shells, rotations have the standard interpretation of orthogonal transformations, usually non-commutative. Emphasis was placed on the geometric approach, which proves essential in the formulation of algorithms. The update procedure of the configuration becomes the algorithmic counterpart of the exponential map. The computational implementation is based on the formula for the exponential of a skew-symmetric matrix, where the incremental, infinitesimal, rotation is defined by a skew-symmetric matrix and the orthogonal matrix, finite rotation, is found by exponentiation of this skew-symmetric matrix. Consistent linearization procedures are employed to obtain linearized weak forms of the equilibrium equations. The update is done by multiplying this matrix by the existing rotation. Even for a conservative loading, the resulting geometric stiffness is still non-symmetric away from equilibrium configurations and symmetric at the equilibrium configuration provided that the loading is conservative.

Cardona and Geradin (1988) [15] studied a beam finite element with non-linearity and finite rotations. They used an approach that consists in deriving directly the beam equations from a three-dimensional non-linear theory, with a full account of finite rotations, and afterwards introducing the appropriate beam kinematical assumption and used a rotational vector to parameterize rotations, this procedure does not allow an easy manipulation of rotations exceeding π, so they used the updated Lagrangian formulation: rotations are described as increments with respect to a previous configuration.

One of the first to address the term geometrically exact was Simo and Fox (1989) [56] for shells, they define it by, when accepting the kinematics assumption, the class of admissible motions, the geometry of the shell, as well as the balance equations are treated exactly. The geometrically exact formulations attracted a lot of researchers since their beginning. Lots of research was done in geometrically exact theories, Simo and Vu-Quoc (1986) [60], Simo and Vu-Quoc (1991) [57], Simo (1992) [54], Pimenta and Yojo (1993) [41], Pimenta (1996) [42], Gruttmann, Sauer and Wagner (1997, 1999, 2000) [29, 30, 31] , Pimenta and Campello (2003) [46], Sokolov, Krylov and Harari (2015) [62] to name just a few.

Simo and Vu-Quoc (1991) [57] extended their earlier formulation by incorporating shear warping deformation and torsion. They presented a model of a finitely deformable beam accommodating transverse shear and torsion warping of the cross section and the coupling torsion-bending -warping. The model was fully non-linear and geometrically exact within the assumed kinematics.

Simo (1992) [54], Simo and Fox (1992) [55] analyzed some aspects related to the symmetry of the tangent operator for conservatives loading, this non-symmetry is attributed to the fact that the tangent operator is not given by the directional derivative formula of the weak form of the equations. Simo (1992) [54] points out that if the directional derivative is replaced by the covariant derivative an intrinsic definition of the Hessian is obtained which is always symmetric even away from equilibrium

According to Bufler (1993) [10] the tangent stiffness of any conservative mechanical system must be symmetric as far as the position (or displacement) vector acts as the configuration variable which is usually the case. Certain problem formulations, however, require considering the rotation tensor as an independent configuration variable. In this case, as a rule, investigators end up with a non-symmetric tangent stiffness, like Simo (1985) [53], Simo and Vu-Quoc (1986) [60]. As shown by Simo (1992) [54], symmetry is attained formally by replacing the Gâteaux derivative by the covariant one or by symmetrizing the conventionally evaluated stiffness. Simo (1992) [54] shows that correct tangent stiffness of a conservative system is always symmetric, as in a conservative system no work can be lost if a particle is in a closed loop and the work is path-independent.

Pimenta and Yojo (1993) [41] was one of the first to present geometrically exact rod theory in three-dimensional space with the Fréchet derivative of the weak form of the equilibrium being exact and the rotations in three-dimensional space treated in a consistent and convenient way through the Euler-Rodrigues formula. The theory derives a geometrically exact rod model from the kinematic assumption that cross sections, which are initially orthogonal to the axis, remain plane and undistorted during the deformation. The theory accommodates finite strains, large displacements and rotations, and accounts for shear distortion in bending, like the Timoshenko model for plane problems. The tangent operator is always symmetric for conservative loadings, even far from an equilibrium state.

Researchers widely developed and discussed shear deformable shell elements in the last decades for example Başar and Ding (1992) Simo, Fox and Rifai (1990) [58], Eberlein and Wriggers (1999) [21], Gruttmann et al. (1993) [28], Hughes and Liu (1981) [32], Campello, Pimenta and Wriggers (2003) [11], Pimenta, Campello and Wriggers (2004) [45],to name just a few.

Jelenic and Saje (1995) [35] studied a kinematically exact three-dimensional finite strain beam model with finite element formulation by generalized virtual work principle and using the classical Euler-Rodrigues parametrization on rotation matrix expressed by the exponentiation of the skew-symmetric matrix associated with the rotational vector and using the Bernoulli Euler assumption and as Simo and Vu-Quoc (1991) [57] the tangent stiffness matrix is non-symmetric.

As Campello (2000) [14] points out, it is evident that these early theories did not have rigor and precision in their conceptualizations, mainly because they are derived from simplifications imposed in the theories of three-dimensional solids. And when working in the three-dimensional space in nonlinear theories, many misconceptions were committed until the non-vectorial character of the Rotation Tensor was addressed. He also says that only the theories of geometrically nonlinear character are fully consistent with the Principles of Mechanics of Deformable Solids, and do not need to impose any kinematic constraint on the magnitude of the deformations.

Pimenta and Campello (2001) [40] advanced on Pimenta and Yojo (1993) [41] including non-uniform torsion-warping deformation and using a different parametrization than the classic Euler-Rodrigues rod model.

Then Pimenta and Campello (2003) [46] incorporated general cross-sectional in-plane distortions and out-of-plane warping in an extension on their earlier works. The restrictions to a rigid cross section and to a Saint-Venant-like elastic warping were removed from the theory and they used the classical parametrization of Euler-Rodrigues for the rotation.

Dasambiagio, Campello and Pimenta (2009) [20] presented numerical examples for the theory formulated Pimenta and Campello (2003) [46].

Dasambiagio (2008) [19] also presented numerical examples referring to rectangular cross sections, where the results obtained lead to believe in the success of this model and indicates that more expressive results will be obtained when the theory is applied in thin walled cross sections, mainly with opened cross-sectional shapes, where the effects of distortion and warping are important in situations with large displacements and he indicated that it can be developed in future works.

Auricchio, Carotenuto and Reali (2008) [5] derived the equations of the model for the general case finite deformation, as well as for the case of the finite deformation with small deformations using Simo (1985) [53]'s beam model. They did an extended polar decomposition of the beam deformation gradient, based on the composition of a rotation tensor.

Gonçalves, Ritto-corrêa and Camotim (2010) [23] presents a new formulation for thin-walled rods that includes cross-sectional deformation.

Sokolov, Krylov and Harari (2015) [62] extend the work of Dasambiagio, Campello and Pimenta [20] to allow distortion of the cross section.

Wackerfuss and Gruttmann, (2011) [67] introduces a mixed finite element formulation restricted to rectangular cross sections. In Wackerfuss and Gruttmann, (2009) [66] the authors introduce a nonlinear three-dimensional finite beam element based on a Hu–Washizu variational formulation. They used a 3D material law, subject to be discussed in a future work.

All those geometrically exact shell and rod models are not shear rigid as it is done herein. Similar works in Bernoulli-Euler theory has drawn some attention in the last few years, which, however, are different in key aspects.

In the last decade there were some development about rod theories with Bernoulli-Euler's assumption like Armero and Valverde (2012) [4], Bauer et al. (2016) [7] , Boyer and Primault (2004) [9], Boyer et al. (2011) [8], Greco and Cuomo (2013) [25], Greco and Cuomo (2016) [26], Meier, Popp and Wall (2014) [38], Meier et al. (2018) [37], Meier, Popp and Wall (2017) [39], to name just a few.

Meier et al. (2018) [37] developed a geometrically exact beam theory considering Bernoulli's hypothesis of undeformable cross sections. Consequently, the configuration of the beam is uniquely defined by the beam centerline curve. They focus on the development of finite element formulations that are capable of accurately modeling the dynamics of slender components and their contact interaction. The parametrization he used is different from the one proposed in the present work, and he analyzed only one kind of interpolation function, whereas 4 different schemes are addressed in this work.

Few researchers discussed shear-rigid shell, like Viebahn, Pimenta and Schröder (2016) [65], Pimenta, Neto and Campelo (2010) [44], Kiendl (2015) [36]. Greco et al. (2019) [27] developed triangular elements only for the analysis of Kirchhoff plates.

Armero and Valverde (2012) [4] develops finite elements for the simulation of thin Kirchhoff rods, that is, rods where the influence of transverse shear strain can be neglected leading to governing equations that require C1-continuous finite element interpolations, but for the linear plane case. Boyer and Primault (2004) [9] presents a geometrically exact non-linear Euler–Bernoulli model for beams with constant circular cross sections and a straight initial configuration, in Boyer et al. (2011) [8] the same theory is applied to cable dynamics, in these mentioned references the kinematical considerations are similar to this paper`s approach. The basic difference, besides the circular cross section, is that they parameterize the rotation differently. In the present approach one can have arbitrary cross sections, and the initial configuration is also straight, although initially curved rods could be accomplished in the same it way as in Pimenta (1996) [42], Pimenta and Campello (2009) [43], if one regards the initial configuration as a stress-free deformed state from the plane position, this will not be subject of this work.

Bauer et al. (2016) [7] extends Boyer and Primault (2004) [9] into a non-linear isogeometric spatial Bernoulli-Euler rod theory that is treated spatially curved and a rotation around the center line of the rod is adopted as a degree of freedom, that also differs from this work, as it can be seen later. Greco and Cuomo (2013, 2016) [25, 26] made some advances in non-linear Bernoulli-Euler rod theory, they use an isogeometric approach. Meier, Popp and Wall (2014, 2017) [38, 39] have similar approach for the geometrically exact Bernoulli-Euler rod theory, in terms of initial kinematics configuration, but presents different parameterization for the rotation. They also indicate two portions of motion on the beam axes, and 4 degrees of freedom, but they connect the elements in a usual manner in the finite element method, what imposes a continuous rotational degree of freedom. This cannot be true in many examples and is not consistent with the theory. Meier et al. (2018) [37] extends Meier, Popp and Wall (2014) [38], a geometrically exact beam theory was developed considering discrete Bernoulli hypothesis of rigid cross sections that remain orthogonal to the chosen axis during deformation. Focuses on the development of finite element formulations that are capable of accurately modeling the dynamics of slender components and their contact interaction with circular cross sections.

All the papers referred to above describes the rotation in a different way as is done in our work.

This literature review does not intend to be complete. The major contributions to rod and shell formulations are mentioned.

To the authors knowledge little is written about the connection of beam and shell elements. There is some information about how to do it on a commercial program, lacks theoretical foundation. For this theory the connection is not trivial like in the linear case.

3. Nonlinear Bernoulli-Euler rod theory

3.1. Kinematics

For the kinematics assumption of this work it is assumed that the rod is initially straight, and this is the reference configuration.

An orthogonal system $\{\boldsymbol{e}_1^r, \boldsymbol{e}_2^r, \boldsymbol{e}_3^r\}$ is placed at the reference configuration of the rod. Every time $(\cdot)^r$ is used, it refers to the material counterpart of $(\cdot)$, it is not affected by superimposed rigid body motions. Back-rotated means that the vector is calculated in the reference configuration, that is $(\cdot) = \boldsymbol{Q}(\cdot)^r \Leftrightarrow (\cdot)^r = \boldsymbol{Q}^T(\cdot)$ where $\boldsymbol{Q}$ is the cross section rotation tensor described in section 5.

The vectors $\boldsymbol{e}_\alpha^r$ with $\alpha = 1{,}2$ describe the basis on the cross section plane. Thus, $\boldsymbol{e}_3^r$ is orthogonal to this plane and coincides with the axis of the rod. The position of the rod material points in the reference configuration can be described by

$$\xi = \zeta + \boldsymbol{r}^r \ , \tag{1}$$

where the vector ζ defines the position along the axis rod on the reference configuration, therefore,

$$\zeta = \zeta \boldsymbol{e}_3^r + \zeta_0 \tag{2}$$

$\boldsymbol{r}^r$ is the director given by

$$\boldsymbol{r}^r = \xi_\alpha \boldsymbol{e}_\alpha^r \tag{3}$$

that describes the relative position of the points on the cross section at the reference configuration.

The coordinate $\zeta = \boldsymbol{\zeta} \cdot \boldsymbol{e}_3^r$ is introduced, $\zeta \in \Omega = (0, \ell)$, where ℓ is the rod length at reference configuration. The boundary of the domain Ω is denoted by Γ. So, Γ contains the two ends of the rod, that is $\Gamma = \{0, \ell\}$. The cross section domain at the reference configuration is $A \subset \mathbb{R}^2$. The boundary of A is denoted by C. Coordinates $\xi_\alpha = \boldsymbol{r}^r \cdot \boldsymbol{e}_\alpha^r$ are such that $\{\xi_1, \ \xi_2\} \ \in A$. Thus, $\xi_1, \ \xi_2$ and ζ build a Cartesian coordinate system.

In the current configuration, as it can be seen in Figure 1, the position of the material points is given by

$$\boldsymbol{x} = \boldsymbol{z} + \boldsymbol{r} \ , \tag{4}$$

where $\boldsymbol{z} = \hat{\boldsymbol{z}}(\zeta)$ describes the position of the rod axis at the current configuration and $\boldsymbol{r}$ is the current director given by

$$\boldsymbol{r} = \boldsymbol{Q}\boldsymbol{r}^{r} \ , \tag{5}$$

This assumption embeds our basic kinematical hypothesis, i.e. the director remains rigid during the motion (no cross-sectional deformations or thickness changes occur) and may only rotate as a rigid body.

Figure 1: Rod description and basic kinematical quantities.

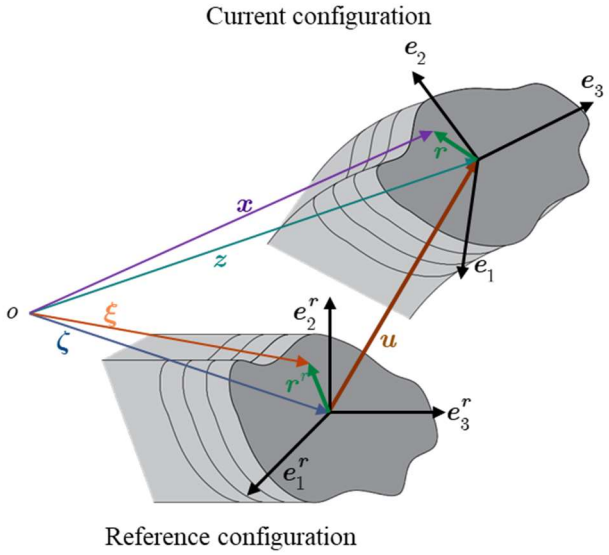

Source: Author

3.2. Strains

The set of vectors $\{\boldsymbol{e}_1, \boldsymbol{e}_2, \boldsymbol{e}_3\}$ are the base local orthogonal system in the current configuration, with

$$\boldsymbol{e}_3 \ = \|\boldsymbol{z}'\|^{-1}\boldsymbol{z}'. \tag{6}$$

It is remarked that $\boldsymbol{e}_3$ is tangent to the rod axis in the current configuration and orthogonal to the cross section, that is defined by the Bernoulli constraint. The displacements of the points on the rod axis are defined by

$$\boldsymbol{u} = \boldsymbol{z} - \boldsymbol{\zeta} \ . \tag{7}$$

Note also that

$$\boldsymbol{z}' = \boldsymbol{e}_3^r + \boldsymbol{u}' \quad \text{and} \quad \boldsymbol{z}'' = \boldsymbol{u}'' \ . \tag{8}$$

The Bernoulli-Euler assumption states that the director $\boldsymbol{r}$ remains orthogonal to the axis of the rod. The cross-sectional rotation tensor, with the Rodrigues parameter, can be expressed by

$$\boldsymbol{Q} = \widehat{\boldsymbol{Q}}(\boldsymbol{e}_3, \varphi) = \widehat{\boldsymbol{Q}}(\boldsymbol{u}', \varphi) \ . \tag{9}$$

where $\varphi = \hat{\varphi}(\zeta)$ is a scalar which is a torsion parameter explained section 5.

Note that

$$\boldsymbol{e}_i = \boldsymbol{Q}\boldsymbol{e}_i^r \quad \text{and} \quad \boldsymbol{Q} = \boldsymbol{e}_i \otimes \boldsymbol{e}_i^r \ . \tag{10}$$

If the displacements field is derived in relation to the position vector $\boldsymbol{\xi}$, one gets the deformation gradient

$$\boldsymbol{F} = \frac{\partial \boldsymbol{x}}{\partial \boldsymbol{\xi}} = \frac{\partial \boldsymbol{x}}{\partial \xi_\alpha} \otimes \boldsymbol{e}_\alpha^r + \frac{\partial \boldsymbol{x}}{\partial \zeta} \otimes \boldsymbol{e}_3^r \tag{11}$$

Considering $(\cdot)_{,\alpha} = \frac{\partial(\cdot)}{\partial \xi_\alpha}$ and $(\cdot)' = \frac{\partial(\cdot)}{\partial \zeta}$ one gets,

$$\boldsymbol{F} = \boldsymbol{x}_{,\alpha} \otimes \boldsymbol{e}_\alpha^r + \boldsymbol{x}' \otimes \boldsymbol{e}_3^r \tag{12}$$

Deriving (4) one has

$$\boldsymbol{x}_{,\alpha} = \boldsymbol{z}_{,\alpha} + \boldsymbol{r}_{,\alpha} = \boldsymbol{r}_{,\alpha} = \boldsymbol{Q}\boldsymbol{r}^r{}_{,\alpha} = \boldsymbol{Q}\left(\xi_\alpha \boldsymbol{e}_\alpha^r\right)_{,\alpha} = \boldsymbol{Q}\boldsymbol{e}_\alpha^r \tag{13}$$

and

$$\boldsymbol{x}' = \boldsymbol{z}' + \boldsymbol{r}' = \boldsymbol{\zeta}' + \boldsymbol{u}' + (\boldsymbol{Q}\boldsymbol{r}^r)' = (\boldsymbol{\zeta}\boldsymbol{e}_3^r)' + \boldsymbol{u}' + \boldsymbol{Q}'\boldsymbol{r}^r = \boldsymbol{e}_3^r + \boldsymbol{u}' + \boldsymbol{Q}'\boldsymbol{Q}^T\boldsymbol{r} \tag{14}$$

The curvature tensor and its correspondent axial curvature vector are defined as

$$\boldsymbol{K} = \boldsymbol{Q}'\boldsymbol{Q}^T = \text{Skew}(\boldsymbol{\kappa}) \ \text{ and } \ \boldsymbol{\kappa} = \text{axial}(\boldsymbol{K}) \tag{15}$$

this skew-symmetric tensor relates the director to its derivative.

An important result from Pimenta and Campello (2001) [40] is

$$\boldsymbol{\kappa} = \boldsymbol{\Xi}\boldsymbol{\alpha}' \quad \text{and} \quad \boldsymbol{\kappa}^r = \boldsymbol{\Xi}^T\boldsymbol{\alpha}' \tag{16}$$

where $\boldsymbol{\alpha}$ is the Rodrigues vector and,

$$\boldsymbol{\Xi} = \frac{4}{4 + \boldsymbol{\alpha}\cdot\boldsymbol{\alpha}}\left(\boldsymbol{I} + \frac{1}{2}\boldsymbol{A}\right) \tag{17}$$

with $\boldsymbol{A} = \text{Skew}(\boldsymbol{\alpha})$.

For further knowledge of how to reach (17) see attachment C.

In $(16)_2$ the property $\boldsymbol{Q}^T\boldsymbol{\Xi} = \boldsymbol{\Xi}^T$ was employed, then

$$\boldsymbol{\Xi}^T = \tfrac{4}{4+\alpha^2}\left(\boldsymbol{I} - \tfrac{1}{2}\boldsymbol{A}\right). \tag{18}$$

There are the following valuable properties

$$\boldsymbol{\Xi}\boldsymbol{\alpha} = \frac{4}{4+\alpha^2}\boldsymbol{\alpha}, \qquad \det\boldsymbol{\Xi} = \left(\frac{4}{4+\alpha^2}\right)^2 \quad \text{and} \quad \frac{4}{4+\alpha^2}\boldsymbol{\Xi}^{-T} = \frac{1}{2}(\boldsymbol{I} + \boldsymbol{Q}). \tag{19}$$

In Bernoulli theory $\boldsymbol{\kappa}$ is the real curvature of the beam axis. If the work conjugated to the bending strain is derived, the actual curvature of the beam axis is achieved and given by $(16)_1$.

Thus,

$$\boldsymbol{r}' = \boldsymbol{Q}'\boldsymbol{Q}^T\boldsymbol{r} = \boldsymbol{K}\boldsymbol{r} = \boldsymbol{\kappa}\times\boldsymbol{r} = \boldsymbol{Q}(\boldsymbol{\kappa}^r\times\boldsymbol{r}^r) \tag{20}$$

with (13), (14) and (20) in (12) one has

$$\boldsymbol{F} = \boldsymbol{Q}\boldsymbol{e}_\alpha^r \otimes \boldsymbol{e}_\alpha^r + (\boldsymbol{e}_3^r + \boldsymbol{u}' + \boldsymbol{\kappa}\times\boldsymbol{r}) \otimes \boldsymbol{e}_3^r. \tag{21}$$

In (21) the following generalized strain vector is noted

$$\boldsymbol{\eta} = \boldsymbol{z}' - \boldsymbol{e}_3 \;\; = \boldsymbol{u}' + \boldsymbol{e}_3^r - \boldsymbol{e}_3 \tag{22}$$

then,

$$\boldsymbol{F} = \boldsymbol{Q}\boldsymbol{e}_\alpha^r \otimes \boldsymbol{e}_\alpha^r + (\boldsymbol{e}_3 + \boldsymbol{\eta} + \boldsymbol{\kappa}\times\boldsymbol{r}) \otimes \boldsymbol{e}_3^r. \tag{23}$$

In (23) the following generalized strains are noted

$$\boldsymbol{\gamma} = \boldsymbol{\eta} + \boldsymbol{\kappa} \times \boldsymbol{r} \tag{24}$$

and their back-rotated counterparts are

$$\boldsymbol{\gamma}^r = \boldsymbol{\eta}^r + \boldsymbol{\kappa}^r \times \boldsymbol{r}^r \tag{25}$$

Thus

$$\boldsymbol{F} = \boldsymbol{Q}\boldsymbol{e}_\alpha^r \otimes \boldsymbol{e}_\alpha^r + \boldsymbol{Q}(\boldsymbol{e}_3^r + \boldsymbol{\gamma}^r) \otimes \boldsymbol{e}_3^r = \boldsymbol{Q}(\boldsymbol{e}_i^r \otimes \boldsymbol{e}_i^r + \boldsymbol{\gamma}^r \otimes \boldsymbol{e}_3^r) = \boldsymbol{Q}(\boldsymbol{I} + \boldsymbol{\gamma}^r \otimes \boldsymbol{e}_3^r) \tag{26}$$

The deformation gradient can be expressed by

$$\boldsymbol{F} = \boldsymbol{Q}\boldsymbol{F}^r \ , \tag{27}$$

One can see by (26) and (27) that

$$\boldsymbol{F}^r = \boldsymbol{I} + \boldsymbol{\gamma}^r \ \otimes \boldsymbol{e}_3^r \tag{28}$$

is the back-rotated deformation gradient.

Note that

$$\begin{aligned} \boldsymbol{\eta}^r = \boldsymbol{Q}^T\boldsymbol{\eta} = \boldsymbol{Q}^T(\boldsymbol{z}' - \boldsymbol{e}_3) \ &= \boldsymbol{Q}^T(\|\boldsymbol{z}'\|\boldsymbol{e}_3 - \boldsymbol{e}_3) = (\|\boldsymbol{z}'\| - 1)\boldsymbol{Q}^T\boldsymbol{e}_3 \\ &= (\|\boldsymbol{z}'\| - 1)\boldsymbol{e}_3^r \, . \end{aligned} \tag{29}$$

With $\varepsilon = (\|\boldsymbol{z}'\| - 1)$, that will be considered as a degree of freedom.

$$\boldsymbol{\eta}^r = \varepsilon \boldsymbol{e}_3^r \, . \tag{30}$$

It is observed that the projection of $\boldsymbol{\eta}^r$ in $\boldsymbol{e}_\alpha^r$ is zero, because there is no shear strain then,

$$\boldsymbol{\eta}^r \ \cdot \boldsymbol{e}_\alpha^r = \boldsymbol{\eta}^r \ \times \boldsymbol{e}_3^r = 0 \ . \tag{31}$$

due to the Bernoulli-Euler assumption.

3.3. Strain rates

The velocity gradient is given by time differentiation of (27).

$$\dot{\boldsymbol{F}} = \dot{\boldsymbol{Q}}\boldsymbol{F}^r + \boldsymbol{Q}\dot{\boldsymbol{F}}^r = \dot{\boldsymbol{Q}}\boldsymbol{Q}^T\boldsymbol{F} + \boldsymbol{Q}\dot{\boldsymbol{F}}^r \tag{32}$$

where the superposed dot denotes the differentiation with respect to time.

Analogous to $\boldsymbol{K}$ there is the skew-symmetric tensor $\boldsymbol{\Omega}$ that relates the director to its time derivative the way shown in the following

$$\dot{\boldsymbol{r}} = \dot{\boldsymbol{Q}}\boldsymbol{Q}^T\boldsymbol{r} = \boldsymbol{\Omega}\boldsymbol{r} = \boldsymbol{\omega} \times \boldsymbol{r} \tag{33}$$

Thus, the following skew-symmetric spin tensor and its corresponding axial spin vector are considered. The spin tensor ($\boldsymbol{\Omega} = \mathrm{Skew}(\boldsymbol{\omega})$ and $\boldsymbol{\omega} = \mathrm{axial}(\boldsymbol{\Omega})$) is

$$\boldsymbol{\Omega} = \dot{\boldsymbol{Q}}\boldsymbol{Q}^T \, . \tag{34}$$

Introducing $(10)_2$ in (34), one gets

$$\boldsymbol{\Omega} = \dot{\boldsymbol{e}}_i \otimes \boldsymbol{e}_i \, . \tag{35}$$

Analogous to (16) the spin vector is

$$\boldsymbol{\omega} = \boldsymbol{\Xi}\dot{\boldsymbol{\alpha}} \tag{36}$$

with (33) and (28) in (32) one has

$$\dot{\boldsymbol{F}} = \boldsymbol{\Omega}\boldsymbol{F} + \boldsymbol{Q}(\dot{\boldsymbol{\gamma}}^r \otimes \boldsymbol{e}_3^r) \, , \tag{37}$$

where

$$\dot{\boldsymbol{\gamma}}^r = \dot{\boldsymbol{\eta}}^r + \dot{\boldsymbol{\kappa}}^r \times \boldsymbol{r}^r \, . \tag{38}$$

Time derivative of (6) leads to

$$\begin{aligned} &\dot{\boldsymbol{e}}_3 = \dot{\boldsymbol{z}}'\|\boldsymbol{z}'\|^{-1} - \|\boldsymbol{z}'\|^{-3}\boldsymbol{z}'\left(\boldsymbol{z}' \cdot \dot{\boldsymbol{z}}'\right) = \dot{\boldsymbol{u}}'\|\boldsymbol{z}'\|^{-1} - \|\boldsymbol{z}'\|^{-1}\boldsymbol{e}_3\left(\boldsymbol{e}_3 \cdot \dot{\boldsymbol{u}}'\right) = \\ &= \|\boldsymbol{z}'\|^{-1}(\boldsymbol{I} - \boldsymbol{e}_3 \otimes \boldsymbol{e}_3)\dot{\boldsymbol{u}}' \end{aligned} \tag{39}$$

where $\boldsymbol{I}$ is the identity tensor.

Hence, one may write

$$\boldsymbol{z}' \times \boldsymbol{\omega} = -\boldsymbol{\Omega}\boldsymbol{z}' = -\|\boldsymbol{z}'\|(\dot{\boldsymbol{e}}_i \otimes \boldsymbol{e}_i)\boldsymbol{e}_3 = -\|\boldsymbol{z}'\|\dot{\boldsymbol{e}}_3 = -(\boldsymbol{I} - \boldsymbol{e}_3 \otimes \boldsymbol{e}_3)\dot{\boldsymbol{u}}' \tag{40}$$

Consequently, one has

$$\dot{\boldsymbol{u}}' + \boldsymbol{z}' \times \boldsymbol{\omega} = (\boldsymbol{e}_3 \otimes \boldsymbol{e}_3)\dot{\boldsymbol{u}}' \tag{41}$$

Time differentiation of (29) considering $\dot{\boldsymbol{Q}}^T = \left(\dot{\boldsymbol{Q}}\boldsymbol{Q}^T\boldsymbol{Q}\right)^T = (\boldsymbol{\Omega}\boldsymbol{Q})^T = \boldsymbol{Q}^T\boldsymbol{\Omega}^T = -\boldsymbol{Q}^T\boldsymbol{\Omega}$ yields

$$\dot{\boldsymbol{\eta}}^r = \boldsymbol{Q}^T\dot{\boldsymbol{u}}' + \dot{\boldsymbol{Q}}^T\boldsymbol{z}' = \boldsymbol{Q}^T\left(\dot{\boldsymbol{u}}' + \boldsymbol{z}' \times \boldsymbol{\omega}\right) \, . \tag{42}$$

Introducing (44) in (45) one gets

$$\dot{\boldsymbol{\eta}}^{r} = \boldsymbol{Q}^{T}(\boldsymbol{e}_3 \otimes \boldsymbol{e}_3)\dot{\boldsymbol{u}}'. \tag{43}$$

Time differentiation of $\boldsymbol{Q}' = \boldsymbol{K}\boldsymbol{Q}$ leads to

$$\dot{\boldsymbol{Q}}' = \dot{\boldsymbol{K}}\boldsymbol{Q} + \boldsymbol{K}\dot{\boldsymbol{Q}} = \left(\dot{\boldsymbol{K}} + \boldsymbol{K}\dot{\boldsymbol{Q}}\boldsymbol{Q}^{T}\right)\boldsymbol{Q} = \left(\dot{\boldsymbol{K}} + \boldsymbol{K}\boldsymbol{\Omega}\right)\boldsymbol{Q}. \tag{44}$$

Differentiation of $\dot{\boldsymbol{Q}} = \boldsymbol{\Omega}\boldsymbol{Q}$. leads to

$$\dot{\boldsymbol{Q}}' = \boldsymbol{\Omega}'\boldsymbol{Q} + \boldsymbol{\Omega}\boldsymbol{Q}' = \left(\boldsymbol{\Omega}' + \boldsymbol{\Omega}\boldsymbol{Q}'\boldsymbol{Q}^{T}\right)\boldsymbol{Q} = (\boldsymbol{\Omega}' + \boldsymbol{\Omega}\boldsymbol{K})\boldsymbol{Q}. \tag{45}$$

Thus, one gets

$$\boldsymbol{\Omega}' + \boldsymbol{\Omega}\boldsymbol{K} = \dot{\boldsymbol{K}} + \boldsymbol{K}\boldsymbol{\Omega}. \tag{46}$$

Since $\left(\dot{\boldsymbol{Q}}\right)' = (\boldsymbol{Q}')^{\cdot}$, considering (46) and the property shown in (239) one reaches the conclusion

$$\boldsymbol{\omega}' = \dot{\boldsymbol{\kappa}} - \boldsymbol{\omega} \times \boldsymbol{\kappa} \tag{47}$$

and

$$\dot{\boldsymbol{\kappa}} = \boldsymbol{\omega}' + \boldsymbol{\omega} \times \boldsymbol{\kappa} \tag{48}$$

which leads to $\dot{\boldsymbol{\kappa}}^{r} = \boldsymbol{Q}^{T}(\dot{\boldsymbol{\kappa}} - \boldsymbol{\omega} \times \boldsymbol{\kappa})$. Hence, from (47), the important relation displayed below is settled

$$\dot{\boldsymbol{\kappa}}^{r} = \boldsymbol{Q}^{T}\boldsymbol{\omega}'. \tag{49}$$

Considering (36) in (49) one gets,

$$\dot{\boldsymbol{\kappa}}^{r} = \boldsymbol{Q}^{T}(\boldsymbol{\Xi}\dot{\boldsymbol{\alpha}})'. \tag{50}$$

3.4. Stresses

Let the 1st Piola-Kirchhoff stress tensor be expressed by

$$\boldsymbol{P} = \boldsymbol{\tau}_i \otimes \boldsymbol{e}_i^r = \boldsymbol{Q}(\boldsymbol{\tau}_i^r \otimes \boldsymbol{e}_i^r) = \boldsymbol{Q}(\boldsymbol{\tau}_\alpha^r \otimes \boldsymbol{e}_\alpha^r + \boldsymbol{\tau}_3^r \otimes \boldsymbol{e}_3^r) \ . \tag{51}$$

Now the back-rotated 1st Piola-Kirchhoff stress tensor is introduced by

$$\boldsymbol{P}^r = \boldsymbol{Q}^T\boldsymbol{P} = \boldsymbol{\tau}_\alpha^r \otimes \boldsymbol{e}_\alpha^r + \boldsymbol{\tau}_3^r \otimes \boldsymbol{e}_3^r, \tag{52}$$

Where

$$\boldsymbol{\tau}_i^r = \boldsymbol{Q}^T\boldsymbol{\tau}_i \quad , \quad i = 1,2,3 \ , \tag{53}$$

are the back-rotated stress vectors.

The following generalized cross-sectional forces are obtained by integration of the stresses $\boldsymbol{\tau} = \boldsymbol{\tau}_3$ on the cross section

$$\boldsymbol{n} = \int_A \boldsymbol{\tau} dA \quad \text{and} \quad \boldsymbol{m} = \int_A (\boldsymbol{r} \times \boldsymbol{\tau}) dA \tag{54}$$

$\boldsymbol{n}$ represents the true forces and $\boldsymbol{m}$ the true moments, acting on a cross section. Their back-rotated counterparts are

$$\boldsymbol{n}^r = \boldsymbol{Q}^T\boldsymbol{n} \quad \text{and} \quad \boldsymbol{m}^r = \boldsymbol{Q}^T\boldsymbol{m} \ . \tag{55}$$

Hence, it may also be written as

$$\boldsymbol{n}^r = \int_A \boldsymbol{\tau}^r \, dA \quad \text{and} \quad \boldsymbol{m}^r = \int_A (\boldsymbol{r}^r \times \boldsymbol{\tau}^r) dA \tag{56}$$

$\boldsymbol{n}^r$ represents the back-rotated cross section forces and $\boldsymbol{m}^r$ the back-rotated cross section moments.

The axial (membrane) and transversal (shear due to bending) parts of the force $\boldsymbol{n}$ are defined by

$$\boldsymbol{n}^m = (\boldsymbol{e}_3 \otimes \boldsymbol{e}_3)\boldsymbol{n} = N\boldsymbol{e}_3 \quad \text{and} \quad \boldsymbol{n}^b = (\boldsymbol{I} - \boldsymbol{e}_3 \otimes \boldsymbol{e}_3)\boldsymbol{n} = V_\alpha \boldsymbol{e}_\alpha \ , \tag{57}$$

respectively, where

$$N = \boldsymbol{n} \cdot \boldsymbol{e}_3 \quad \text{and} \quad V_\alpha = \boldsymbol{n} \cdot \boldsymbol{e}_\alpha \tag{58}$$

are the normal and shear forces acting on the cross section, respectively. The back-rotated counterparts of (57) are

$$\boldsymbol{n}^{mr} = N\boldsymbol{e}_3^r \quad \text{and} \quad \boldsymbol{n}^{br} = V_\alpha \boldsymbol{e}_\alpha^r \tag{59}$$

The bending moments are defined as

$$M_\alpha = \boldsymbol{m} \cdot \boldsymbol{e}_\alpha \ . \tag{60}$$

For the torsion moment, one has

$$T = \boldsymbol{m} \cdot \boldsymbol{e}_3 = \boldsymbol{m}^r \cdot \boldsymbol{e}_3^r. \tag{61}$$

Hence, one may write

$$\begin{array}{lll} \boldsymbol{n} = V_\alpha \boldsymbol{e}_\alpha + N\boldsymbol{e}_3 \ , & & \boldsymbol{n}^r = V_\alpha \boldsymbol{e}_\alpha^r + N\boldsymbol{e}_3^r \ , \\ \boldsymbol{m} = M_\alpha \boldsymbol{e}_\alpha + T\boldsymbol{e}_3 & \text{and} & \boldsymbol{m}^r = M_\alpha \boldsymbol{e}_\alpha^r + T\boldsymbol{e}_3^r \ . \end{array} \tag{62}$$

Remark 1: Local moment balance

The local moment balance is formulated as

$$\text{Skew}(\boldsymbol{P}\boldsymbol{F}^T) = \boldsymbol{O}, \tag{63}$$

where $\boldsymbol{O}$ is the null tensor. Equation (63) enforces

$$\boldsymbol{P}\boldsymbol{F}^T : \boldsymbol{\Omega} = 0 \tag{64}$$

3.5. Power

From (51), (37) and, (64) one gets

$$\begin{array}{l} \boldsymbol{P} : \dot{\boldsymbol{F}} = \boldsymbol{P} : \left(\boldsymbol{\Omega}\boldsymbol{F} + \boldsymbol{Q}\dot{\boldsymbol{F}}^r\right) = \ \boldsymbol{P} : \boldsymbol{Q}\dot{\boldsymbol{F}}^r = \boldsymbol{P} : \boldsymbol{Q}(\dot{\boldsymbol{\gamma}}^r \otimes \boldsymbol{e}_3^r) \ = \\ = \boldsymbol{Q}^T\boldsymbol{P} : (\dot{\boldsymbol{\gamma}}^r \otimes \boldsymbol{e}_3^r) = \boldsymbol{Q}^T\boldsymbol{Q}(\boldsymbol{\tau}^r \otimes \boldsymbol{e}_3^r) : (\dot{\boldsymbol{\gamma}}^r \otimes \boldsymbol{e}_3^r) = \boldsymbol{\tau}^r \cdot \dot{\boldsymbol{\gamma}}^r \end{array} \tag{65}$$

that is the stress power per unit reference volume. Introducing (38) in (65) and after some manipulation, one gets

$$\boldsymbol{P} : \dot{\boldsymbol{F}} = \boldsymbol{\tau}^r \cdot \dot{\boldsymbol{\gamma}}^r \ = \boldsymbol{\tau}^r \cdot \dot{\boldsymbol{\eta}}^r + (\boldsymbol{r}^r \times \boldsymbol{\tau}^r) \cdot \dot{\boldsymbol{\kappa}}^r \tag{66}$$

Note that $\boldsymbol{\tau}_\alpha^r$ are powerless in this model, because there is no distortion. With the aid of the definitions (56), the integration of (66) over the cross section furnishes

$$\int_A \left(\boldsymbol{P}:\dot{\boldsymbol{F}}\right) dA = \boldsymbol{n}^r \cdot \dot{\boldsymbol{\eta}}^r + \boldsymbol{m}^r \cdot \dot{\boldsymbol{\kappa}}^r \tag{67}$$

that is the stress power per unit length of the reference axis. It is important to remark that $\boldsymbol{n}^r$, $\boldsymbol{m}^r$, $\boldsymbol{\eta}^r$ and $\boldsymbol{\kappa}^r$ are not affected by superimposed rigid body motions. Regarding (43) and $(59)_1$, one has

$$\boldsymbol{n}^r \cdot \dot{\boldsymbol{\eta}}^r + \boldsymbol{m}^r \cdot \dot{\boldsymbol{\kappa}}^r = \boldsymbol{n}^{mr} \cdot \dot{\boldsymbol{\eta}}^r + \boldsymbol{m}^r \cdot \dot{\boldsymbol{\kappa}}^r \,. \tag{68}$$

The cross-sectional resultants that do work and their back-rotated counterparts are collected in two vectors, respectively, as shown in

$$\boldsymbol{\sigma} = \begin{bmatrix} \boldsymbol{n}^m \\ \boldsymbol{m} \end{bmatrix} \quad \text{and} \quad \boldsymbol{\sigma}^r = \begin{bmatrix} \boldsymbol{n}^{mr} \\ \boldsymbol{m}^r \end{bmatrix} . \tag{69}$$

The differentiation with respect to time of the cross section back-rotated generalized strains are

$$\dot{\boldsymbol{\varepsilon}}^r = \begin{bmatrix} \dot{\boldsymbol{\eta}}^r \\ \dot{\boldsymbol{\kappa}}^r \end{bmatrix}. \tag{70}$$

With the aid of (69) and (70), (67) can be written as follows

$$\int_A \left(\boldsymbol{P}:\dot{\boldsymbol{F}}\right) dA = \boldsymbol{\sigma}^r \cdot \dot{\boldsymbol{\varepsilon}}^r \,. \tag{71}$$

The internal power on the domain Ω is then given by

$$P_{\text{int}}^{\Omega} = \int_{\Omega} \boldsymbol{\sigma}^r \cdot \dot{\boldsymbol{\varepsilon}}^r \, d\Omega \,. \tag{72}$$

On the other hand, the external power on the same domain can be expressed by

$$P_{\text{ext}}^{\Omega} = \int_{\Omega} \left[\int_C (\bar{\boldsymbol{t}} \cdot \dot{\boldsymbol{x}}) dC + \int_A \left(\overline{\boldsymbol{b}} \cdot \dot{\boldsymbol{x}}\right) dA \right] d\Omega \,, \tag{73}$$

where $\bar{\boldsymbol{t}}$ is the surface traction per unit reference area prescribed on the lateral surface of the rod and $\overline{\boldsymbol{b}}$ is the body force per unit reference volume. The time differentiation of (4) yields

$$\dot{\boldsymbol{x}} = \dot{\boldsymbol{u}} + \boldsymbol{\omega} \times \boldsymbol{r} \,. \tag{74}$$

Introducing the following generalized external forces

$$\bar{\boldsymbol{n}}^{\Omega} = \int_C \bar{\boldsymbol{t}} dC + \int_A \bar{\boldsymbol{b}} dA \quad \text{and} \quad \bar{\boldsymbol{m}}^{\Omega} = \int_C (\boldsymbol{r} \times \bar{\boldsymbol{t}}) dC + \int_A (\boldsymbol{r} \times \bar{\boldsymbol{b}}) dA \tag{75}$$

and (74), there is

$$P_{\text{ext}}^{\Omega} = \int_{\Omega} \bar{\boldsymbol{n}}^{\Omega} \cdot \dot{\boldsymbol{u}} + \bar{\boldsymbol{m}}^{\Omega} \cdot \boldsymbol{\omega} d\Omega \; = \int_{\Omega} \bar{\boldsymbol{n}}^{\Omega} \cdot \dot{\boldsymbol{u}} + \bar{\boldsymbol{m}}^{\Omega} \cdot \boldsymbol{\Xi} \dot{\boldsymbol{\alpha}} d\Omega \tag{76}$$

where $\bar{\boldsymbol{n}}^{\Omega}$ is the applied external force per unit length and $\bar{\boldsymbol{m}}^{\Omega}$ is the applied external moment per unit length.

Since $\boldsymbol{\alpha} = \hat{\boldsymbol{\alpha}}(\boldsymbol{u}', \varphi)$ the time derivative of $\boldsymbol{\alpha}$ furnishes

$$\dot{\boldsymbol{\alpha}} = \frac{\partial \boldsymbol{\alpha}}{\partial \boldsymbol{z}'} \dot{\boldsymbol{u}}' + \frac{\partial \boldsymbol{\alpha}}{\partial \varphi} \dot{\varphi} \tag{77}$$

with (36), one arrives at

$$\boldsymbol{\omega} = \boldsymbol{W} \dot{\boldsymbol{u}}' + \boldsymbol{w} \dot{\varphi} \tag{78}$$

where

$$\boldsymbol{W} = \boldsymbol{\Xi} \frac{\partial \boldsymbol{\alpha}}{\partial \boldsymbol{z}'} \quad \text{and} \quad \boldsymbol{w} = \boldsymbol{\Xi} \frac{\partial \boldsymbol{\alpha}}{\partial \varphi}. \tag{79}$$

The pseudo moment $\boldsymbol{\Xi}^T \bar{\boldsymbol{m}}^{\Omega}$ can then be divided into

$$\bar{\boldsymbol{\mu}}^{\Omega} = \boldsymbol{W}^T \bar{\boldsymbol{m}}^{\Omega} \quad \text{and} \quad \bar{\mu}^{\Omega} = \boldsymbol{w} \cdot \bar{\boldsymbol{m}}^{\Omega} \tag{80}$$

that are the bending pseudo-moment and the torsion pseudo-moment applied along the rod, respectively.

Similarly applied forces on the ends of the rod can be expressed by $\bar{\boldsymbol{n}}^{\Gamma}$ and,

$$\bar{\boldsymbol{\mu}}^{\Gamma} = \boldsymbol{W}^T \bar{\boldsymbol{m}}^{\Gamma} \quad \text{and} \quad \bar{\mu}^{\Gamma} = \boldsymbol{w} \cdot \bar{\boldsymbol{m}}^{\Gamma} \tag{81}$$

are the force, the bending pseudo-moment and the torsion pseudo-moment applied on the rod ends, respectively, while $\bar{\boldsymbol{m}}^{\Gamma}$ is the true moment applied on the rod ends.

3.6. Weak form of the local equilibrium equation

The internal virtual work on a domain $\Omega \subset \mathbb{R}$ is given by

$$\delta W_{\text{int}}^{\Omega} = \int_{\Omega} \boldsymbol{\sigma}^{r} \cdot \delta \boldsymbol{\varepsilon}^{r} \, d\Omega \ , \tag{82}$$

where δ defines virtual quantities with,

$$\boldsymbol{\sigma}^{r} = \begin{bmatrix} \boldsymbol{n}^{mr} \\ \boldsymbol{m}^{r} \end{bmatrix} \tag{83}$$

and

$$\delta \boldsymbol{\varepsilon}^{r} = \begin{bmatrix} \delta \boldsymbol{\eta}^{r} \\ \delta \boldsymbol{\kappa}^{r} \end{bmatrix} \tag{84}$$

Introducing (43) and (50) in (82) one gets,

$$\delta W_{\text{int}}^{\Omega} = \int_{\Omega} (\boldsymbol{n}^{mr} \cdot \boldsymbol{Q}^{T} (\boldsymbol{e}_3 \otimes \boldsymbol{e}_3) \delta \boldsymbol{u}' + \boldsymbol{m}^{r} \cdot \boldsymbol{Q}^{T} (\boldsymbol{\Xi} \delta \boldsymbol{\alpha})') d\Omega \ , \tag{85}$$

and

$$\delta W_{\text{int}}^{\Omega} = \int_{\Omega} (\boldsymbol{Q}^{T} \boldsymbol{n}^{m} \cdot \boldsymbol{Q}^{T} (\boldsymbol{e}_3 \otimes \boldsymbol{e}_3) \delta \boldsymbol{u}' + \boldsymbol{Q}^{T} \boldsymbol{m} \cdot \boldsymbol{Q}^{T} (\boldsymbol{\Xi} \delta \boldsymbol{\alpha})') d\Omega \ , \tag{86}$$

concluding

$$\delta W_{\text{int}}^{\Omega} = \int_{\Omega} (\boldsymbol{n}^{m} \cdot \delta \boldsymbol{u}' + \boldsymbol{m} \cdot (\boldsymbol{\Xi} \delta \boldsymbol{\alpha})') d\Omega \ , \tag{87}$$

The external virtual work on a domain $\Omega \subset \mathbb{R}$ is similarly given by

$$\delta W_{\text{ext}}^{\Omega} = \int_{\Omega} \bar{\boldsymbol{n}}^{\Omega} \cdot \delta \boldsymbol{u} + \bar{\boldsymbol{m}}^{\Omega} \cdot \boldsymbol{\omega} d\Omega \ = \int_{\Omega} \bar{\boldsymbol{n}}^{\Omega} \cdot \delta \boldsymbol{u} + \bar{\boldsymbol{m}}^{\Omega} \cdot \boldsymbol{\Xi} \, \delta \boldsymbol{\alpha} d\Omega \tag{88}$$

The local equilibrium equations of the rod are obtained by applying the Virtual Work Theorem valid for statics as follows

$$\delta W_{\text{int}}^{\Omega} - \delta W_{\text{ext}}^{\Omega} = \delta W_{\text{ext}}^{\Gamma} \ , \quad \forall \delta \boldsymbol{d} \quad \text{in } \Omega \ . \tag{89}$$

where $\delta W_{\text{ext}}^{\Gamma}$ is the external virtual work on the boundary Γ and $\boldsymbol{d}$ are the displacements and rotation. Introducing (86) and (88) in (89), one gets

$$\int_{\Omega} (\boldsymbol{n}^{m} \cdot \delta \boldsymbol{u}' - \bar{\boldsymbol{n}}^{\Omega} \cdot \delta \boldsymbol{u} + \boldsymbol{m} \cdot (\boldsymbol{\Xi} \delta \boldsymbol{\alpha})' - \bar{\boldsymbol{m}}^{\Omega} \cdot \boldsymbol{\Xi}\, \delta \boldsymbol{\alpha}) d\Omega = \delta W_{\text{ext}}^{\Gamma} \quad . \tag{90}$$

Performing integration by parts on (90), one obtains

$$\begin{aligned} \int_{\Omega} (\boldsymbol{n}^{m} \cdot \delta \boldsymbol{u}' - \bar{\boldsymbol{n}}^{\Omega} \cdot \delta \boldsymbol{u} - \boldsymbol{m}' \cdot \boldsymbol{\Xi} \delta \boldsymbol{\alpha} - \bar{\boldsymbol{m}}^{\Omega} \cdot \boldsymbol{\Xi}\, \delta \boldsymbol{\alpha}) d\Omega + \\ + (\boldsymbol{m} \cdot \boldsymbol{\Xi} \delta \boldsymbol{\alpha})_{\Gamma} = \delta W_{\text{ext}}^{\Gamma} \quad . \end{aligned} \tag{91}$$

Applying integration by parts on (91), one obtains

$$\begin{aligned} - \int_{\Omega} \left[\left(\boldsymbol{n}^{m\prime} + \bar{\boldsymbol{n}}^{\Omega} \right) \cdot \delta \boldsymbol{u} + (\boldsymbol{m}' + \bar{\boldsymbol{m}}^{\Omega}) \cdot \boldsymbol{\Xi} \delta \boldsymbol{\alpha} \right] d\Omega + \\ + (\boldsymbol{n}^{m} \cdot \delta \boldsymbol{u} + \boldsymbol{\Xi}^{\boldsymbol{T}} \boldsymbol{m} \cdot \delta \boldsymbol{\alpha})_{\Gamma} = \delta W_{\text{ext}}^{\Gamma} \quad , \end{aligned} \tag{92}$$

By fundamental Lemma of Variational Calculus, (92) delivers the following local equilibrium equations in Ω

$$\boldsymbol{n}' + \bar{\boldsymbol{n}}^{\Omega} = \boldsymbol{o} \quad \text{and} \quad (\boldsymbol{m}' + \bar{\boldsymbol{m}}^{\Omega}) \cdot \boldsymbol{e}_3 = 0. \tag{93}$$

It remains the following boundary term on Γ

$$(\boldsymbol{n}^{m} \cdot \delta \boldsymbol{u} + \boldsymbol{\Xi}^{\boldsymbol{T}} \boldsymbol{m} \cdot \delta \boldsymbol{\alpha})_{\Gamma} = \delta W_{\text{ext}}^{\Gamma} \quad . \tag{94}$$

With (94) it is concluded that the natural (Neumann) boundary conditions are

$$\bar{\boldsymbol{n}}^{\Gamma} = \boldsymbol{n}^{m} \quad , \quad \bar{\boldsymbol{m}}^{\Gamma} = \boldsymbol{m} \, , \tag{95}$$

on both ends.

3.7. Rod local equilibrium equations

The rod local equilibrium equations can be directly derived by Statics (see for example Pimenta and Yojo (1993) [41]). They are displayed below

$$\boldsymbol{n}' + \bar{\boldsymbol{n}}^{\Omega} = \boldsymbol{o} \quad \text{and} \quad \boldsymbol{m}' + \boldsymbol{z}' \times \boldsymbol{n} + \bar{\boldsymbol{m}}^{\Omega} = \boldsymbol{o} \ . \tag{96}$$

From $(96)_2$, one gets $\boldsymbol{z}' \times \boldsymbol{n} = -(\boldsymbol{m}' + \bar{\boldsymbol{m}}^{\Omega})$, which, with the aid of $\boldsymbol{n} = \boldsymbol{n}^m + \boldsymbol{n}^b$ and $\boldsymbol{z}' \times \boldsymbol{n}^m = \boldsymbol{o}$, leads to the result below

$$\boldsymbol{z}' \times \boldsymbol{n}^b = -(\boldsymbol{m}' + \bar{\boldsymbol{m}}^{\Omega}) \tag{97}$$

From (97), with $\boldsymbol{n}^b = V_\alpha \boldsymbol{e}_\alpha$, one can derive

$$\boldsymbol{e}_\beta \cdot (\boldsymbol{z}' \times \boldsymbol{n}^b) = \|\boldsymbol{z}'\| V_\alpha \big(\boldsymbol{e}_\beta \cdot \boldsymbol{e}_3 \times \boldsymbol{e}_\alpha\big) = \varepsilon_{\alpha\beta} \|\boldsymbol{z}'\| V_\alpha = -\boldsymbol{e}_\beta \cdot (\boldsymbol{m}' + \bar{\boldsymbol{m}}^{\Omega}) \tag{98}$$

where

$$\varepsilon_{\alpha\beta} = \boldsymbol{e}_\alpha \cdot \boldsymbol{e}_\beta \times \boldsymbol{e}_3 \tag{99}$$

is a permutation symbol. From (98) one arrives at

$$V_\alpha = -\|\boldsymbol{z}'\|^{-1} \varepsilon_{\alpha\beta} \boldsymbol{e}_\beta \cdot (\boldsymbol{m}' + \bar{\boldsymbol{m}}^{\Omega}) \tag{100}$$

An alternative to (100) is

$$\begin{aligned} \boldsymbol{n}^b = V_\alpha \boldsymbol{e}_\alpha &= -\|\boldsymbol{z}'\|^{-1} \big[\varepsilon_{\alpha\beta} \boldsymbol{e}_\beta \cdot (\boldsymbol{m}' + \bar{\boldsymbol{m}}^{\Omega})\big] \boldsymbol{e}_\alpha \\ &= -\|\boldsymbol{z}'\|^{-1} (\boldsymbol{e}_1 \otimes \boldsymbol{e}_2 - \boldsymbol{e}_2 \otimes \boldsymbol{e}_1)(\boldsymbol{m}' + \bar{\boldsymbol{m}}^{\Omega}) \ . \end{aligned} \tag{101}$$

From (101), with the aid of

$$\boldsymbol{e}_2 \otimes \boldsymbol{e}_1 - \boldsymbol{e}_1 \otimes \boldsymbol{e}_2 = \mathrm{Skew}(\boldsymbol{e}_3) \tag{102}$$

one arrives at

$$\boldsymbol{n}^b = \|\boldsymbol{z}'\|^{-1} \boldsymbol{e}_3 \times (\boldsymbol{m}' + \bar{\boldsymbol{m}}^{\Omega}) = \|\boldsymbol{z}'\|^{-2} \boldsymbol{z}' \times (\boldsymbol{m}' + \bar{\boldsymbol{m}}^{\Omega}) \ . \tag{103}$$

Hence, the transversal shear forces can be directly recovered from the bending moments, as in the linear theory.

4. Nonlinear Kirchhoff-Love shell theory

4.1. Kinematics

For the kinematics assumption that the shell is flat with straight edges at reference configuration.

An orthogonal system $\{\boldsymbol{e}_1^r, \boldsymbol{e}_2^r, \boldsymbol{e}_3^r\}$ is placed at the reference configuration of the shell.

The vectors $\boldsymbol{e}_\alpha^r$ with $\alpha = 1{,}2$ describe the shell plane and $\boldsymbol{e}_3^r$ is orthogonal to this plane. The position of the shell material points in the reference configuration along the height of the shell can be described by

$$\boldsymbol{\xi} = \boldsymbol{\zeta} + \boldsymbol{r}^r \tag{104}$$

where the vector $\boldsymbol{\zeta}$ defines the middle plane and $\boldsymbol{r}^r$ is the director, normal to the middle plane,

The thickness coordinate $\xi_3 \in H = \left[-\frac{h}{2}, \frac{h}{2}\right]$ with (h being the shell reference thickness) the director is given by

$$\boldsymbol{r}^r = \xi_3 \boldsymbol{e}_3^r\,, \tag{105}$$

that describes the relative position of the points on the cross section at the reference configuration. Coordinates $\xi_1, \xi_2 \in \Omega$ are such that , where $\Omega \subset \mathbb{R}^2$ is the shell domain. The boundary of the domain Ω is denoted by Γ, as usual. Thus, ξ_1, ξ_2 and ξ_3 build a Cartesian coordinate system.

Then,

$$\boldsymbol{\zeta} = \xi_\alpha \boldsymbol{e}_\alpha^r. \tag{106}$$

In the current configuration, as it can be seen in Figure 2, the position of the material points is given by

$$\boldsymbol{x} = \boldsymbol{z} + \boldsymbol{r} \tag{107}$$

Where $\boldsymbol{r}$ is the current director and $\boldsymbol{z} = \hat{\boldsymbol{z}}(\xi_\alpha)$ describes the position on the middle surface of the shell at the current configuration

$$\boldsymbol{z} = \boldsymbol{\zeta} + \mathbf{u} \tag{108}$$

the current director given by

$$\boldsymbol{r} = \boldsymbol{Q}\boldsymbol{r}^r \ , \tag{109}$$

where $\boldsymbol{Q}$ is the rotation tensor. Relation $\boldsymbol{e}_i = \boldsymbol{Q}\boldsymbol{e}_i^r$ holds for the local systems.

Figure 2: Shell description and basic kinematical quantities.

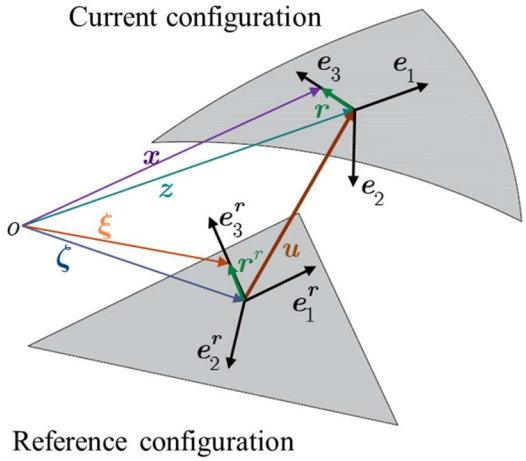

Source: Author

The set of vectors $\{\boldsymbol{e}_1, \boldsymbol{e}_2, \boldsymbol{e}_3\}$ is the local orthogonal system in the current configuration. $\boldsymbol{e}_\alpha$ is tangential to the middle surface of the shell, with $\boldsymbol{e}_3$ always being orthogonal to this plane of the shell and $\boldsymbol{e}_1$ parallel to one of the sides of the shell. $\boldsymbol{e}_1$ and $\boldsymbol{e}_3$ are material vectors because they are always tangent the same material fiber of the shell. The derivatives of the material points of the shell mid-plane are

$$\boldsymbol{z}_{,\alpha} = \boldsymbol{e}_\alpha^r + \boldsymbol{u}_{,\alpha} \quad \text{and} \quad \boldsymbol{z}_{,\alpha\beta} = \boldsymbol{u}_{,\alpha\beta} \, . \tag{110}$$

With the derivatives (110) one can define the base for the shell on the current deformed state.

$$\begin{aligned} \boldsymbol{e}_1 &= \|\boldsymbol{z}_{,1}\|^{-1}\boldsymbol{z}_{,1}\ , \\ \boldsymbol{e}_3 &= \|\boldsymbol{z}_{,1}\times\boldsymbol{z}_{,2}\|^{-1}(\boldsymbol{z}_{,1}\times\boldsymbol{z}_{,2}), \\ \boldsymbol{e}_2 &= \boldsymbol{e}_3\times\boldsymbol{e}_1\ . \end{aligned} \tag{111}$$

4.2. Strains

The Kirchhoff-Love assumption states that the director $\boldsymbol{r}$ remains orthogonal to the middle surface of the shell. The rotation tensor is expressed by

$$\boldsymbol{Q} = \boldsymbol{e}_i \otimes \boldsymbol{e}_i^r \quad \text{and} \quad \boldsymbol{e}_i = \boldsymbol{Q}\boldsymbol{e}_i^r. \tag{112}$$

If the displacements field are derived in relation to the position vector $\boldsymbol{\xi}$, one gets the transformation gradient

$$\boldsymbol{F} = \frac{\partial \boldsymbol{x}}{\partial \boldsymbol{\xi}} = \frac{\partial \boldsymbol{x}}{\partial \xi_\alpha}\otimes \boldsymbol{e}_\alpha^r + \frac{\partial \boldsymbol{x}}{\partial \xi_3}\otimes \boldsymbol{e}_3^r \tag{113}$$

Considering $(\cdot)_{,\alpha} = \frac{\partial(\cdot)}{\partial \xi_\alpha}$, $(\cdot)_{,3} = \frac{\partial(\cdot)}{\partial \xi_3}$, $\boldsymbol{x} = \boldsymbol{z} + \boldsymbol{Q}\boldsymbol{r}^r$ and $\boldsymbol{r}^r = \xi_3\boldsymbol{e}_3^r$, one gets,

$$\boldsymbol{x}_{,\alpha} = \boldsymbol{z}_{,\alpha} + \boldsymbol{r}_{,\alpha} = \boldsymbol{z}_{,\alpha} + (\boldsymbol{Q}\boldsymbol{r}^r)_{,\alpha} = \boldsymbol{z}_{,\alpha} + \boldsymbol{Q}_{,\alpha}\boldsymbol{r}^r \tag{114}$$

and

$$\boldsymbol{x}_{,3} = \boldsymbol{z}_{,3} + \boldsymbol{r}_{,3} = (\boldsymbol{Q}\xi_3\boldsymbol{e}_3^r)_{,3} = \boldsymbol{Q}\boldsymbol{e}_3^r \tag{115}$$

then,

$$\boldsymbol{F} = \left(\boldsymbol{z}_{,\alpha} + \boldsymbol{Q}_{,\alpha}\boldsymbol{r}^r\right)\otimes \boldsymbol{e}_\alpha^r + \boldsymbol{Q}\boldsymbol{e}_3^r \otimes \boldsymbol{e}_3^r. \tag{116}$$

In (116) the following membrane strain vector is noted

$$\boldsymbol{\eta}_\alpha = \boldsymbol{z}_{,\alpha} - \boldsymbol{e}_\alpha. \tag{117}$$

Then the deformation gradient can be written as,

$$\boldsymbol{F} = \left(\boldsymbol{\eta}_\alpha + \boldsymbol{e}_\alpha + \boldsymbol{Q}_{,\alpha}\boldsymbol{r}^r\right)\otimes \boldsymbol{e}_\alpha^r + \boldsymbol{e}_3 \otimes \boldsymbol{e}_3^r = \left(\boldsymbol{\eta}_\alpha + \boldsymbol{Q}_{,\alpha}\boldsymbol{r}^r\right)\otimes \boldsymbol{e}_\alpha^r + \boldsymbol{e}_i \otimes \boldsymbol{e}_i^r \tag{118}$$

The deformation gradient can be expressed by

$$\boldsymbol{F} = \boldsymbol{Q}\boldsymbol{F}^r, \tag{119}$$

and back-rotated transformation gradient is

$$\boldsymbol{F}^r = \boldsymbol{Q}^T\boldsymbol{F} = \boldsymbol{Q}^T\left(\boldsymbol{\eta}_\alpha + \boldsymbol{Q}_{,\alpha}\boldsymbol{r}^r\right) \otimes \boldsymbol{e}_\alpha^r + \boldsymbol{Q}^T\boldsymbol{Q}. \tag{120}$$

Which can be established as

$$\boldsymbol{F}^r = \boldsymbol{\gamma}_\alpha^r \otimes \boldsymbol{e}_\alpha^r + \boldsymbol{I} \tag{121}$$

with $\boldsymbol{\gamma}_\alpha^r = \boldsymbol{\eta}_\alpha^r + \boldsymbol{\kappa}_\alpha^r \times \boldsymbol{r}^r$ being the back-rotated generalized strains and $\boldsymbol{\eta}_\alpha^r$ the back-rotated membrane strains.

The following generalized back-rotated strain has been introduced

$$\boldsymbol{\eta}_\alpha^r = \boldsymbol{Q}^T\boldsymbol{z}_{,\alpha} - \boldsymbol{e}_\alpha^r. \tag{122}$$

The curvature tensor and its correspondent axial curvature vector are defined as

$$\boldsymbol{K}_\alpha = \boldsymbol{Q}_{,\alpha}\boldsymbol{Q}^T = \text{Skew}(\boldsymbol{\kappa}_\alpha) \text{ and } \boldsymbol{\kappa}_\alpha = \text{axial}(\boldsymbol{K}_\alpha). \tag{123}$$

The back-rotated curvature of the shell is given by

$$\boldsymbol{\kappa}_\alpha^r = \text{axial}\left(\boldsymbol{Q}^T\boldsymbol{Q}_{,\alpha}\right). \tag{124}$$

A result from Viebahn, Pimenta and Schröder 2016 [65] is

$$\boldsymbol{\kappa}_\alpha = \boldsymbol{\Gamma}_\beta \boldsymbol{u}_{,\beta\alpha} \tag{125}$$

where $\boldsymbol{\Gamma}_\beta$ are

$$\begin{aligned} \boldsymbol{\Gamma}_1 &= \left(\boldsymbol{e}_1 \cdot \boldsymbol{z}_{,1}\right)^{-1}\left[\text{Skew}(\boldsymbol{e}_1) - \left(\boldsymbol{e}_1 \cdot \boldsymbol{z}_{,2}\right)\left(\boldsymbol{e}_2 \cdot \boldsymbol{z}_{,2}\right)^{-1}(\boldsymbol{e}_1 \otimes \boldsymbol{e}_3)\right], \\ \boldsymbol{\Gamma}_2 &= \left(\boldsymbol{e}_2 \cdot \boldsymbol{z}_{,1}\right)^{-1}(\boldsymbol{e}_1 \otimes \boldsymbol{e}_3). \end{aligned} \tag{126}$$

It is observed that

$$\boldsymbol{\gamma}_\alpha^r \cdot \boldsymbol{e}_3^r = \boldsymbol{\eta}_\alpha^r \cdot \boldsymbol{e}_3^r = 0 \tag{127}$$

due to the Kirchhoff–Love assumption.

The back-rotated counterpart of (125) is

$$\boldsymbol{\kappa}_\alpha^r = \boldsymbol{Q}^T\boldsymbol{\Gamma}_\beta \boldsymbol{u}_{\beta\alpha}. \tag{128}$$

A generalized strain vector can be written as,

$$\boldsymbol{\varepsilon}_{\alpha}^{r} = \begin{bmatrix} \boldsymbol{\eta}_{\alpha}^{r} \\ \boldsymbol{\kappa}_{\alpha}^{r} \end{bmatrix}. \tag{129}$$

4.3. Strain rates

The velocity gradient is given by time differentiation of (119)

$$\dot{\boldsymbol{F}} = \dot{\boldsymbol{Q}}\boldsymbol{F}^{r} + \boldsymbol{Q}\dot{\boldsymbol{F}}^{r} = \dot{\boldsymbol{Q}}\boldsymbol{Q}^{T}\boldsymbol{F} + \boldsymbol{Q}\dot{\boldsymbol{F}}^{r}. \tag{130}$$

The skew-symmetric tensor $\boldsymbol{\Omega}$ that relates the director to its time derivative like in the following

$$\dot{\boldsymbol{r}} = \dot{\boldsymbol{Q}}\boldsymbol{Q}^{T}\boldsymbol{r} = \boldsymbol{\Omega}\boldsymbol{r} = \boldsymbol{\omega} \times \boldsymbol{r} \tag{131}$$

and it is considered the following skew-symmetric spin tensor and its corresponding axial spin vector.

$$\boldsymbol{\Omega} = \dot{\boldsymbol{Q}}\boldsymbol{Q}^{T} = \text{Skew}(\boldsymbol{\omega}) \text{ and } \boldsymbol{\omega} = \text{axial}(\boldsymbol{\Omega}). \tag{132}$$

Considering $(112)_1$ and (132), one gets

$$\boldsymbol{\Omega} = (\dot{\boldsymbol{e}}_i \otimes \boldsymbol{e}_i^{r})(\boldsymbol{e}_i^{r} \otimes \boldsymbol{e}_i) = (\dot{\boldsymbol{e}}_i \otimes \boldsymbol{e}_i)\,. \tag{133}$$

The spin vector is

$$\boldsymbol{\omega} = \boldsymbol{\Xi}\dot{\boldsymbol{\alpha}}. \tag{134}$$

Considering time differentiation of (121), (130) can be rewritten as,

$$\dot{\boldsymbol{F}} = \boldsymbol{\Omega}\boldsymbol{F} + \boldsymbol{Q}(\dot{\boldsymbol{\gamma}}_{\alpha}^{r} \otimes \boldsymbol{e}_{\alpha}^{r}) \ , \tag{135}$$

where

$$\dot{\boldsymbol{\gamma}}_{\alpha}^{r} = \dot{\boldsymbol{\eta}}_{\alpha}^{r} + \dot{\boldsymbol{\kappa}}_{\alpha}^{r} \times \boldsymbol{r}^{r} \ . \tag{136}$$

with

$$\dot{\boldsymbol{\kappa}}_{\alpha}^{r} = \boldsymbol{Q}^{T}\boldsymbol{\omega}_{,\boldsymbol{\alpha}}. \tag{137}$$

On the other hand, time differentiation of (122) yields

$$\dot{\boldsymbol{\eta}}_{\alpha}^{r} = \boldsymbol{Q}^{T}\dot{\boldsymbol{u}}_{,\alpha} + \dot{\boldsymbol{Q}}^{T}\boldsymbol{z}_{,\alpha} = \boldsymbol{Q}^{T}\left(\dot{\boldsymbol{u}}_{,\alpha} + \boldsymbol{z}_{,\alpha} \times \boldsymbol{\omega}\right). \tag{138}$$

Time differentiation of the curvatures $\boldsymbol{\kappa}_{\alpha}$ gives

$$\dot{\boldsymbol{\kappa}}_{\alpha} = \dot{\boldsymbol{\Gamma}}_{\beta}\boldsymbol{u}_{,\beta\alpha} + \boldsymbol{\Gamma}_{\beta}\dot{\boldsymbol{u}}_{,\beta\alpha} \tag{139}$$

and

$$\dot{\boldsymbol{\kappa}}_{\alpha}^{r} = \boldsymbol{Q}^{T}\dot{\boldsymbol{\Gamma}}_{\beta}\boldsymbol{u}_{,\beta\alpha} + \boldsymbol{Q}^{T}\boldsymbol{\Gamma}_{\beta}\dot{\boldsymbol{u}}_{,\beta\alpha}. \tag{140}$$

4.4. Stresses

The 1st Piola-Kirchhoff stress tensor is used because it relates the deformed stressed configuration to undeformed geometry and can be stated by its columns as shown

$$\boldsymbol{P} = \boldsymbol{\tau}_{i} \otimes \boldsymbol{e}_{i}^{r} = \boldsymbol{Q}(\boldsymbol{\tau}_{i}^{r} \otimes \boldsymbol{e}_{i}^{r}) \ . \tag{141}$$

Then, the back-rotated counterpart of (141) can be introduced by

$$\boldsymbol{P}^{r} = \boldsymbol{Q}^{T}\boldsymbol{P} = \boldsymbol{\tau}_{i}^{r} \otimes \boldsymbol{e}_{i}^{r} \ , \tag{142}$$

where the back-rotated stress vectors are

$$\boldsymbol{\tau}_{i}^{r} = \boldsymbol{Q}^{T}\boldsymbol{\tau}_{i} \ , \quad i = 1,2,3 \ , \tag{143}$$

$\boldsymbol{\tau}_{i}$ are the nominal stress vectors acting on points of the shell at the current configuration whose unitary normal vectors at the reference configuration are $\boldsymbol{e}_{i}^{r}$.

Notice that, $\boldsymbol{e}_{\alpha}^{r}$ are the vectors that describe the plane of the shell. Integration of $\boldsymbol{\tau}_{\alpha}^{r}$ over the shell reference thickness domain H furnishes the stress resultants as below

$$\boldsymbol{n}_{\boldsymbol{\alpha}} = \int_{H} \boldsymbol{\tau}_{\boldsymbol{\alpha}} dH \quad \text{and} \quad \boldsymbol{m}_{\boldsymbol{\alpha}} = \int_{H} (\boldsymbol{r} \times \boldsymbol{\tau}_{\boldsymbol{\alpha}}) dH. \tag{144}$$

The vectors $\boldsymbol{n}_{\boldsymbol{\alpha}}$ are the true internal forces and $\boldsymbol{m}_{\boldsymbol{\alpha}}$ are the true internal moments that are acting on the shell plane, these quantities are both per unit length of the reference configuration.

Considering (143), the back-rotated counterparts of (144) may be written

$$\boldsymbol{n}_\alpha^r = \boldsymbol{Q}^T\boldsymbol{n}_\alpha = \int_H \boldsymbol{\tau}_\alpha^r dH \quad \text{and} \quad \boldsymbol{m}_\alpha^r = \boldsymbol{Q}^T\boldsymbol{m}_\alpha = \int_H (\boldsymbol{r}\times\boldsymbol{\tau}_\alpha^r) dH. \tag{145}$$

4.5. Power

From (141), (135) and the angular momentum balance $\boldsymbol{P}\boldsymbol{F}^T:\boldsymbol{\Omega} = 0$, one gets the following result

$$\begin{aligned}&\boldsymbol{P}:\dot{\boldsymbol{F}} = \boldsymbol{P}:\left(\boldsymbol{\Omega}\boldsymbol{F} + \boldsymbol{Q}\dot{\boldsymbol{F}}^r\right) = \ \boldsymbol{P}:\boldsymbol{Q}\dot{\boldsymbol{F}}^r = \boldsymbol{P}:\boldsymbol{Q}(\dot{\boldsymbol{\gamma}}_\alpha^r \otimes \boldsymbol{e}_\alpha^r) \ = \\ &= \boldsymbol{Q}^T\boldsymbol{P}:(\dot{\boldsymbol{\gamma}}_\alpha^r \otimes \boldsymbol{e}_\alpha^r) = \boldsymbol{Q}^T\boldsymbol{Q}(\boldsymbol{\tau}_\alpha^r \otimes \boldsymbol{e}_3^r):(\dot{\boldsymbol{\gamma}}_\alpha^r \otimes \boldsymbol{e}_\alpha^r) = \boldsymbol{\tau}_\alpha^r \cdot \dot{\boldsymbol{\gamma}}_\alpha^r\end{aligned} \tag{146}$$

that is the stress power per unit reference volume. With the aid of (136) one gets,

$$\boldsymbol{P}:\dot{\boldsymbol{F}} = \boldsymbol{\tau}_\alpha^r \cdot \dot{\boldsymbol{\eta}}_\alpha^r + (\boldsymbol{r}^r \times \boldsymbol{\tau}_\alpha^r)\cdot \dot{\boldsymbol{\kappa}}_\alpha^r. \tag{147}$$

With the aid of the definitions on (145) , the integration of (147) over the height furnishes

$$\int_H \left(\boldsymbol{P}:\dot{\boldsymbol{F}}\right) dH = \boldsymbol{n}_\alpha^r \cdot \dot{\boldsymbol{\eta}}_\alpha^r + \boldsymbol{m}_\alpha^r \cdot \dot{\boldsymbol{\kappa}}_\alpha^r. \tag{148}$$

that is the stress power per unit length of the reference. It is important to remark that $\boldsymbol{n}_\alpha^r$, $\boldsymbol{m}_\alpha^r$, $\boldsymbol{\eta}_\alpha^r$ and $\boldsymbol{\kappa}_\alpha^r$ are not affected by superimposed rigid body motions.

The internal power on the domain Ω is then given by

$$P_{\text{int}}^{\Omega} = \int_\Omega (\boldsymbol{n}_\alpha^r \cdot \dot{\boldsymbol{\eta}}_\alpha^r + \boldsymbol{m}_\alpha^r \cdot \dot{\boldsymbol{\kappa}}_\alpha^r) d\Omega. \tag{149}$$

On the other hand, the external power on the same domain can be expressed by

$$P_{\text{ext}}^{\Omega} = \int_\Omega \left[(\bar{\boldsymbol{t}}^t \cdot \dot{\boldsymbol{x}}^t + \bar{\boldsymbol{t}}^b \cdot \dot{\boldsymbol{x}}^t) + \int_H \left(\overline{\boldsymbol{b}} \cdot \dot{\boldsymbol{x}}\right) dH\right] d\Omega, \tag{150}$$

$\bar{\boldsymbol{t}}$ is the normal surface stresses and $\overline{\boldsymbol{b}}$ is the body force per unit reference volume. $\bar{\boldsymbol{t}}^t$ is the top surface traction and $\bar{\boldsymbol{t}}^b$ is bottom surface traction.

The time differentiation of (107) yields

$$\dot{\boldsymbol{x}} = \dot{\boldsymbol{u}} + \boldsymbol{\omega}\times\boldsymbol{r} \tag{151}$$

The following definitions are stated

$$\overline{\boldsymbol{n}}^{\Omega} = \bar{\boldsymbol{t}}^{t} + \bar{\boldsymbol{t}}^{b} + \int_{H} \bar{\boldsymbol{b}}\, dH \quad \text{and} \quad \overline{\boldsymbol{m}}^{\Omega} = \boldsymbol{r}^{t} \times \bar{\boldsymbol{t}}^{t} + \boldsymbol{r}^{\boldsymbol{b}} \times \bar{\boldsymbol{t}}^{b} + \int_{H} \left(\boldsymbol{r} \times \bar{\boldsymbol{b}}\right) dH \tag{152}$$

With (150), (151), (152) and knowing that $\boldsymbol{\omega} = \boldsymbol{\Gamma}_{\alpha}\dot{\boldsymbol{u}}_{,\alpha}$ one may write

$$P_{\text{ext}}^{\Omega} = \int_{\Omega} \left(\overline{\boldsymbol{n}}^{\Omega} \cdot \dot{\boldsymbol{u}} + \overline{\boldsymbol{\mu}}_{\alpha}^{\Omega} \cdot \dot{\boldsymbol{u}}_{,\alpha}\right) d\Omega \tag{153}$$

where

$$\overline{\boldsymbol{\mu}}_{\alpha}^{\Omega} = \boldsymbol{\Gamma}_{\alpha}^{T} \overline{\boldsymbol{m}}^{\Omega} \tag{154}$$

are the pseudo-moments applied on the shell. And $\overline{\boldsymbol{n}}^{\Omega}$ is the applied external force per unit length at reference configuration and $\overline{\boldsymbol{m}}^{\Omega}$ is the applied external moment per unit length at reference configuration. $\overline{\boldsymbol{\mu}}_{\alpha}^{\Omega}$ are the pseudo-moments

4.6. Weak form of the local equilibrium equation

The internal virtual work on the domain Ω is given by

$$\delta W_{\text{int}}^{\Omega} = \int_{\Omega} (\boldsymbol{n}_{\alpha}^{r} \cdot \delta \boldsymbol{\eta}_{\alpha}^{r} + \boldsymbol{m}_{\alpha}^{r} \cdot \delta \boldsymbol{\kappa}_{\alpha}^{r}) d\Omega\,. \tag{155}$$

Considering (153) for the shell the external virtual work is

$$\delta W_{\text{ext}}^{\Omega} = \int_{\Omega} \left(\overline{\boldsymbol{n}}^{\Omega} \cdot \delta \boldsymbol{u} + \overline{\boldsymbol{\mu}}_{\alpha}^{\Omega} \cdot \delta \boldsymbol{u}_{,\alpha}\right) d\Omega \tag{156}$$

The local equilibrium equations are obtained by applying the Virtual Work Theorem, valid for statics, as follows

$$\delta W_{\text{int}}^{\Omega} - \delta W_{\text{ext}}^{\Omega} = \delta W_{\text{ext}}^{\Gamma}\,, \quad \forall \delta \boldsymbol{d} \ \text{ in } \Omega. \tag{157}$$

With $\boldsymbol{d}$ being the displacements degrees of freedom

5. Rotation

5.1. Total description

The rotation is described by employing the Rodrigues rotation parameters, for more information on how to get these parameters see Pimenta and Campello (2001) [40] or attachment B. Let $\boldsymbol{\alpha}$ denote the vector of Rodrigues parameters. The Rodrigues parameterization furnishes

$$\widehat{\boldsymbol{Q}}(\boldsymbol{\alpha}) = \boldsymbol{I} + \frac{4}{4+\alpha^2}\left(\boldsymbol{A} + \frac{1}{2}\boldsymbol{A}^2\right) \tag{158}$$

Where $\boldsymbol{A} = \text{Skew}(\boldsymbol{\alpha})$ and $\alpha^2 = \boldsymbol{\alpha} \cdot \boldsymbol{\alpha}$.

Another way to display Rodrigues formula shown in Appendix B is

$$\widehat{\boldsymbol{Q}}(\boldsymbol{\alpha}) = \left(\boldsymbol{I} - \frac{1}{2}\boldsymbol{A}\right)^{-1}\left(\boldsymbol{I} + \frac{1}{2}\boldsymbol{A}\right) \tag{159}$$

Vector $\boldsymbol{\alpha}$ can be obtained from $\boldsymbol{Q}$ with the aid of

$$\boldsymbol{\alpha} = \frac{4}{1+\text{tr}\boldsymbol{Q}}\text{axial}(\text{Skew}\boldsymbol{Q}) \tag{160}$$

From (159) and $\boldsymbol{e} = \boldsymbol{Q}\boldsymbol{e}^r$ with $\boldsymbol{e}$ and $\boldsymbol{e}^r$ being a considered axis, like $\boldsymbol{e}_3$ and $\boldsymbol{e}_3^r$ for the rod, one has

$$\left(\boldsymbol{I} - \frac{1}{2}\boldsymbol{A}\right)\boldsymbol{e} = \left(\boldsymbol{I} + \frac{1}{2}\boldsymbol{A}\right)\ \boldsymbol{e}^r \tag{161}$$

And

$$\boldsymbol{e} - \frac{1}{2}\boldsymbol{A}\boldsymbol{e} = \boldsymbol{e}^r + \frac{1}{2}\boldsymbol{A}\boldsymbol{e}^r \tag{162}$$

Arriving at the important result

$$\boldsymbol{e} - \boldsymbol{e}^r = \frac{1}{2}(\boldsymbol{A}\boldsymbol{e}^r + \boldsymbol{A}\boldsymbol{e}) = \boldsymbol{A}\boldsymbol{e}^m = \boldsymbol{\alpha} \times \boldsymbol{e}^m \tag{163}$$

Figure 3: vectors $\boldsymbol{e}^r$ and $\boldsymbol{e}$.

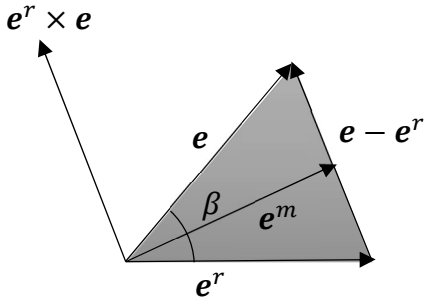

Source: Author

Looking at Figure 3, one gets

$$\boldsymbol{e}^m = \frac{1}{2}(\boldsymbol{e} + \boldsymbol{e}^r). \tag{164}$$

It is remarked that $\boldsymbol{e}^m$ is not a unit vector. And one can get the relation

$$\boldsymbol{e} - \boldsymbol{e}^r = \frac{(\boldsymbol{e}^r \times \boldsymbol{e}) \times \boldsymbol{e}^m}{\|(\boldsymbol{e}^r \times \boldsymbol{e}) \times \boldsymbol{e}^m\|} \|\boldsymbol{e} - \boldsymbol{e}^r\|. \tag{165}$$

Considering (165) and some mathematical manipulation applied, one gets

$$(\boldsymbol{e}^r \times \boldsymbol{e}) \times \boldsymbol{e}^m = \frac{1 + \boldsymbol{e}^r \cdot \boldsymbol{e}}{2}(\boldsymbol{e} - \boldsymbol{e}^r). \tag{166}$$

Let β denote the angle from $\boldsymbol{e}^r$ to $\boldsymbol{e}$. Then, one has

$$\boldsymbol{e}^r \times \boldsymbol{e} = \sin\beta \|\boldsymbol{e}^r \times \boldsymbol{e}\|^{-1}(\boldsymbol{e}^r \times \boldsymbol{e}) = 2\tan\frac{\beta}{2}\cos^2\frac{\beta}{2}\|\boldsymbol{e}^r \times \boldsymbol{e}\|^{-1}(\boldsymbol{e}^r \times \boldsymbol{e}). \tag{167}$$

Note that

$$\begin{aligned} \|\boldsymbol{e}^m\| &= \cos\frac{\beta}{2} = \sqrt{\frac{1 + \cos\beta}{2}} = \sqrt{\frac{1 + \boldsymbol{e}^r \cdot \boldsymbol{e}}{2}}, \\ \boldsymbol{e}^m \cdot \boldsymbol{e} &= \frac{1 + \boldsymbol{e}^r \cdot \boldsymbol{e}}{2} = \cos^2\frac{\beta}{2} = \|\boldsymbol{e}^m\|^2 . \end{aligned} \tag{168}$$

Considering (166) and$(168)_2$ one reaches the following result

$$\|\boldsymbol{e}^m\|^{-2}(\boldsymbol{e}^r \times \boldsymbol{e}) \times \boldsymbol{e}^m = \boldsymbol{e} - \boldsymbol{e}^r. \tag{169}$$

Comparing (163) and (169) one gets part of $\boldsymbol{\alpha}$, because $\boldsymbol{\alpha} = \widehat{\boldsymbol{\alpha}}(\boldsymbol{u}', \varphi)$ and (163) only has the part concerning $\boldsymbol{u}'$, then one more scalar parameter φ is needed. For (169) to be true this scalar has to be in the direction of $\boldsymbol{e}^m$

Now, to comply with the previous relations $\boldsymbol{e} - \boldsymbol{e}^r = \boldsymbol{\alpha} \times \boldsymbol{e}^m$ a new formula is achieved

$$\boldsymbol{\alpha} = \|\boldsymbol{e}^m\|^{-2}(\boldsymbol{e}^r \times \boldsymbol{e}) + \varphi\|\boldsymbol{e}^m\|^{-1}\boldsymbol{e}^m \tag{170}$$

which is a relevant contribution in this work.

Definition (170) preserves relation (163). According to (170), $\boldsymbol{\alpha}$ has the following components

$$\begin{aligned} &\boldsymbol{\alpha} \cdot \|\boldsymbol{e}^m\|^{-1}\boldsymbol{e}^m = \varphi \text{ and} \\ &\boldsymbol{\alpha} \cdot \|\boldsymbol{e}^r \times \boldsymbol{e}\|^{-1}(\boldsymbol{e}^r \times \boldsymbol{e}) = \|\boldsymbol{e}^m\|^{-2}\|\boldsymbol{e}^r \times \boldsymbol{e}\| = \|\boldsymbol{e}^m\|^{-1}\|\boldsymbol{e} - \boldsymbol{e}^r\| = 2\tan\frac{\beta}{2} \end{aligned} \tag{171}$$

There are the following results, as well

$$\begin{aligned} &\boldsymbol{\alpha} \cdot \boldsymbol{e} = \varphi\|\boldsymbol{e}^m\|^{-1}\boldsymbol{e}^m \cdot \boldsymbol{e} = \varphi\|\boldsymbol{e}^m\| \\ &\boldsymbol{\alpha} \times \boldsymbol{e} = +\frac{1}{2}\|\boldsymbol{e}^m\|\boldsymbol{\alpha} - \varphi\boldsymbol{e}^m - \|\boldsymbol{e}^m\|^{-2}(\boldsymbol{I} - \boldsymbol{e} \otimes \boldsymbol{e})\boldsymbol{e}^r \text{and} \\ &\alpha^2 = \boldsymbol{\alpha} \cdot \boldsymbol{\alpha} = \|\boldsymbol{e}^m\|^{-4}\|\boldsymbol{e}^r \times \boldsymbol{e}\|^2 + \varphi^2 = \|\boldsymbol{e}^m\|^{-1}\|\boldsymbol{e} - \boldsymbol{e}^r\| = 4\tan^2\frac{\beta}{2} + \varphi^2. \end{aligned} \tag{172}$$

5.2. Incremental description

Let $(\cdot)_i$ and $(\cdot)_{i+1}$ denote a quantity $(\cdot)$ at instants t_i and t_{i+1}, respectively. And let $(\cdot)_\Delta$ be an incremental quantity. Thus, one gets for the rotation tensor the following relations

$$\begin{aligned} &\boldsymbol{Q}_{i+1} = \boldsymbol{Q}_\Delta \boldsymbol{Q}_i \ , \quad \text{where} \\ &\boldsymbol{Q}_{i+1} = \widehat{\boldsymbol{Q}}(\boldsymbol{\alpha}_{i+1}) \ , \quad \boldsymbol{Q}_\Delta = \widehat{\boldsymbol{Q}}(\boldsymbol{\alpha}_\Delta) \quad \text{and} \quad \boldsymbol{Q}_i = \widehat{\boldsymbol{Q}}(\boldsymbol{\alpha}_i). \end{aligned} \tag{173}$$

The following result by Rodrigues is recalled, which is probably his the most relevant result,

$$\boldsymbol{\alpha}_{i+1} = \frac{4}{4 - \boldsymbol{\alpha}_i \cdot \boldsymbol{\alpha}_\Delta}\left(\boldsymbol{\alpha}_i + \boldsymbol{\alpha}_\Delta - \frac{1}{2}\boldsymbol{\alpha}_i \times \boldsymbol{\alpha}_\Delta\right) \tag{174}$$

The curvature vector at instant t_{i+1} is given by $\boldsymbol{\kappa}_{i+1} = \text{axial}(\boldsymbol{Q}'_{i+1}\boldsymbol{Q}_{i+1}^T)$ or $\boldsymbol{\kappa}_{i+1} = \text{axial}((\boldsymbol{Q}_\Delta \boldsymbol{Q}_i)'\boldsymbol{Q}_i^T\boldsymbol{Q}_\Delta^T)$. This delivers

$$\boldsymbol{\kappa}_{i+1} = \boldsymbol{Q}_{\Delta}\,\boldsymbol{\kappa}_{i} \;+ \boldsymbol{\Xi}_{\Delta}\boldsymbol{\alpha}'_{\Delta} \tag{175}$$

where

$$\boldsymbol{\Xi}_{\Delta} = \frac{4}{4+\alpha_{\Delta}^{2}}\left(\boldsymbol{I} + \frac{1}{2}\boldsymbol{A}_{\Delta}\right) \tag{176}$$

In (176), both $\boldsymbol{A}_{\Delta} = \mathrm{Skew}(\boldsymbol{\alpha}_{\Delta})$ and $\alpha_{\Delta}^{2} = \boldsymbol{\alpha}_{\Delta}\cdot\boldsymbol{\alpha}_{\Delta}$ appear.On the other hand, the back-rotated curvature vector at instant t_{i+1} is given by $\boldsymbol{\kappa}_{i+1}^{r} = \mathrm{axial}(\boldsymbol{Q}_{i+1}^{T}\boldsymbol{Q}'_{i+1}) = \mathrm{axial}(\boldsymbol{Q}_{i}^{T}\boldsymbol{Q}_{\Delta}^{T}(\boldsymbol{Q}_{\Delta}\boldsymbol{Q}_{i})')$ or

$$\boldsymbol{\kappa}_{i+1}^{r} = \boldsymbol{\kappa}_{i}^{r} + \boldsymbol{Q}_{i+1}^{T}\boldsymbol{\Xi}_{\Delta}\boldsymbol{\alpha}'_{\Delta} = \boldsymbol{\kappa}_{i}^{r} + \boldsymbol{Q}_{i}^{T}\boldsymbol{\Xi}_{\Delta}^{T}\boldsymbol{\alpha}'_{\Delta} \tag{177}$$

where

$$\boldsymbol{\Xi}_{\Delta}^{T} = \frac{4}{4+\alpha_{\Delta}^{2}}\left(\boldsymbol{I} - \frac{1}{2}\boldsymbol{A}_{\Delta}\right). \tag{178}$$

Time derivative of (175) leads to

$$\dot{\boldsymbol{\kappa}}_{i+1}^{r} = \boldsymbol{Q}_{i}^{T}\left(\dot{\boldsymbol{\Xi}}_{\Delta}^{T}\boldsymbol{\alpha}'_{\Delta} + \boldsymbol{\Xi}_{\Delta}^{T}\dot{\boldsymbol{\alpha}}'_{\Delta}\right) = \boldsymbol{Q}_{i+1}^{T}\left(\boldsymbol{Q}_{\Delta}\dot{\boldsymbol{\Xi}}_{\Delta}^{T}\boldsymbol{\alpha}'_{\Delta} + \boldsymbol{\Xi}_{\Delta}\dot{\boldsymbol{\alpha}}'_{\Delta}\right). \tag{179}$$

The spin vector at instant t_{i+1} is given by

$$\boldsymbol{\omega}_{i+1} = \mathrm{axial}\left(\dot{\boldsymbol{Q}}_{i+1}\boldsymbol{Q}_{i+1}^{T}\right) = \mathrm{axial}\left(\dot{\boldsymbol{Q}}_{\Delta}\boldsymbol{Q}_{i}\boldsymbol{Q}_{i}^{T}\boldsymbol{Q}_{\Delta}^{T}\right) = \mathrm{axial}\left(\dot{\boldsymbol{Q}}_{\Delta}\boldsymbol{Q}_{\Delta}^{T}\right) = \boldsymbol{\Xi}_{\Delta}\dot{\boldsymbol{\alpha}}_{\Delta}. \tag{180}$$

An interesting result, which is an alternative to (179), is

$$\dot{\boldsymbol{\kappa}}_{i+1}^{r} = \boldsymbol{Q}_{i+1}^{T}\boldsymbol{\omega}'_{i+1} = \boldsymbol{Q}_{i+1}^{T}\left(\boldsymbol{\Xi}'_{\Delta}\dot{\boldsymbol{\alpha}}_{\Delta} + \boldsymbol{\Xi}_{\Delta}\dot{\boldsymbol{\alpha}}'_{\Delta}\right) = \boldsymbol{Q}_{i}^{T}\left(\boldsymbol{Q}_{\Delta}^{T}\boldsymbol{\Xi}'_{\Delta}\dot{\boldsymbol{\alpha}}_{\Delta} + \boldsymbol{\Xi}_{\Delta}^{T}\dot{\boldsymbol{\alpha}}'_{\Delta}\right) \tag{181}$$

where

$$\boldsymbol{\Xi}'_{\Delta} = \frac{2}{4+\alpha_{\Delta}^{2}}\left[\boldsymbol{A}'_{\Delta} - (\boldsymbol{\alpha}_{\Delta}\cdot\boldsymbol{\alpha}'_{\Delta})\boldsymbol{\Xi}_{\Delta}\right] \tag{182}$$

Now, considering the incremental counterpart of (170) one gets,

$$\boldsymbol{\alpha}_{\Delta} = \|\boldsymbol{e}^{m}\|^{-2}\left(\boldsymbol{e}^{i}\times\boldsymbol{e}^{i+1}\right) + \varphi_{\Delta}\|\boldsymbol{e}^{m}\|^{-1}\,\boldsymbol{e}^{m} \tag{183}$$

The incremental parameter $\boldsymbol{\alpha}_{\Delta}$ has the same properties as $\boldsymbol{\alpha}$,

$$\begin{aligned} &\boldsymbol{\alpha}_{\Delta}\cdot\|\boldsymbol{e}^{m}\|^{-1}\,\boldsymbol{e}^{m} = \varphi_{\Delta}\ , \\ &\boldsymbol{\alpha}_{\Delta}\cdot\boldsymbol{\alpha}_{\Delta} = \alpha_{\Delta}^{2}\ . \end{aligned} \tag{184}$$

Bearing in mind (183), one gets

$$\boldsymbol{\alpha}_{\Delta} \cdot \boldsymbol{e}^{i} = \boldsymbol{\alpha}_{\Delta} \cdot \boldsymbol{e}^{i+1} = \varphi_{\Delta} \|\boldsymbol{e}^{m}\|^{-1} \frac{1 + \boldsymbol{e}^{i} \cdot \boldsymbol{e}^{i+1}}{2} = \varphi_{\Delta} \|\boldsymbol{e}^{m}\| \tag{185}$$

with aid of (160) and knowing that $\mathrm{tr}\left(\boldsymbol{e}_{\mathrm{j}}^{i+1} \otimes \boldsymbol{e}_{j}^{i}\right) = \boldsymbol{e}_{j}^{i+1} \cdot \boldsymbol{e}_{j}^{i}$, $\boldsymbol{Q} = \boldsymbol{e}_{\mathrm{j}}^{i+1} \otimes \boldsymbol{e}_{j}^{r}$ and axial $\left(\mathrm{Skew}\left(\boldsymbol{e}_{\mathrm{j}}^{i+1} \otimes \boldsymbol{e}_{\mathrm{j}}^{i}\right)\right) = -\frac{1}{2}\boldsymbol{e}_{j}^{i+1} \times \boldsymbol{e}_{\mathrm{j}}^{i}$ the important formula for the Rodrigues vector can be reached

$$\boldsymbol{\alpha}_{\Delta} = \frac{-2}{1+\boldsymbol{e}_{k}^{i+1} \cdot \boldsymbol{e}_{k}^{i}} \boldsymbol{e}_{j}^{i+1} \times \boldsymbol{e}_{j}^{i}, \tag{186}$$

$\left\{\boldsymbol{e}_{1}^{i+1}, \boldsymbol{e}_{2}^{i+1}, \boldsymbol{e}_{3}^{i+1}\right\}$ is the basis in the current configuration and $\{\boldsymbol{e}_{1}, \boldsymbol{e}_{2}, \boldsymbol{e}_{3}\}$ the basis in the reference configuration. This formula is also an important contribution on this work.

6. Constitutive equations

6.1. Rods

If the rod axis is placed along with the cross section shear centers, the following linear elastic constitutive equation for small strain isotropic elasticity can be adopted.

$$\boldsymbol{\sigma}^r = \boldsymbol{D}\boldsymbol{\varepsilon}^r \tag{187}$$

Where

$$\boldsymbol{D} = \begin{bmatrix} \boldsymbol{D}_{\eta\eta} & \boldsymbol{D}_{\eta\kappa} \\ \boldsymbol{D}_{\kappa\eta} & \boldsymbol{D}_{\kappa\kappa} \end{bmatrix} \tag{188}$$

The strain energy per unit reference length is then given by

$$\psi(\boldsymbol{\varepsilon}^r) = \frac{1}{2}\boldsymbol{\varepsilon}^r \cdot \boldsymbol{D}\boldsymbol{\varepsilon}^r \tag{189}$$

In (188), one has

$$\begin{aligned} &\boldsymbol{D}_{\eta\eta} = EA\boldsymbol{e}_3^r \otimes \boldsymbol{e}_3^r \\ &\boldsymbol{D}_{\eta\kappa} = ES_\alpha \boldsymbol{e}_3^r \otimes \boldsymbol{e}_\alpha^r = \boldsymbol{D}_{\kappa\eta}^T \text{and} \\ &\boldsymbol{D}_{\kappa\kappa} = EJ_{\alpha\beta}\boldsymbol{e}_\alpha^r \otimes \boldsymbol{e}_\beta^r + GJ_T \boldsymbol{e}_3^r \otimes \boldsymbol{e}_3^r, \end{aligned} \tag{190}$$

where E is the elasticity modulus, G is the shear modulus, A is the cross-sectional area, J_T is the cross-sectional torsion constant, $S_\alpha = \varepsilon_{\alpha\beta}\int_A \xi_\beta \, dA$ are the cross-sectional static moments and $J_{\alpha\beta} = \varepsilon_{\alpha\gamma}\varepsilon_{\beta\delta}\int_A \xi_\gamma \xi_\delta dA$ are the cross-sectional inertia moments. It is recalled that J_T is given by

$$J_T = J_0 - \int_A \varepsilon_{\alpha\beta}\xi_\beta \, \phi_{,\alpha} dA, \tag{191}$$

where $\phi = \hat{\phi}(\xi_\alpha)$ is the St.-Venant warping function and

$$J_0 = \int_A \xi_\alpha \xi_\alpha \, dA = J_{11} + J_{22} \tag{192}$$

is the cross-sectional polar moment of inertia. For circular or annular sections, with the origin at the barycenter $S_\alpha = 0$, $J_{12} = J_{21} = 0, \phi = 0$ .and $J_T = J_0$ For bisymmetrical cross sections with the origin at the barycenter and $\boldsymbol{e}_\alpha^r$ along the principal axes of the cross section, one has $S_\alpha = 0,\ J_{12} = J_{21} = 0,$ and J_T given by (191).

6.2. Shells

For the shell the material is assumed to be isotropic, then the strain energy of a neo-Hookean hyperelastic material shown in Simo and Hughes (1998) [59] is described by

$$\bar{\psi}(\boldsymbol{\varepsilon}_\alpha^r) = \bar{\psi}(I_1, J) = \frac{1}{2}\lambda\left[\frac{1}{2}\left(J^2 - 1\right) - \ln J\right] + \frac{1}{2}\mu(I_1 - 3 - 2\ln J) \tag{193}$$

Where the function $\bar{\psi}(\boldsymbol{\varepsilon}_\alpha^r)$ is written in terms of strain invariants $I_1 = \boldsymbol{F}:\boldsymbol{F}$, $J = \det\boldsymbol{F}$ and λ, μ are the Lamé constants. More general, fully three-dimensional hyperelastic materials for shells (i.e. without the plane-stress enforcement) can be considered as Pimenta, Campello and Wriggers (2004) [45].

6.2.1. Plane stress condition

In order to enforce plane stress condition, the expression for the back-rotated deformation gradient (121) can be rewritten as

$$\boldsymbol{F}^r = \boldsymbol{I} + \boldsymbol{\gamma}_\alpha^r \otimes \boldsymbol{e}_\alpha^r + \boldsymbol{\gamma}_3^r \otimes \boldsymbol{e}_3^r \tag{194}$$

Which $\boldsymbol{\gamma}_\alpha^r$ are the shell strain vectors and $\boldsymbol{\gamma}_3^r = \gamma_{33}^r \boldsymbol{e}_3^r$ is the vector of the thickness strain corresponding to the plane stress state and the scalar γ_{33}^r is introduced to allow thickness deformation (transversal strains). It can be considered as an additional degree of freedom and should be eliminated at constitutive level by a shell plane stress condition.

The following plane stress condition is stated

$$\tau_{33}^r = \boldsymbol{\tau}_3^r \cdot \boldsymbol{e}_3^r = 0 \tag{195}$$

and

$$(\boldsymbol{P}\boldsymbol{e}_3^r) \cdot \boldsymbol{e}_3 = 0\ . \tag{196}$$

which means that the projection of the traction $\boldsymbol{P}\boldsymbol{e}_3^r$ on the director $\boldsymbol{r} = \xi_3 \boldsymbol{e}_3$ is zero. So, τ_{33}^r is powerless.

For specific cases one can define this scalar by analytical enforcement as done in Viebahn, Pimenta and Schröder (2016) [65]. This is considered in all shell examples.

$$\gamma_{33}^r = \sqrt{\frac{\lambda + 2\mu}{\lambda \bar{J}^2 + 2\mu}} - 1 \tag{197}$$

7. Finite element

Bearing in mind that the potential is nonlinear, a Newton-Raphson iteration scheme is chosen to solve this problem. The simulations presented are performed within the AceFEM finite element software. Both AceGen and AceFEM programs are developed and maintained by Joze Korelc (University of Ljubljana). The interested reader is referred to Korelc and Wriggers (2016) [34].

The presented model allows the formulation of an internal and an external potential, which can be given by

$$\Pi = \sum_{e} (\Pi^{e}_{\text{int}} + \Pi^{e}_{\text{ext}}) \tag{198}$$

where $(\cdot)^e$ is the contribution of each element $e = 1,2, \dots N_{elements}$. The strain energy of an element is

$$\Pi^{e}_{\text{int}} = \int_{\Omega^e} \psi d\Omega \tag{199}$$

with ψ given by (189) for rods or (193) for shells.

The finite element method is used to discretize these potentials on a computational domain in terms of the nodal degrees of freedom. The minimization of the potential energy leads to the equilibrium state, this minimization in the context as a Theorem of Potential Energy, which states that the solution of a static problem is a stationary (in some cases minimum) of the total potential energy. The residual vector, also known as unbalanced forces, and the tangent stiffness matrix are respectively given by

$$\begin{aligned} \boldsymbol{R}(\boldsymbol{d}) &= \frac{\partial \Pi(\boldsymbol{d})}{\partial \boldsymbol{d}} = 0 \quad \text{and} \\ \boldsymbol{K}(\boldsymbol{d}) &= \frac{\partial^2 \Pi(\boldsymbol{d})}{\partial \boldsymbol{d}^2} \end{aligned} \tag{200}$$

where $\boldsymbol{d}$ is the vector of the nodal degrees-of-freedom. A Newton iteration is then given by

$$\frac{\partial \Pi(\boldsymbol{d}_{k+1})}{\partial \boldsymbol{d}} \cong \boldsymbol{R}(\boldsymbol{d}_k) + \boldsymbol{K}(\boldsymbol{d}_k)\Delta\boldsymbol{d} = \boldsymbol{0} \tag{201}$$

The application of this procedure leads to the standard form of the local linear equation system, given in equation (201). Here $\boldsymbol{R}$ and $\boldsymbol{K}$ are known as the global residual and global stiffness matrix. Solution of this linear system leads to the incremental update $\Delta\boldsymbol{d}$ of the vector of unknowns within the iterative solution procedure.

7.1. Rods

7.1.1. First connection strategy - Finite elements with $\boldsymbol{u}$, $\boldsymbol{u}'$ and $\boldsymbol{\varphi}$ as DOFs

For a smooth axis at reference configuration, a finite element must be continuous for $\boldsymbol{u}$, $(\boldsymbol{I} - \boldsymbol{e}_3 \otimes \boldsymbol{e}_3)\boldsymbol{u}'$ and φ (or$\boldsymbol{\varphi}_\Delta$). If there is no cross section or material change from an element to the other, a C_1 interpolation for the displacements $\boldsymbol{u}$ and a C_0 interpolation for the incremental rotation $\boldsymbol{\varphi}_\Delta$ is sufficient. For non-smooth connection or for the case of cross section or material change from an element to the other, the connection of elements must be carefully performed. A connection can be generally formulated by enforcing the equality of $\boldsymbol{u}$ and $\boldsymbol{\alpha}_\Delta$ at connecting ends.

Figure 4: Connection strategy - Finite elements with u, u' and φ as basic degrees of freedom.

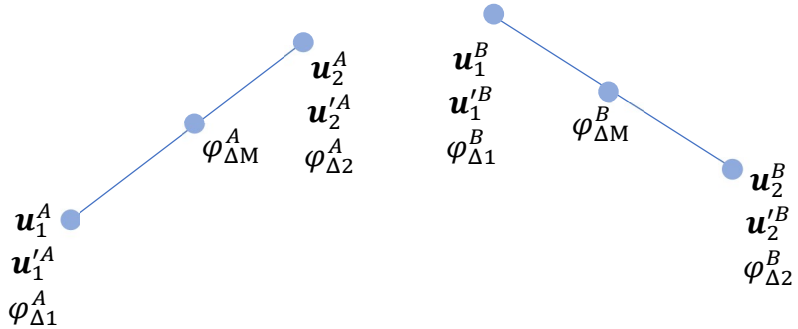

Source: Author

Then, the continuity of the degrees of freedom are given by

$$\begin{aligned} \boldsymbol{u}_2^A &= \boldsymbol{u}_1^B \\ \boldsymbol{u}_2'^A &\neq \boldsymbol{u}_1'^B \\ \varphi_{\Delta 2}^A &\neq \varphi_{\Delta 1}^B \end{aligned} \tag{202}$$

The displacements constraint is standard, but for the second and third continuity a penalty or Lagrangian term must be added to the potential energy, as follows

$$\frac{1}{2} k(\boldsymbol{\alpha}_\Delta^A - \boldsymbol{\alpha}_\Delta^B) \cdot (\boldsymbol{\alpha}_\Delta^A - \boldsymbol{\alpha}_\Delta^B) \quad \text{or} \quad \boldsymbol{\lambda} \cdot (\boldsymbol{\alpha}_\Delta^A - \boldsymbol{\alpha}_\Delta^B) \tag{203}$$

where A and B designate the connecting element ends, k is a penalty parameter and $\boldsymbol{\lambda}$ is the associated vector of Lagrange multipliers. $\varphi_{\Delta \mathrm{M}}$ is illustrated in the Figure 4 being an option for the interpolation polynomials, but that is a degree of freedom only when the polynomial used requires it.

7.1.2. Second connection strategy - $\boldsymbol{u}$ and $\boldsymbol{\alpha}$ as DOFs

There is another element option that needs no special treatment where the degrees of freedom are the $\boldsymbol{u}$, $\boldsymbol{\alpha}$ and ε, leaving ε discontinuous. Evaluating both options this was the chosen method for the example illustrations, as no difference in results were found between both strategies.

$$\begin{aligned} \varepsilon_I &= \|\boldsymbol{z}'_I\| - 1 \\ \varphi_I &= \|\boldsymbol{e}_{3I}^m\|^{-1} (\boldsymbol{\alpha}_I \cdot \boldsymbol{e}_{3I}^m), \\ \boldsymbol{u}'_I &= \big(1 + \varepsilon_I\big) \boldsymbol{e}_{3I} - \boldsymbol{e}_3^r. \end{aligned} \tag{204}$$

where I=1,2 designate the element nodes. $\boldsymbol{u}$, $\boldsymbol{u}'$ and φ are still the one interpolated, but the nodal values are achieved through $\boldsymbol{u}$, $\boldsymbol{\alpha}$ and ε. φ_I is the rotation around e $\boldsymbol{e}_{3I}^m$ which is a moving axis and ε_I is the elongation of the axis.

At nodes $I = 1,2$, with the nodal values $\boldsymbol{\alpha}_I^i$, $\boldsymbol{\alpha}_{\Delta I}$, ε_I^i and ε_I^{i+1}, one gets

$$
\begin{aligned}
&\boldsymbol{e}_{iI}^{i} = \widehat{\boldsymbol{Q}}(\boldsymbol{\alpha}_{iI})\boldsymbol{e}_{iI}^{r},\\
&\boldsymbol{e}_{iI}^{i+1} = \widehat{\boldsymbol{Q}}(\boldsymbol{\alpha}_{\Delta I})\boldsymbol{e}_{iI}^{i}\ ,\\
&\boldsymbol{e}_{1I}^{m} = \frac{1}{2}\left(\boldsymbol{e}_{1I}^{i} + \boldsymbol{e}_{1I}^{i+1}\right),\\
&\varphi_{\Delta I} = \|\boldsymbol{e}_{1I}^{m}\|^{-1}(\boldsymbol{\alpha}_{\Delta I}\cdot\boldsymbol{e}_{1I}^{m}),\\
&\boldsymbol{u'}_{I}^{i} = \left(1+\varepsilon_{I}^{i}\right)\boldsymbol{e}_{1I}^{i} - \boldsymbol{e}_{1}^{r}\quad\text{and}\\
&\boldsymbol{u'}_{I}^{i+1} = \left(1+\varepsilon_{I}^{i+1}\right)\boldsymbol{e}_{1I}^{i+1} - \boldsymbol{e}_{1}^{r}.
\end{aligned}
\tag{205}
$$

Along the rod, with the interpolations $\boldsymbol{u}^{i+1}$, $\boldsymbol{u'}^{i+1}$, $\boldsymbol{u''}^{i+1}$, $\boldsymbol{u}^{i}$, $\boldsymbol{u'}^{i}$, $\boldsymbol{u''}^{i}$, φ_{Δ} and φ'_{Δ} are computed. Afterwards, $\boldsymbol{\alpha}_{\Delta}$ and $\boldsymbol{\alpha'}_{\Delta}$ are obtained with the aid of

$$
\begin{aligned}
&\boldsymbol{e}_{1}^{i} = \left\|\boldsymbol{e}_{1}^{r} + \boldsymbol{u'}^{i}\right\|^{-1}\left(\boldsymbol{e}_{1}^{r} + \boldsymbol{u'}^{i}\right)\ ,\\
&\boldsymbol{e}_{1}^{i+1} = \left\|\boldsymbol{e}_{1}^{r} + \boldsymbol{u'}^{i+1}\right\|^{-1}\left(\boldsymbol{e}_{1}^{r} + \boldsymbol{u'}^{i+1}\right)\ ,\\
&\boldsymbol{e}_{1}^{m} = \frac{1}{2}\left(\boldsymbol{e}_{1}^{i} + \boldsymbol{e}_{1}^{i+1}\right)\ ,\\
&\boldsymbol{\alpha}_{\Delta} = \|\boldsymbol{e}_{1}^{m}\|^{-2}\left(\boldsymbol{e}_{1}^{i}\times\boldsymbol{e}_{1}^{i+1}\right) + \varphi_{\Delta}\|\boldsymbol{e}_{1}^{m}\|^{-1}\boldsymbol{e}_{1}^{m}
\end{aligned}
\tag{206}
$$

Finally, at the domain, one can compute

$$
\begin{aligned}
&\boldsymbol{\alpha}_{i+1} = \frac{4}{4-\boldsymbol{\alpha}_{i}\cdot\boldsymbol{\alpha}_{\Delta}}\left(\boldsymbol{\alpha}_{i} + \boldsymbol{\alpha}_{\Delta} - \frac{1}{2}\boldsymbol{\alpha}_{i}\times\boldsymbol{\alpha}_{\Delta}\right)\ ,\\
&\boldsymbol{\Xi}_{\Delta} = \frac{4}{4+\boldsymbol{\alpha}_{\Delta}\cdot\boldsymbol{\alpha}_{\Delta}}\left(\boldsymbol{I} + \frac{1}{2}\mathrm{Skew}(\boldsymbol{\alpha}_{\Delta})\right)\ ,\\
&\varepsilon^{i+1} = \left\|\boldsymbol{e}_{1}^{r} + \boldsymbol{u'}^{i+1}\right\| - 1\ ,\\
&\boldsymbol{\eta}_{i+1}^{r} = \varepsilon^{i+1}\,\boldsymbol{e}_{1}^{r}\quad\text{and}\\
&\boldsymbol{\kappa}_{i+1}^{r} = \boldsymbol{\kappa}_{i}^{r} + \boldsymbol{Q}_{i}^{T}\boldsymbol{\Xi}_{\Delta}^{T}\boldsymbol{\alpha'}_{\Delta}\ .
\end{aligned}
\tag{207}
$$

At every integration point, $\boldsymbol{\alpha}_{i}$ and $\boldsymbol{\kappa}_{i}^{r}$ must be stored. In general, only $\boldsymbol{u}$ and $\boldsymbol{\alpha}_{\Delta}$ can be connected by neighboring elements. ε can be shared only in the case of smooth connection of 2 elements, with no change of cross-sectional properties and no nodal external forces.

Figure 5: Connection strategy - Finite elements with $\boldsymbol{u}$, $\boldsymbol{\alpha}$ and ε as basic degrees of freedom.

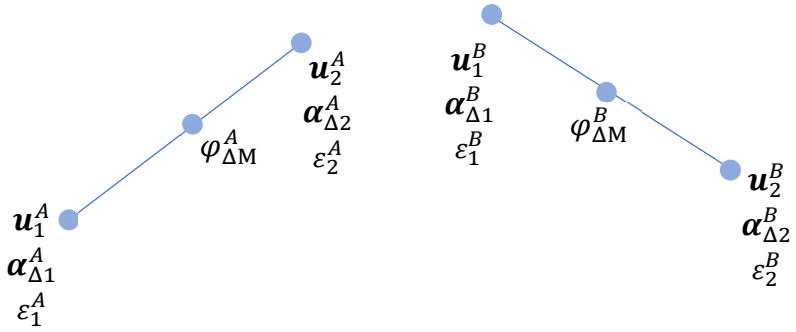

Source: Author

Then, the continuity of the degrees of freedom are

$$\begin{gathered} \boldsymbol{u}_2^A = \boldsymbol{u}_1^B \\ \boldsymbol{\alpha}_{\Delta 2}^A = \boldsymbol{\alpha}_{\Delta 1}^B \\ \varepsilon_2^A \neq \varepsilon_1^B \end{gathered} \tag{208}$$

The constraints are enforced by the assembly of the of the global stiffness matrix as usual in the finite element method.

7.1.3. Interpolation polynomials

In any of the connection strategies the interpolation polynomials are applied in u, u', u'', φ and φ' as demonstrated in the following. u'' and φ' are added to the end nodes as degrees of freedom for the interpolation, but they are discontinuous between elements.

7.1.3.1. Cubic interpolation for the displacements

The FE interpolation can be written as

$$\boldsymbol{u} = N_1^u \boldsymbol{u}_1 + N_1^{u'} \boldsymbol{u}_1' + N_2^u \boldsymbol{u}_2 + N_2^{u'} \boldsymbol{u}_2' \tag{209}$$

where,

$$N_1^u = 1 - \frac{3\zeta^2}{l^2} + \frac{2\zeta^3}{l^3},\ N_1^{u'} = \zeta - \frac{2\zeta^2}{l} + \frac{\zeta^3}{l^2},\ N_2^u = \frac{3\zeta^2}{l^2} - \frac{2\zeta^3}{l^3},\ N_2^{u'} = \frac{\zeta^3}{l^2} - \frac{\zeta^2}{l}, \tag{210}$$

7.1.3.2. Quintic interpolation for the displacements

The FE interpolation can be written as

$$\begin{aligned}&\boldsymbol{u} = N_1^u \boldsymbol{u}_1 + N_1^{u'} \boldsymbol{u}_1' + N_1^{u''} \boldsymbol{u}_1'' + N_2^u \boldsymbol{u}_2 + N_2^{u'} \boldsymbol{u}_2' + N_2^{u''} \boldsymbol{u}_2'' \text{ and}\\ &\varphi = N_1^\varphi \varphi_1 + N_1^{\varphi'} \varphi_1' + N_2^\varphi \varphi_2 + N_2^{\varphi'} \varphi_2' + N_M^\varphi \varphi_M,\end{aligned} \tag{211}$$

where,

$$\begin{aligned}&N_1^u = 1 - \frac{10\zeta^3}{l^3} + \frac{15\zeta^4}{l^4} - \frac{6\zeta^5}{l^5}, \quad N_1^{u'} = \zeta - \frac{6\zeta^3}{l^2} + \frac{8\zeta^4}{l^3} - \frac{3\zeta^5}{l^4},\\ &N_1^{u''} = \frac{\zeta^2}{2} - \frac{3\zeta^3}{2l} + \frac{3\zeta^4}{2l^2} - \frac{\zeta^5}{2l^3}, \quad N_2^u = \frac{10\zeta^3}{l^3} - \frac{15\zeta^4}{l^4} + \frac{6\zeta^5}{l^5},\\ &N_2^{u'} = -\frac{4\zeta^3}{l^2} + \frac{7\zeta^4}{l^3} - \frac{3\zeta^5}{l^4}, \quad N_2^{u''} = \frac{\zeta^3}{2l} - \frac{\zeta^4}{l^2} + \frac{\zeta^5}{2l^3},\end{aligned} \tag{212}$$

7.1.3.3. Linear interpolation for the torsion

The FE interpolation can be written as

$$\varphi = N_1^\varphi \varphi_1 + N_2^\varphi \varphi_2 \tag{213}$$

where,

$$N_1^\varphi = 1 - \frac{\zeta}{l} \text{ and } N_2^\varphi = \frac{\zeta}{l}. \tag{214}$$

7.1.3.4. Quadratic interpolation for the torsion

The FE interpolation can be written as

$$\varphi = N_1^\varphi \varphi_1 + N_2^\varphi \varphi_2 + N_M^\varphi \varphi_M \tag{215}$$

where,

$$N_1^\varphi = 1 - \frac{3\zeta}{l} + \frac{2\zeta^2}{l^2}, \qquad N_2^\varphi = -\frac{\zeta}{l} + \frac{2\zeta^2}{l^2} \text{ and } N_M^\varphi = \frac{4\zeta}{l} - \frac{4\zeta^2}{l^2} \tag{216}$$

7.1.3.5. Cubic interpolation for the torsion

The FE interpolation can be written as

$$\varphi = N_1^{\varphi}\varphi_1 + N_1^{\varphi'}\varphi_1' + N_2^{\varphi}\varphi_2 + N_2^{\varphi'}\varphi_2' \tag{217}$$

where,

$$\begin{aligned} N_1^{\varphi} &= 1 - \frac{3\zeta^2}{l^2} + \frac{2\zeta^3}{l^3}, \\ N_2^{\varphi} &= \frac{3\zeta^2}{l^2} - \frac{2\zeta^3}{l^3}, \\ N_1^{\varphi'} &= \zeta - \frac{2\zeta^2}{l} + \frac{\zeta^3}{l^2} \quad \text{and} \quad N_2^{\varphi'} = -\frac{\zeta^2}{l} + \frac{\zeta^3}{l^2} \end{aligned} \tag{218}$$

7.1.3.6. Quartic interpolation for the torsion

The FE interpolation can be written as

$$\varphi = N_1^{\varphi}\varphi_1 + N_1^{\varphi'}\varphi_1' + N_2^{\varphi}\varphi_2 + N_2^{\varphi'}\varphi_2' + N_M^{\varphi}\varphi_M, \tag{219}$$

where,

$$\begin{aligned} &N_1^{\varphi} = 1 - \frac{11\zeta^2}{l^2} + \frac{18\zeta^3}{l^3} - \frac{8\zeta^4}{l^4}, \quad N_2^{\varphi} = -\frac{5\zeta^2}{l^2} + \frac{14\zeta^3}{l^3} - \frac{8\zeta^4}{l^4}, \\ &N_1^{\varphi'} = \zeta - \frac{4\zeta^2}{l} + \frac{5\zeta^3}{l^2} - \frac{2\zeta^4}{l^3}, \quad N_2^{\varphi'} = \frac{\zeta^2}{l} - \frac{3\zeta^3}{l^2} + \frac{2\zeta^4}{l^3} \\ &\text{and} \quad N_3^{\varphi} = \frac{16\zeta^2}{l^2} - \frac{32\zeta^3}{l^3} + \frac{16\zeta^4}{l^4}. \end{aligned} \tag{220}$$

7.1.3.7. Interpolation polynomials schemes

The simplest element is cubic Hermitian on $\boldsymbol{u}$ (2 nodes) and linear Lagrangian on φ_Δ (2 nodes). This element has 14 DOF's. At each node, it has 7 DOF's, which are $\boldsymbol{u}$, $\boldsymbol{\alpha}$ and ε. $\boldsymbol{u}'$ and φ_Δ as internal degrees of freedom that are computed through $\boldsymbol{\alpha}$ and ε.

The next element is cubic Hermitian on $\boldsymbol{u}$ (2 nodes) and quadratic Lagrangian on φ_Δ (3 nodes). This element can be used together with T6-KL element. At each node, it has 7 DOF's, which are $\boldsymbol{u}$, $\boldsymbol{\alpha}$ and ε like the first element, and one more degree of freedom in the middle node φ_Δ. $\boldsymbol{u}'$ and $\varphi_{\Delta 3}$ as internal degrees of freedom that are computed through $\boldsymbol{\alpha}$ and ε.

Another element presented is a cubic Hermitian on $\boldsymbol{u}$ and φ_Δ (2 nodes). At each node, it has 8 DOF's, which are $\boldsymbol{u}$, $\boldsymbol{\alpha}$, ${\varphi'}_\Delta$ and ε. $\boldsymbol{u}'$ and φ_Δ as internal degrees of freedom that are computed through $\boldsymbol{\alpha}$ and ε.

Another element presented is a quintic Hermitian on $\boldsymbol{u}$ (2 nodes) and a linear Lagrangian on φ_Δ (2 nodes). At each node, it has 10 DOF's, which are $\boldsymbol{u}$, $\boldsymbol{u}''$, $\boldsymbol{\alpha}$ and ε. $\boldsymbol{u}'$ and φ_Δ as internal degrees of freedom that are computed through $\boldsymbol{\alpha}$ and ε.

One more element presented is a quintic Hermitian on $\boldsymbol{u}$ (2 nodes) and a quadratic Lagrangian on φ_Δ (3 nodes). At each node, it has 10 DOF's, which are $\boldsymbol{u}$, $\boldsymbol{u}''$, $\boldsymbol{\alpha}$ and ε, and one more degree of freedom in the middle node $\varphi_{\Delta 3}$. $\boldsymbol{u}'$ and φ_Δ as internal degrees of freedom that are computed through $\boldsymbol{\alpha}$ and ε.

There is also an element with quintic Hermitian on $\boldsymbol{u}$ (2 nodes) and a cubic Hermitian polynomial interpolation on φ_Δ (2 nodes), can be used together with reduced-quintic TUBA3 element. At each node, it has 11 DOF's, which are $\boldsymbol{u}$, $\boldsymbol{u}''$, $\boldsymbol{\alpha}$, ${\varphi'}_\Delta$ and ε. $\boldsymbol{u}'$ and φ_Δ as internal degrees of freedom that are computed through $\boldsymbol{\alpha}$ and ε.

The last one presented is an element with quintic Hermitian on $\boldsymbol{u}$ (2 nodes) and a quartic polynomial interpolation on φ_Δ (3 nodes), can be used together with quintic TUBA6 or TUBA7 shell element. At each node, it has 11 DOF's, which are $\boldsymbol{u}$, $\boldsymbol{u}''$, $\boldsymbol{\alpha}$, ${\varphi'}_\Delta$ and ε, and one more degree of freedom in the middle node $\varphi_{\Delta 3}$. $\boldsymbol{u}'$ and φ_Δ as internal degrees of freedom that are computed through $\boldsymbol{\alpha}$ and ε.

7.2. Shells

A triangular shell element T6-KL is considered. The element is a 6-node displacement-based one, with a plane reference configuration as displayed in Figure 2. In general, the Kirchhoff–Love shell theory requires C^1-continuous approximations. The approach adopted herein is to enforce C^1-continuity at the element boundaries. Therefore, it is sufficient to employ a C^0 interpolation. For the approximation of the triangular shaped finite elements, shape functions based on barycentric parent coordinates are applied. The position vector of the middle surface in the current configuration is interpolated with their corresponding nodal values and shape functions as

$$\boldsymbol{u}^h = \sum_I^e N_I \boldsymbol{u}_I \tag{221}$$

where the superscript h indicates the finite element discretization, and the number of element nodes, N_I a suitable matrix including the shape functions. $\boldsymbol{u}_I$ are the nodal degrees of freedom for the displacements, as in Viebahn, Pimenta and Schröder (2016) [65].

Figure 6: Node on a shell element.

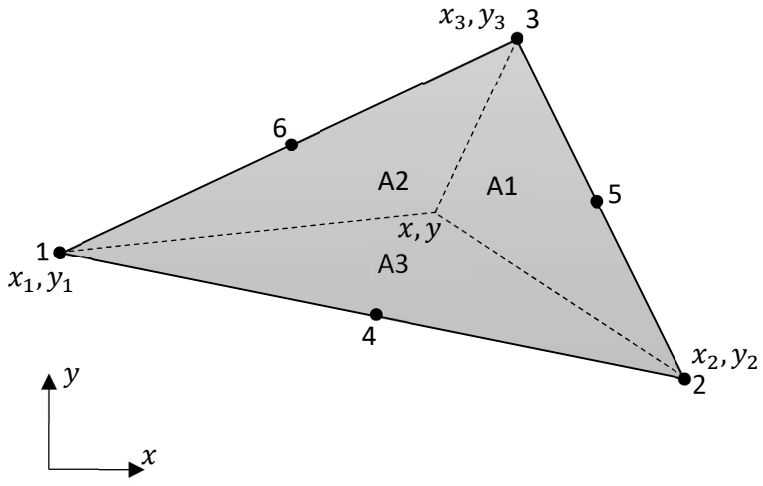

Source: Author

To find the shape functions for the shell element in Figure 6 the area of the element must be known

$$A = \frac{1}{2}\mathrm{Det}\begin{vmatrix} x_1 & y_1 & 1 \\ x_2 & y_2 & 1 \\ x_3 & y_3 & 1 \end{vmatrix} = \Delta \tag{222}$$

also the area opposite to node I A_I

$$A_1 = \frac{1}{2}\mathrm{Det}\begin{vmatrix} x & y & 1 \\ x_2 & y_2 & 1 \\ x_3 & y_3 & 1 \end{vmatrix} \tag{223}$$

$$A_2 = \frac{1}{2}\mathrm{Det}\begin{vmatrix} x_1 & y_1 & 1 \\ x & y & 1 \\ x_3 & y_3 & 1 \end{vmatrix} \tag{224}$$

$$A_3 = \frac{1}{2}\mathrm{Det}\begin{vmatrix} x_1 & y_1 & 1 \\ x_2 & y_2 & 1 \\ x & y & 1 \end{vmatrix}. \tag{225}$$

After that, the side opposite to nodes I, L_I

$$L_I = \frac{A_I}{\Delta} \tag{226}$$

are

$$\begin{aligned} L_1 &= \frac{1}{\Delta}(x\,y_2 + x_2\,y_3 + y\,x_3 - y\,x_2 - x\,y_3 - y_2\,x_3) \\ L_2 &= \frac{1}{\Delta}(x_1\,y + x\,y_3 + y_1\,x_3 - y_1\,x - x_1\,y_3 - y\,x_3) \\ L_3 &= \frac{1}{\Delta}(x_1\,y_2 + x_2\,y + y_1\,x - y_1\,x_2 - x_1\,y - y_2\,x) \end{aligned} \tag{227}$$

There is also a need for the derivatives of L_I in relation to the coordinates are

$$\begin{aligned}
\frac{\partial L_1}{\partial x} &= \frac{1}{\Delta}(y_2 - y_3) \\
\frac{\partial L_1}{\partial y} &= \frac{1}{\Delta}(x_3 - x_2) \\
\frac{\partial L_2}{\partial x} &= \frac{1}{\Delta}(y_3 - y_1) \\
\frac{\partial L_2}{\partial y} &= \frac{1}{\Delta}(x_1 - x_3) \\
\frac{\partial L_3}{\partial x} &= \frac{1}{\Delta}(y_1 - y_2) \\
\frac{\partial L_3}{\partial y} &= \frac{1}{\Delta}(x_2 - x_1)
\end{aligned} \tag{228}$$

The following shape functions are based on Figure 6 and equation (226),

$$\begin{aligned}
N_1 &= 2\,L_1\left(L_1 - \frac{1}{2}\right) \\
N_2 &= 2\,L_2\left(L_2 - \frac{1}{2}\right) \\
N_3 &= 2\,L_3\left(L_3 - \frac{1}{2}\right) \\
N_4 &= 4\,L_1 L_2 \\
N_5 &= 4\,L_2 L_3 \\
N_6 &= 4\,L_1 L_3
\end{aligned} \tag{229}$$

7.2.1. Shell connection strategy

Because of the Kirchhoff–Love`s assumption the deformation gradient of the shell is written in terms of first- and second-order derivatives of the displacements. Consequently, a C1-continuity between the finite elements has to be assured. In this work, this condition is imposed by a penalty approach and by a Lagrange multiplier, which enforces the equality at the kinking of the edge of two neighboring elements. There are two approaches to impose this continuity. One addressed in Viebahn, Pimenta and Schröder (2016) [65] which an angle between the normal vectors $\boldsymbol{e}_3^r$ from neighboring elements has to remain the same between $\boldsymbol{e}_3^{i+1}$of each element. And a new approach that is presented in this work, where a rotation parameter φ_Δ around the medium tangent of the middle node that neighbors the elements being connected is calculated and this parameter has to be the same on both elements. The approach that is presented in this work is easier to calculate (for the author's point of view) but no numerical

advantage was presented. Figure 7 shows the degrees of freedom and this internal rotation parameter along with the base in the middle node.

Figure 7: Degrees of freedom in a shell element.

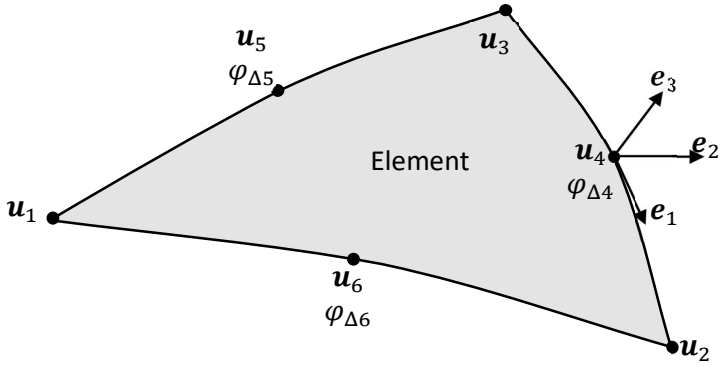

Source: Author

For the shells $\boldsymbol{\alpha}_{\Delta} = \frac{-2}{1+\boldsymbol{e}_k^{i+1}\cdot\boldsymbol{e}_k^i}\boldsymbol{e}_j^{i+1} \times \boldsymbol{e}_j^i$ is used to calculate $\boldsymbol{\alpha}_{\Delta}$ as $\boldsymbol{e}_j^{i+1}$ can be achieved only with the displacements and $\boldsymbol{e}_j^i$ are known from the previous step. Then, φ_{Δ} can be attained by

$$\varphi_{\Delta} = \boldsymbol{\alpha}_{\Delta} \cdot \|\boldsymbol{e}_1^m\|^{-1}\, \boldsymbol{e}_1^m \tag{230}$$

Figure 8: Degrees of freedom in two neighboring elements.

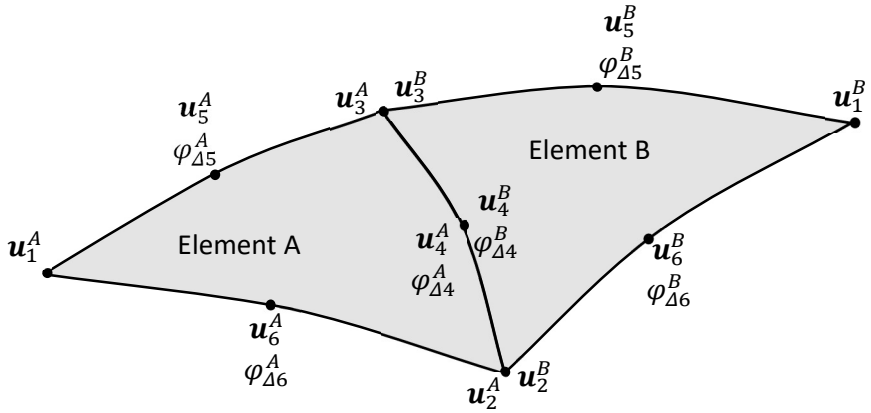

Source: Author

The continuity of the degrees of freedom are

$$\begin{aligned} \boldsymbol{u}^A &= \boldsymbol{u}^B \\ \varphi_{\Delta}^A &= \varphi_{\Delta}^B \end{aligned} \tag{231}$$

The continuity of φ_{Δ} is enforced by adding an artificial energy to the potential (198)

$$\Pi_{cont} = \lambda(\varphi_{\Delta}^A - \varphi_{\Delta}^B) \tag{232}$$

where λ is the Lagrange multiplier.

The continuity of φ_Δ can also be enforced by adding an artificial energy to the potential (198)

$$\Pi_{cont} = \frac{1}{2}\kappa\,(\varphi_\Delta^A - \varphi_\Delta^B)^2 \tag{233}$$

where κ is the penalty parameter. In this work only Lagrange multipliers were considered in the examples.

$\boldsymbol{u}$ are the displacements degrees of freedom from the elements and φ_Δ is an internal degree of freedom that is only needed to connect neighboring elements.

8. Continuity constrains between shells and rods

The connection between shells and rods are done in a similar manner as between shells, φ_{Δ} is calculated as in (230) for the shell and in the rod φ_{Δ} is already a degree of freedom, there is no need to calculate a new parameter. For the connection a Lagrange multiplier was used. Figure 9 shows the degrees of freedom in the rod and shell elements.

Figure 9: General case for the finite elements' threshold.

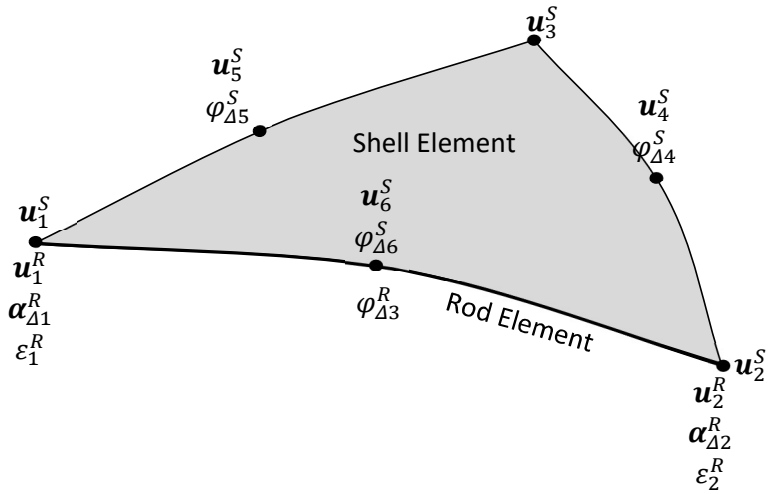

Source: Author

As for the rotation continuity of the shell, the constrain is done internally so that the degree of freedom φ_{Δ}^{S} becomes external and can be connected to the rod element by the assembly of the global stiffness matrix.

$\varphi_{\Delta \mathrm{e}}^{S}$ is attained by (186) and (230) and depends on the element's displacements and φ_{Δ}^{S} is an external degree of freedom and is obtained by adding the following artificial energy function to the potential.

$$\Pi_{cont} = \lambda\left(\varphi_{\Delta}^{S} - \varphi_{\Delta \mathrm{e}}^{S}\right) \tag{234}$$

The procedure to execute this constraint imposes that the rotation field appears as continuous. Here the Lagrange multiplier approach is introduced that ensures the constrain in an exact manner.

Then, the continuity constraint is

$$\varphi_{\Delta}^{S} = \varphi_{\Delta \mathrm{e}}^{S} \tag{235}$$

The displacements continuity is enforced by the assembly of the global stiffness matrix as usual in the finite element method as they are external degrees of freedom.

9. Numerical examples

In this section various numerical examples are presented to verify the model's capabilities. Standard benchmark structural problems were investigated. The first examples aim to verify the general reliability of the derived model especially in terms of correct kinematics and energy formulations as well as application of boundary conditions. First an example is computed to compare Timoshenko rod theory with the one presented in this work. The next example serves to compare the different shape functions schemes. Then a simple two-dimensional cantilever is considered, exposed to conservative and non-conservative loads. Furthermore, the domain of a cantilever is investigated in three dimensions. The considered problem shows a well-known buckling behavior. To show the theory's comprehensiveness the same buckling problem is illustrated with different cross sections. Then for the I cross section different discretizations are applied one as the first example were only rod elements are employed, one where only shell elements are employed then one with rod elements in the flange and shell elements in the web to show the connection between the two theories presented.

An additional buckling analysis is presented on an L-shaped frame section also with the different discretization as it was done for the cantilever. Two more complex boundary value problems are evaluated to show the general capability of the model regarding finite displacement and rotation. Therefore, a snap-through problem on a non-straight reference configuration is presented. Then, the elastic ring, a complex three-dimensional problem is presented, showing all the capabilities of the presented rod formulation. A coil spring under compression is also shown and is another type of buckling problem. Furthermore, a benchmark problem for shells (pinched cylinder) is shown, this is also a complex problem and gives large displacements. And the last example shows a reinforced shell, which is a very usual problem. All the problems showed satisfying results.

9.1. Comparison between Timoshenko and Bernoulli-Euler (BE) - Rods

With this example the intention is to show that Timoshenko and BE rod theory converge to the same results when the structure is sufficiently slender and that BE theory, applied to slender

rods, converges with very few elements while Timoshenko needs more DOFs to converge. A cantilever with its length L=2m clamped at L = 0 is loaded by concentrated force F, starting with F = 1kN. The height of the cross section is h, while the elasticity constants are adopted as E = 210000 MPa and ν = 0.3125, considering a constant area for the cross section. The intensity of the load is properly chosen for different values of the height, according with $F \sim h^2$. Thus, simple bending for both theories with varying slenderness is investigated. Figure 10 shows the tip deflection w (normalized by Bernoulli's analytical solution) versus the degrees of freedom for the cantilever, with different ratios h/L, only the first Newton iteration was considered for the displayed deflections to get the linear solution, and it can be seen that BE solution converges with 2 elements for any slenderness. Timoshenko solution has a much softer response with $h/L=10^{-1}$ due to shear deformation and needs more elements to converge with increasing slenderness, as shown in Figure 10 for this curve the shear is more important and that is why it gives a softer response. In Figure 10 all the Bernoulli-Euler results were the same and are represented by only one curve. Timoshenko's solution the curve differed for $h/L=10^{-1}$, all the other curves were the same and are represented by one curve.

Figure 10: Normalized tip displacements with respect to DOFs.

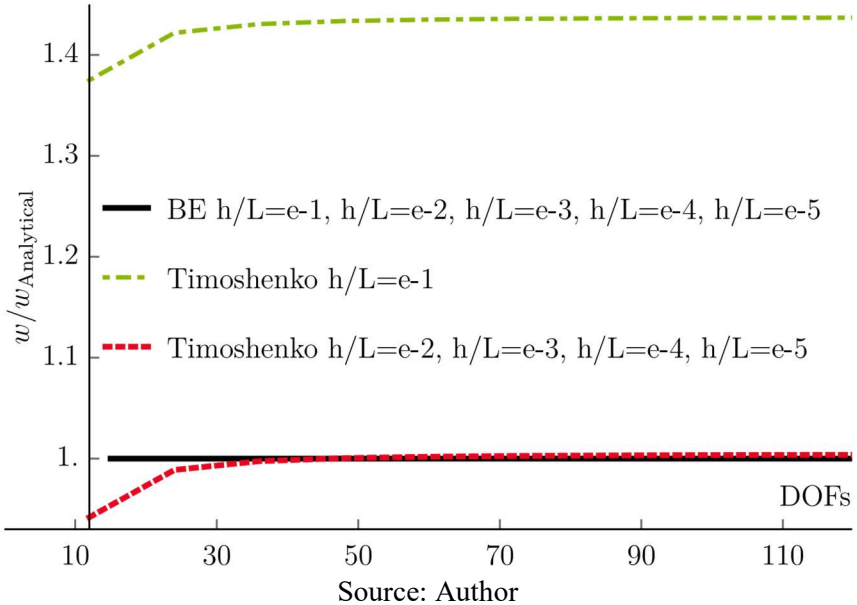

Source: Author

9.2. Convergence study for different interpolating polynomials (rods)

The structure presented in Figure 11 is a right-angle frame that has a force at one end and is clamped in the other end. Material and geometrical properties are also shown in Figure 11, this

example was chosen because it is a simple example where both bending and torsion play a significant role.

A variety of shape functions were presented and compared in Figure 12, Figure 13, Figure 14 the subtitles indicate the polynomial degree, for example, 3/1 is cubic polynomials for the displacements and linear polynomial for the torsion scalar.

Figure 11: Right angle frame.

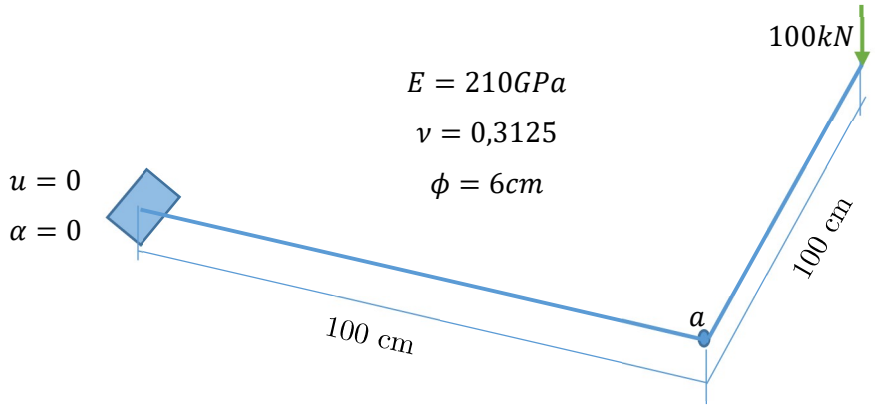

Source: Author

Analyzing Figure 12, clearly, any of the polynomials converge as for Figure 13 and Figure 14 one can see thar cubic/quadratic is the lowest polynomial that converges faster, but any of the polynomials gives satisfying results, and can be chosen as it is suitable. The response is grouped by the displacements interpolations and torsion gives small differences.

Figure 12: Displacements module.

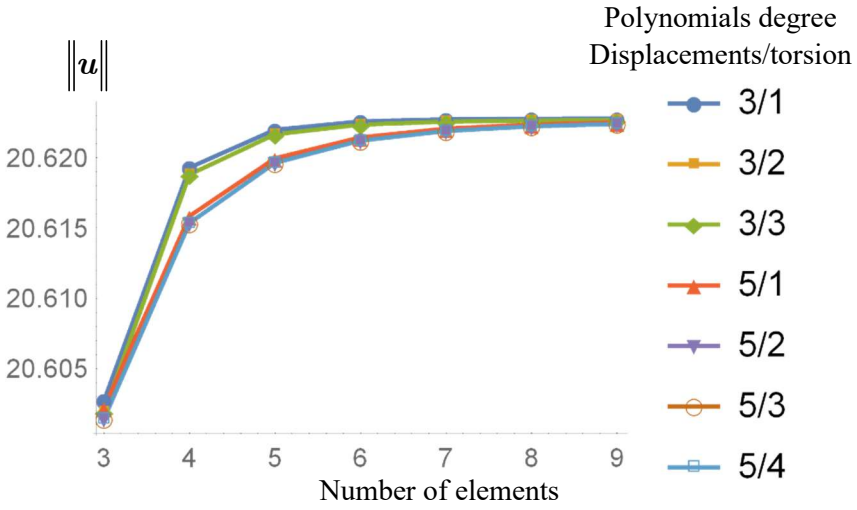

Source: Author

Figure 13: log x log - error for the displacements.

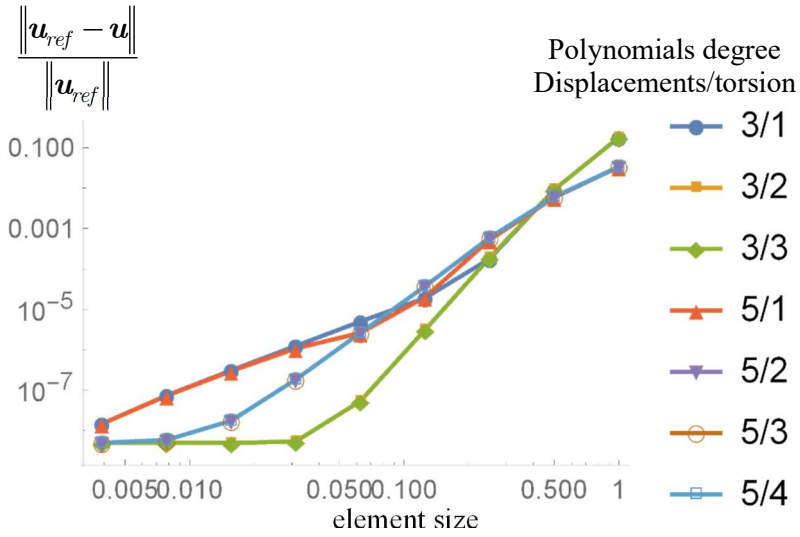

Source: Author

Figure 14: log x log - error for the rotation.

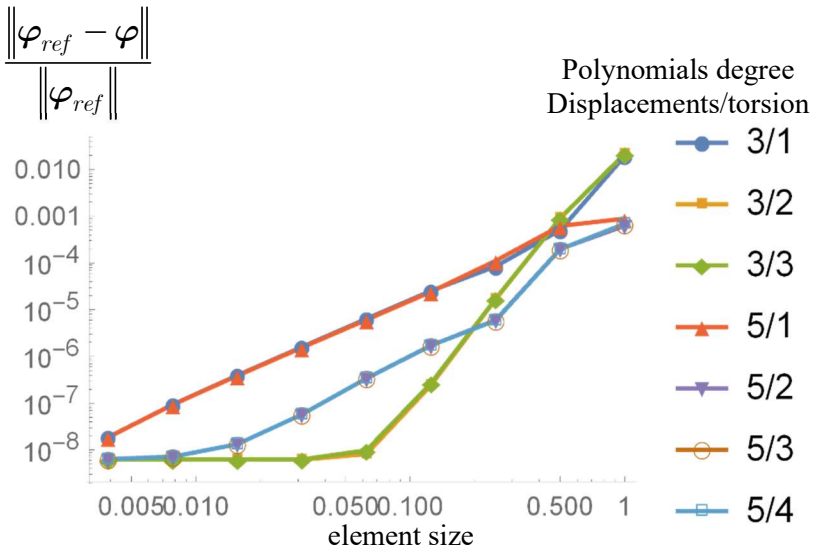

Source: Author

9.3. 2D Cantilever investigations

For general verification of the presented model, the computational problem of a cantilever exposed to two different load cases is considered. The problems are of two-dimensional nature, which is realized by restricting the displacements in the thickness direction, bending around the height direction as well as the torsional degree of freedom. Hence all deformation lies in the X-Y plane. A straight reference configuration and constant geometry and material is considered.

The fully clamped support is fulfilled by restricting the displacements and $\boldsymbol{\alpha}_\Delta$ at the left-end of the cantilever.

The first load case (a) is given by an external bending moment on the right-end of the cantilever Its length is L = 1 m clamped at L = 0. The material properties of the beam are EA = 5 kN, EI = 2 kN.m^2. The problem is known from the literature as, for example, investigated in Gruttmann, Sauer and Wagner (2000) [31], Simo and Vu-Quoc (1986) [60]. The pure bending of the beam results in a full circle for the considered material parameters. The cantilever was modelled with 16 finite elements after a convergence study with respect to the reference solution, but even with as little as 3 elements the result has a 0.3% difference from the reference solution. Some deformation states of the problem are shown in Figure 15, including the final state which is indeed the full circle. The shapes are annotated with the current state of the rotation vector $\boldsymbol{\alpha}_\Delta$ at the cantilever tip respectively.

The local beam base system undergoes large rotations within this problem. As discussed in section 2 the rotation vector inherits a singularity at a rotation of π, which is the reason for the introduced incremental rotation scheme. In this example a two-dimensional problem is given and thus only rotation around the z-axis is observed. Hence the rotation vector only contains one nonzero entry. In Figure 15, the mentioned singularities can easily be recognized at $m = 2\pi\ kN.m$ when $\theta = \pi$ because the total α is recovered, since an incremental formulation was used, there are no singularities during the calculations because the increment is always $< \pi$.

Figure 15: Deformed states at different load levels with local basis at the beam tip - case a.

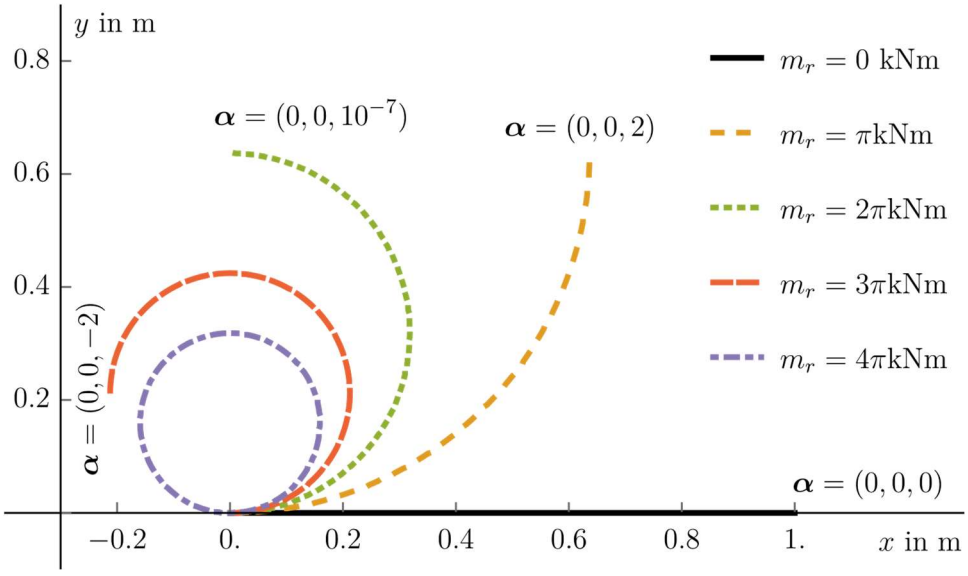

Source: Author

On the next load case (b), the cantilever is exposed to a follower load. The initially straight beam has a length L = 100 cm. Its material properties are EA = 4.20×10^5 kN, EI = 3.5×10^4 kN.cm^2. The follower end load takes successively the values F = 5, 20, 50, 70, 90, 110 and 130 kN. The problem was first investigated by Argyris and Symeonidis (1981) [2] while Simo and Vu-Quoc (1991) [57] covers the results as well. A comparison of Bernoulli-Euler versus Timoshenko beam models on this problem can be found in Boyer and Primault (2004) [9]. Throughout the simulation the nodal force stays perpendicular to the beam axis tangent at the right-hand side of the beam. The beam exhibits large displacements and rotation as it deforms. A convergence study was performed with respect to the vertical tip displacement at the final state. A reasonable number of 16 finite elements was determined to model the cantilever. Different deformation states of the problem are shown in Figure 16 while the load displacement curves are presented in Figure 17. The horizontal displacement is plotted in its negative form, as done in the reference, for a better comparison. For both presented two dimensional examples a good agreement with the results from the literature can be observed.

Figure 16: Deformed states at different load levels – follower load.

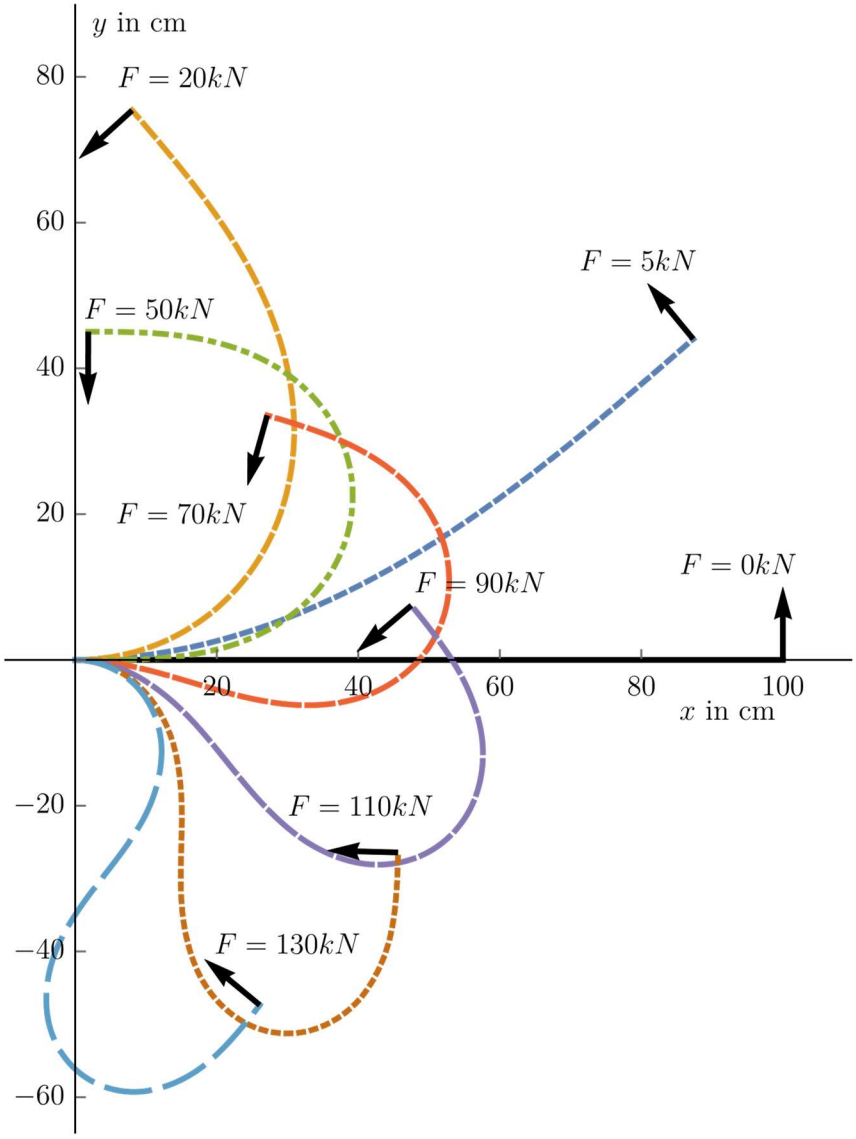

Source: Author

Figure 17: Load displacement curves at beam tip – case b.

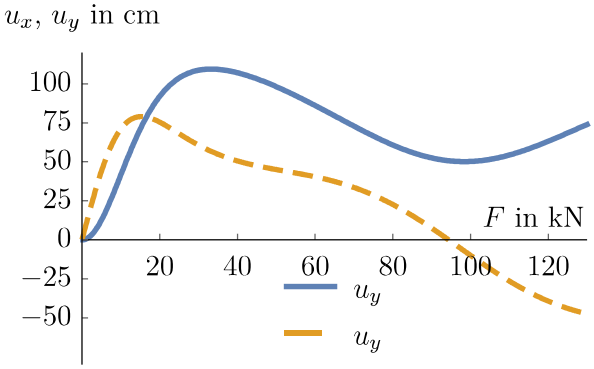

Source: Author

9.4. Lateral buckling analysis of a cantilever

The cantilever problem in Figure 18 is considered in the next numerical examples with cubic interpolations for the displacements and linear interpolation for rotation (the simplest interpolation scheme). This time the problem is no longer restricted to be two dimensional, which leads to a classical buckling problem. Determining the critical point appears to be a standard benchmark problem in this context and is thus considered in many publications as example Pimenta and Yojo (1993) [41], and Smolenski (1999) [61] and Campello and Lago (2014) [13]. The geometrical and material parameters within this paper were adapted from Pimenta and Yojo (1993) [41] shown in Figure 18. To enter the post buckling equilibrium path, a perturbation load is applied. In all the presented forms of this problem, the perturbation load is active during the whole simulation but with a rather small magnitude of 10^{-4} times the primal load. The lateral buckling (displacement in Z-direction) is shown in Figure 19. The critical load can be determined at approximately 2.2kN. Hence a good agreement with the literature can be observed. Figure 19 shows the problem considering the implementation varying the integration points over the rod domain and some deformation states in a 3D picture. For Bernoulli-Euler a 3, 4, 5, 6 Lobatto and 2, 3 ,4 ,5 ,6 ,7 ,8 ,9 ,10 Gauss integration points were implemented. For the shown Timoshenko solution, the formulation from Pimenta and Yojo (1993) [41], with linear interpolation of the degrees of freedom $\boldsymbol{u}$ and $\boldsymbol{\alpha}_{\Delta}$, was implemented and used as reference, only 1 Gauss integration point showed satisfying results, with 2 Gauss points there is locking and the structure does not buckle. With the Bernoulli-Euler solution presented here, the results are the same for any of these integration schemes.

Figure 18: 3D rectangular cantilever problem.

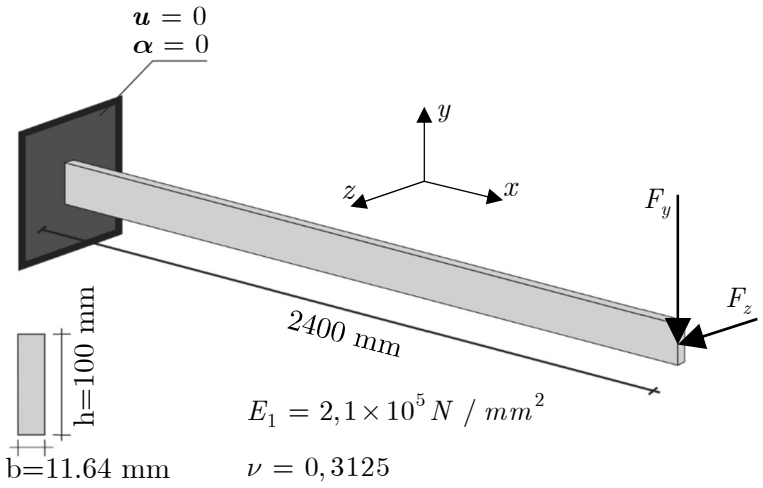

Source: Author

Figure 19: Lateral Buckling of a cantilever with multiple integration points and rectangular cross section.

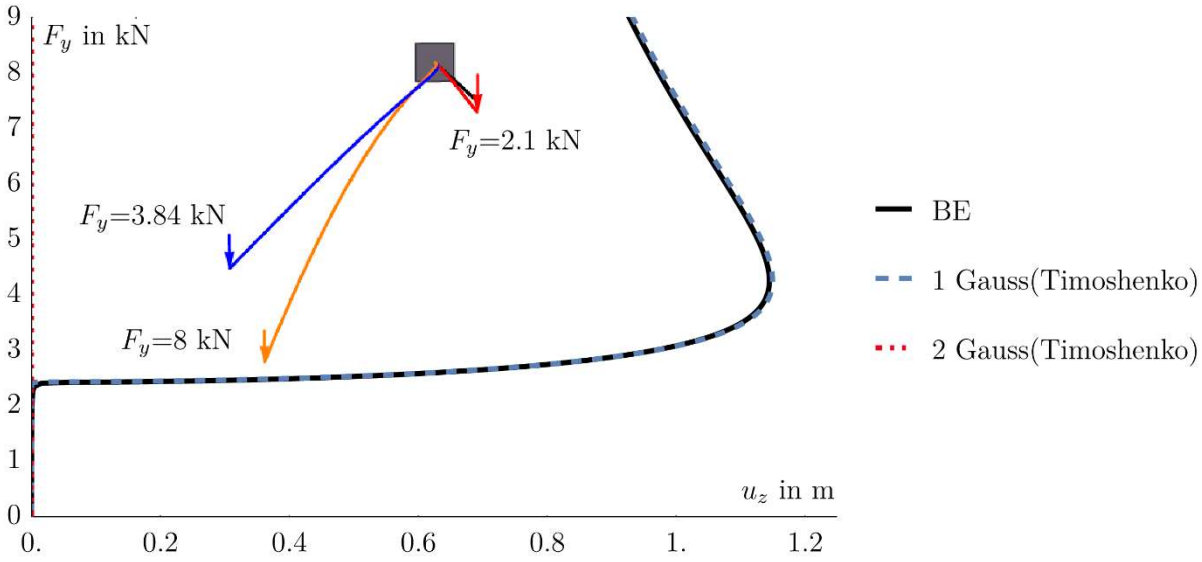

Source: Author

A convergence study with respect to the lateral displacement structure at the final state of the solution was done. As it can be seen in Figure 20, a reasonable discretization of the problem with 16 elements for the structural element was chosen, as it is converged.

Figure 20: Lateral Buckling of a Cantilever with different discretization elements.

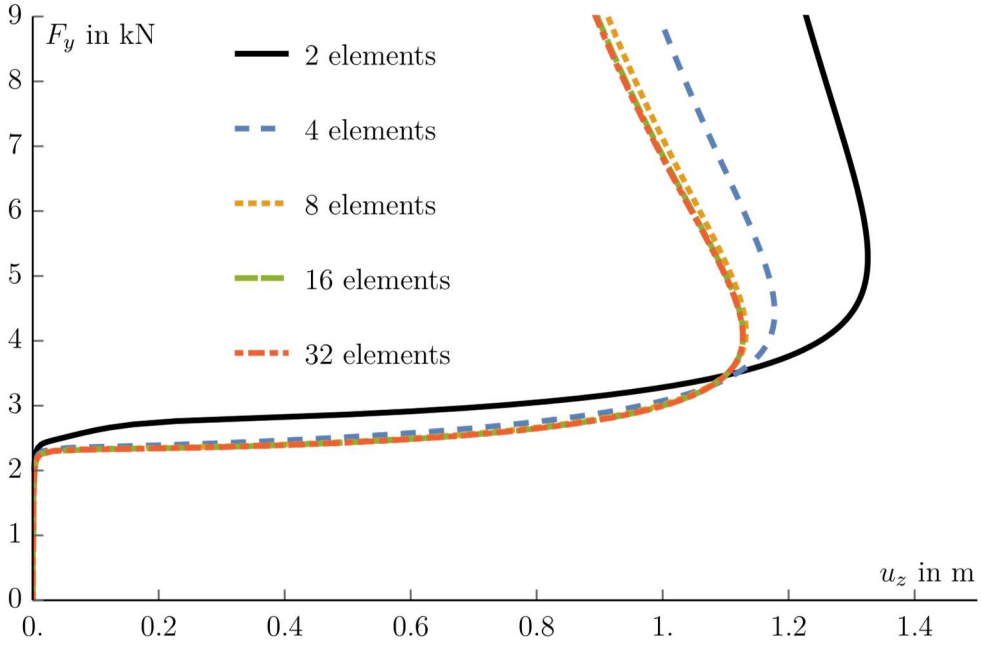

Source: Author

Two different elements were implemented, both geometrically exact, one with the Timoshenko hypothesis from Pimenta, Campello and Wriggers (2008) [45] and the other with the Bernoulli-Euler theory presented. To analyze the convergency the cantilever was divided in 2, 4, 8, 16, 32, 64, 128 and 256 elements so that the finer discretization contains the coarser ones. The smallest eigenvalue was analyzed, one can see that both theories give similar critical force, the difference between them is approximately 1%, which is not relevant because even with different perturbation loads there is already a ~1% difference. Figure 21 shows the critical force vs DOFs. Bernoulli`s theory with 3 elements (22 DOFs) has only a 1% difference from the converged force with 8 elements (57 DOFs), the Timoshenko`s theory with 4 elements (24 DOFs) has 6.5% difference from the converged force with 58 elements (348 DOFs), for a ~1% difference it needs 36 elements (216 DOFs). The BE model needs fewer degrees of freedom to converge.

Figure 21: Convergency behavior regarding the stability point for the rod element.

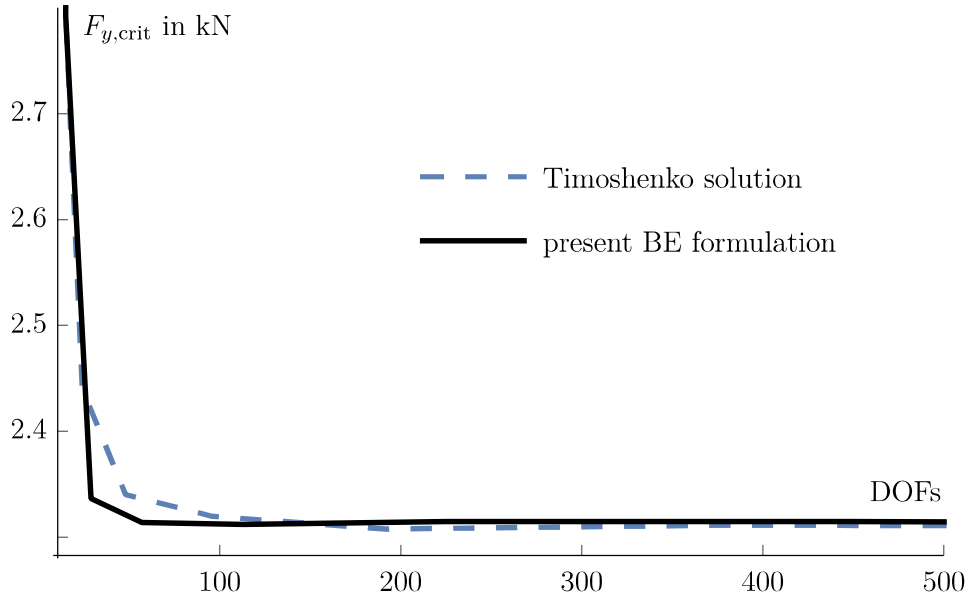

Source: Author

In Figure 19 one can see that the result with geometrically exact 3D Timoshenko beam elements is very similar to geometrically exact 3D Bernoulli beam elements.

The lateral buckling problem was also analyzed to compare 6 different cross sections shown in Figure 23, the first one is the rectangular one that was already introduced in Figure 18. The material properties for the other cross sections are the same and all of them have the same area. As in Pimenta and Yojo (1993) [41] the cross sections are represented by the letters, R, T, I, C, L and V. The load is applied at the shear center as this theory requires. The results are very similar to Pimenta and Yojo (1993) [41]. The T cross section presented the highest critical load as seen in Figure 23 and agrees with the literature.

Figure 22: Cross section geometries for the lateral buckling of a cantilever.

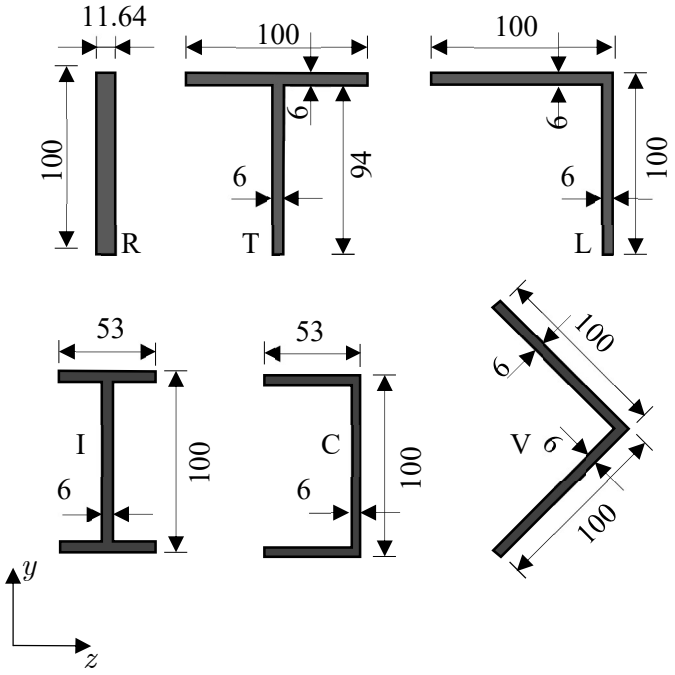

Source: Author

Figure 23: Lateral buckling comparison between different cross sections.

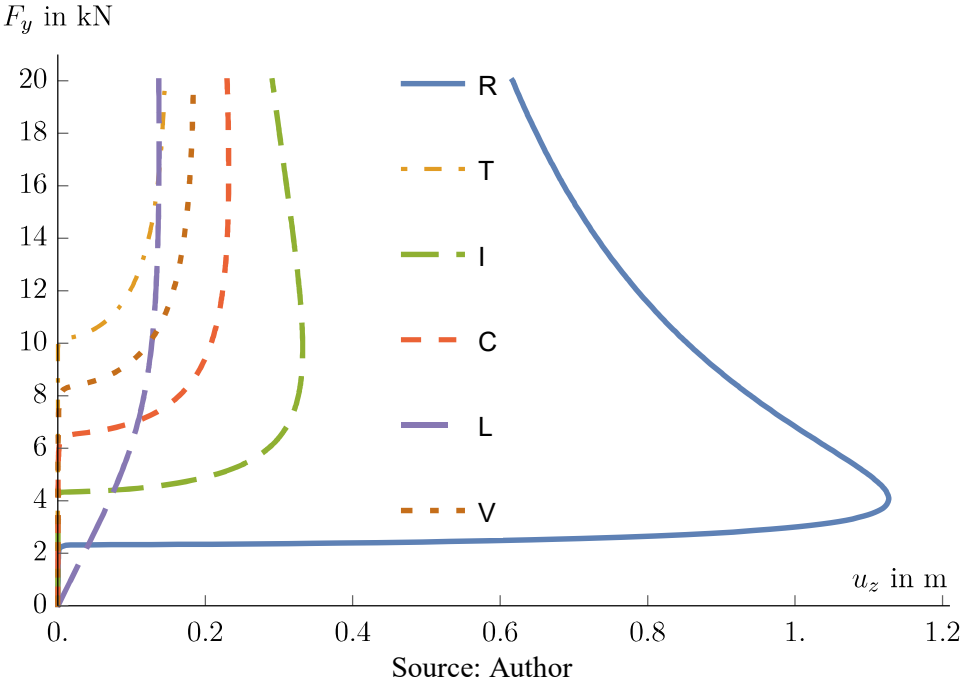

Source: Author

To compare the capabilities of the rod and shell theory, the cantilever problem in Figure 24 is considered. This example is the same as the I cross section from before, so it is also a classical buckling problem. This is example was considered in many publications as Campello and Lago (2014) [13], Pimenta and Yojo (1993) [41] and Smolenski (1999) [61]. The critical point is

determined and compared to the cantilever with the rod element developed in this work and the shell element from Viebahn, Pimenta and Schröder (2016) [65] using the Rodrigues rotation parameter for the continuity of the shell. The geometrical and material parameters within this paper were adapted from Pimenta and Yojo (1993) [41] and is shown in Figure 24. After a convergency study three kinds of discretization are considered for the problem:

case a - the cantilever is discretized with 10 rod elements;

case b – the cantilever is discretized with 2x2x40 shell elements in the web and 2x2x40 shell elements in each flange; and

case c – the cantilever is discretized with 2x2x40 shell elements in the web and 40 rod elements in each flange.

To enter the post buckling equilibrium path, a perturbation load is applied in case a and case c. Case b is not symmetric because of the mesh and doesn't need a perturbation load to enter the post buckling equilibrium path. The perturbation load, in the cases that it is needed, is active during the whole simulation but with a rather small magnitude of 10^{-4} times the original load. The lateral buckling (displacement in Z-direction) is shown in Figure 26. The critical load can be determined at approximately 4.35kN.

A good agreement with the literature can be observed. The cantilever with shell element in the web and rod element in the flange also has good results as the critical load is almost the same as the others. It and can be perceived in Figure 26 the agreement between cases, the small difference for the load can be explained because of the boundary applied to the rod and shell. The essential boundary for the rod is enforced at the axis constraining all the motion possible, as for the shell it is not possible to constrain only at the axis and it makes the results differ. For case b and c the essential boundary conditions are shown in Figure 25. The results also differ after the buckling load because of cross section deformations, the rod element has the constrain that the cross section stays undeformed after motion, which doesn't happen to the shells. Another explanation for the differences can be observed because of the constitutive equations used, since for rod/shell the constitutive equations are distinct, distinct behaviors for large strain regimes may be expected. To show the effect of the different boundary conditions one more curve is added to Figure 26, that is of a cantilever rod with only shell elements and all displacements restricted at L=0 no warping is considered, it is a subject of future works.

Figure 24: Cantilever with I cross section.

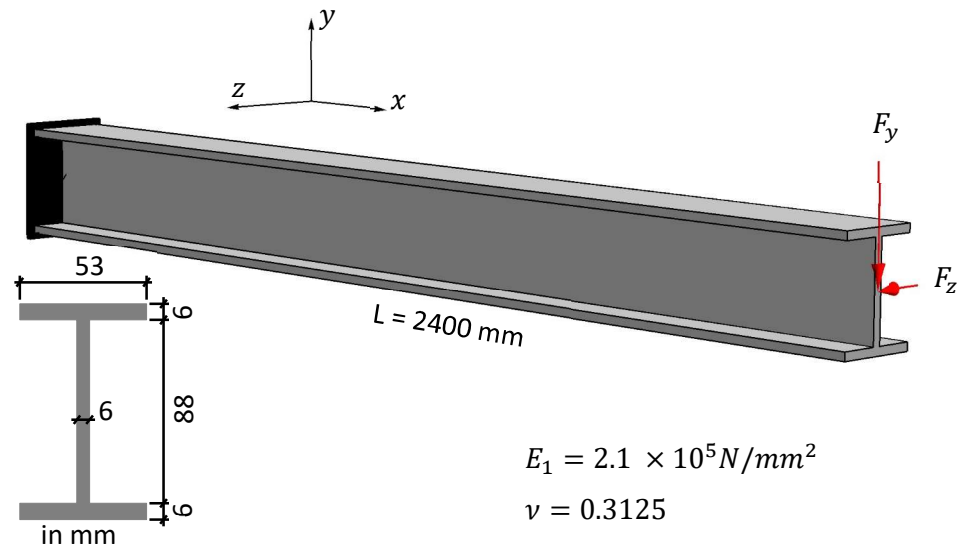

Source: Author

Figure 25: Boundary value problem for the cantilever with I cross section with shell elements in the web.

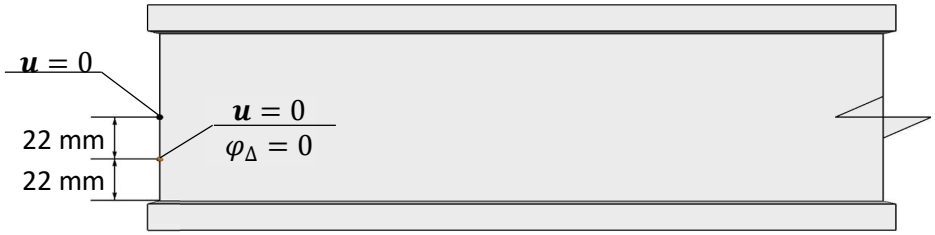

Source: Author

Figure 26: Lateral displacement of the cantilever buckling problem.

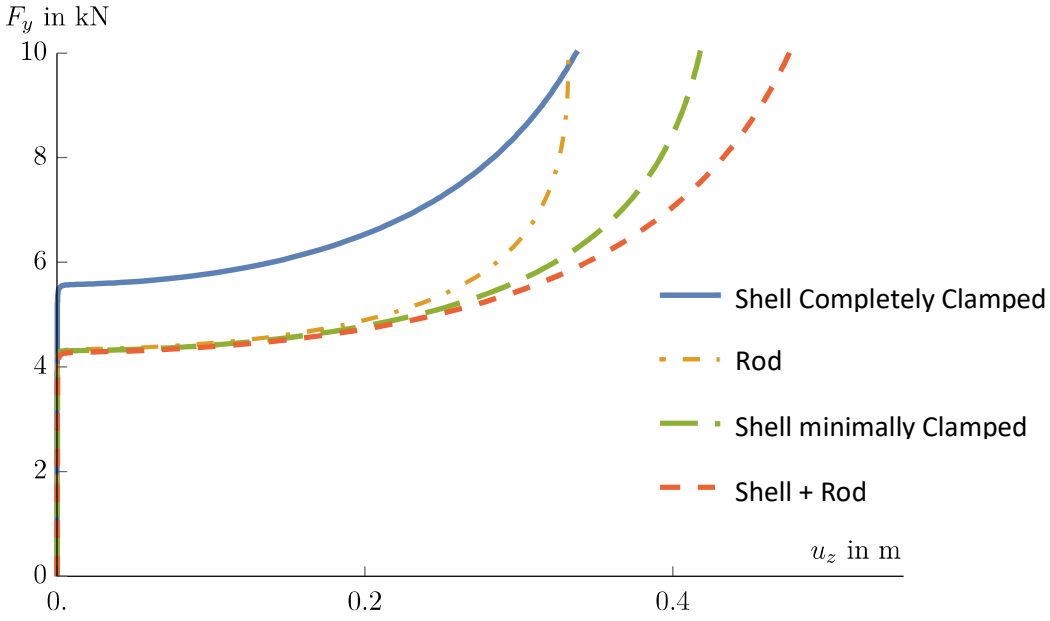

Source: Author

9.5. Lateral buckling analysis an L shaped frame

Investigation of another geometrically discontinuous configuration is the subject to the next example. The cantilever considered before is now extended by a vertical beam at its tip. The resulting structure is known as L-shaped frame and was considered also in Pimenta and Yojo (1993) [41] as well as in Simo and Vu-Quoc (1986) [60]. A loading on the lower structure of the frame is applied such that a buckling problem is constructed again. The material parameters and geometry were adopted from the first mentioned literature and is recovered in Figure 27. A perturbation load in lateral direction is used to drive into the buckling path of the problem again. The connection of the vertical and the horizontal structure represents a non-smooth geometrical discontinuity in the reference configuration of the problem. A convergence study with respect to the lateral displacement at the tip of the vertical structure at the final state of the solution was done and a reasonable discretization of the problem with ten elements for each structural element was chosen. The obtained load displacement curves are given in Figure 28 with an illustration of some deformed configurations. It is first notable that the strategy leads to reasonable results and is able to determine the critical load that is reported form the literature at approximately 0.75 kN.

Figure 27: L-shaped frame buckling problem.

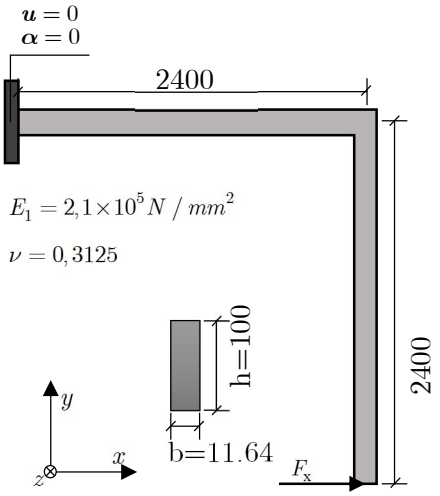

Source: Author

Table 1 shows the quadratic convergency towards equilibrium within the Newton-Raphson scheme for Fx = 3.5 kN. The norm of the increments of the degrees of freedoms (Δd) where

used as sort criteria within the numerical investigation, while the norm of the global residual (R) is given here for completeness.

Figure 28: Lateral buckling and deformed shapes of a L-shaped frame.

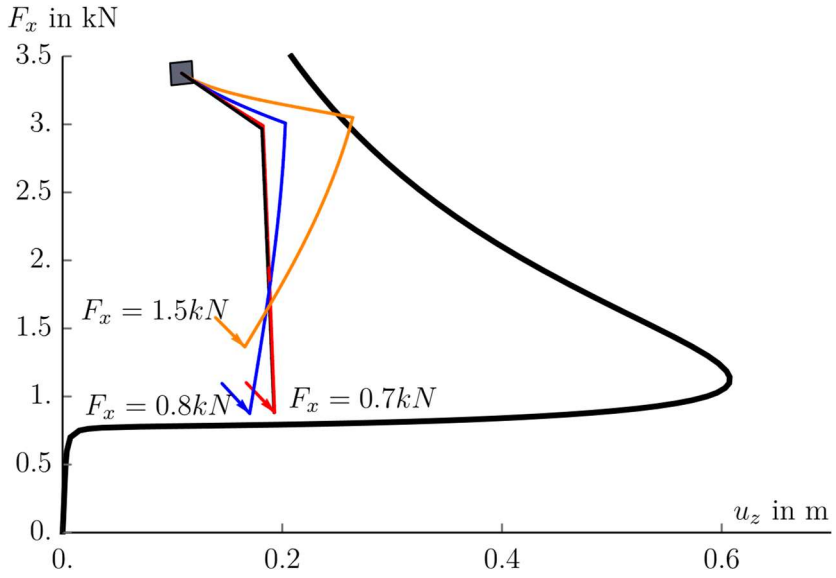

Source: Author

Table 1: Convergence of the Newton-Raphson procedure towards equilibrium at load level 3.5 kN.

iteration	$\|\Delta d\|$	$\|R\|$
2	301.236	285.601
3	48.8237	3.11517
4	0.227885	0.0801331
5	0.0000675315	4.8235×10^{-6}
6	2.55856×10^{-9}	5.34248×10^{-6}

Source: Author

Like shown in the I the cantilever example, the problem is now defined to an I cross section, showing in Figure 29. The discretization of the elements are:

- case a – 40 rod elements, in each part of the L;
- case b – the cantilever is discretized with shell elements in the web and flange seen in Figure 30;

- case c – the cantilever is discretized with shell elements in the web and rod elements in each flange shown in Figure 31.

A perturbation load in lateral direction is also used to drive the frame into the buckling path of the problem. The connection between the vertical and the horizontal structure represents a non-smooth geometrical discontinuity in the reference configuration of the problem. The obtained load displacement curves are given in Figure 32. It is first notable that the strategy leads to reasonable results and is able to determine the critical load that is reported from the literature at approximately 1.77 kN. Just as for the cantilever there are some differences for the results due to the different conditions that each kind of element represent, the boundary conditions were chosen to get the closest result to the cantilever with rod elements, the boundary conditions for the case only with shells and the mesh is shown in Figure 30, as for the case with shell and rod combined it is shown in Figure 31.

Figure 29: L-shaped frame buckling problem.

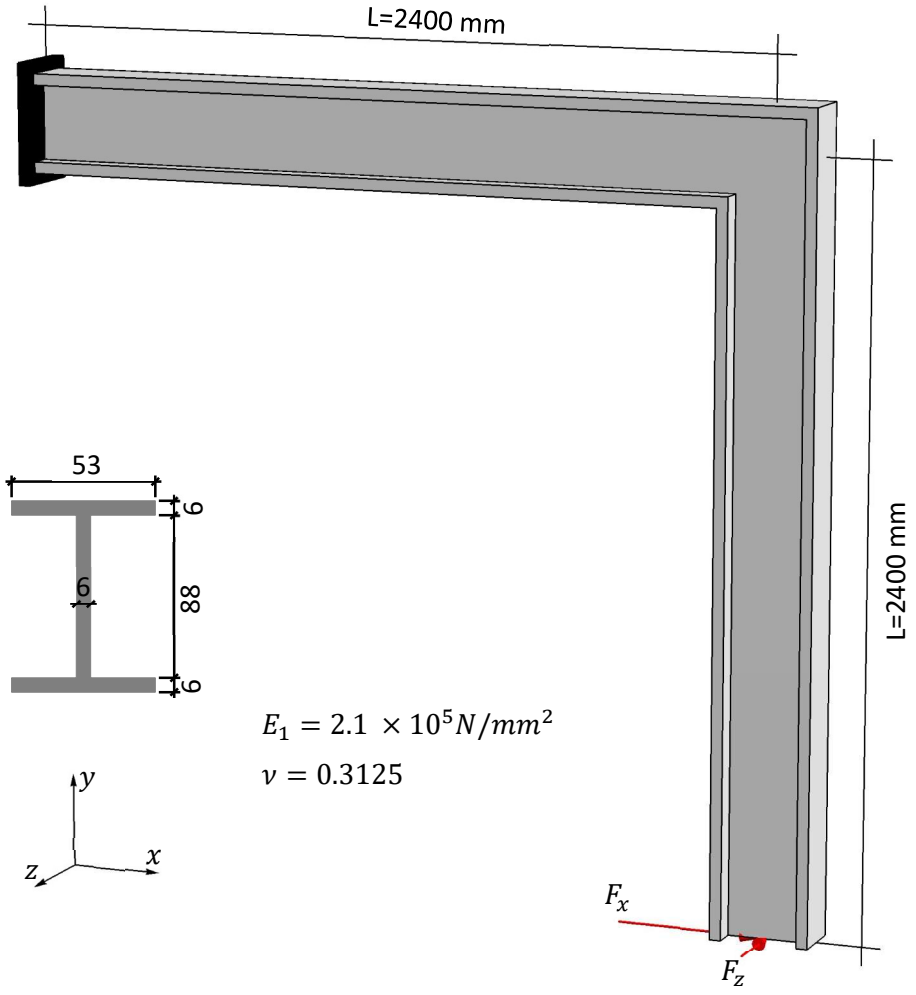

Source: Author

Figure 30: Boundary conditions and mesh for only shell case.

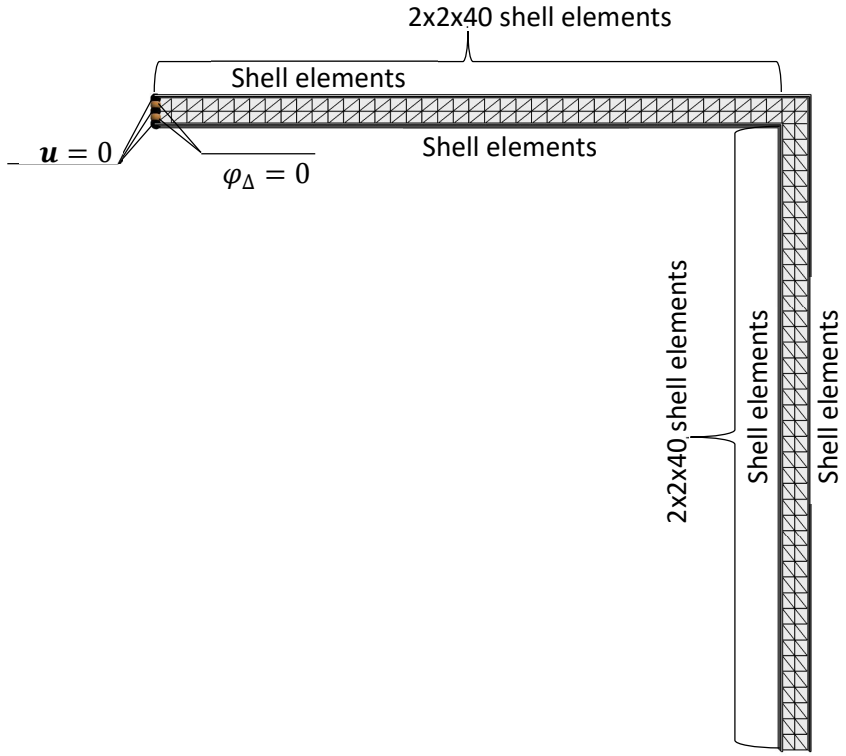

Source: Author

Figure 31: Boundary conditions and mesh for rod + shell case.

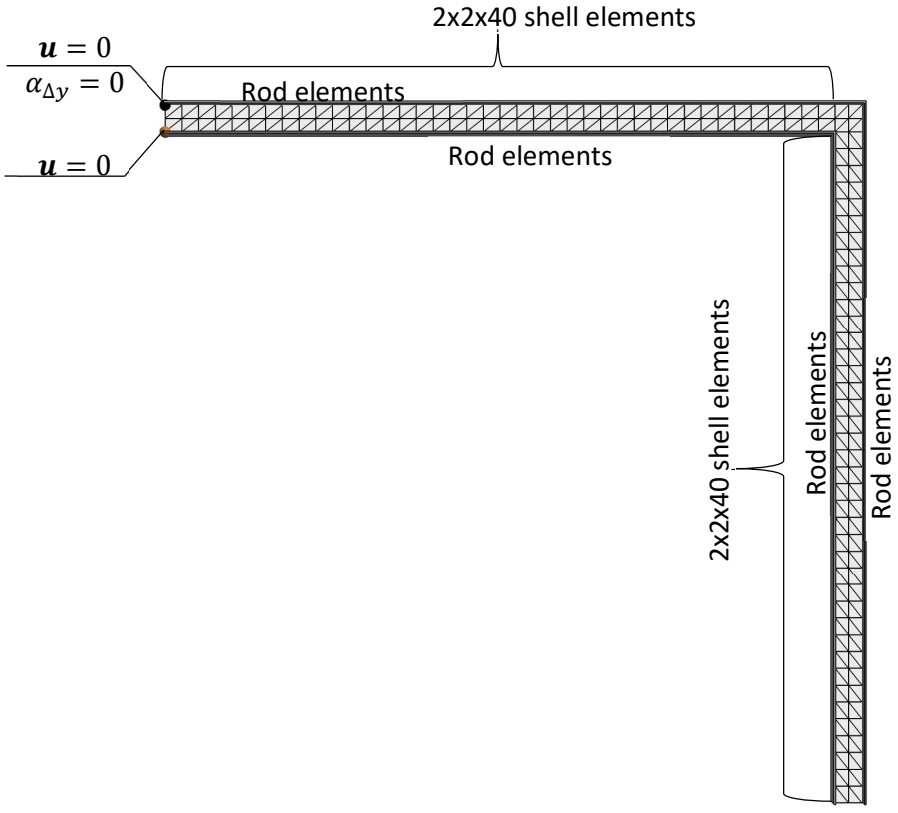

Source: Author

Figure 32: Lateral displacement of the buckling of an L-shaped frame problem.

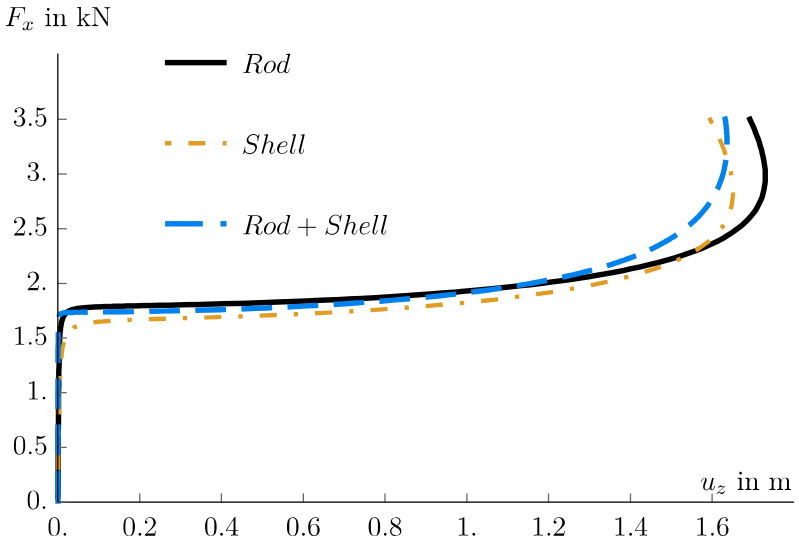

Source: Author

9.6. Snap-through behavior of a clamped/hinged arc

In the next example a non-straight geometry is considered. The arc of the example is approximated by straight finite elements, so it is a curve formed by straight line segments. The presented arc's geometrical and elastic properties are displayed in Figure 33. A full support is given on the right-hand side of it, while on the left-hand side only the displacements are restricted. The problem's displacements are restricted to be two dimensional. The arc is loaded on the top with a single load. The finite element mesh is of such kind that a node is always located on the top center of it. Hence the load is introduced by a classical nodal force. A convergence study with respect to the final displacements of the problem was performed an indicated a reasonable discretization with 20 finite elements, which was chosen for the following investigations.

Figure 33: Clamped/Hinged arc problem.

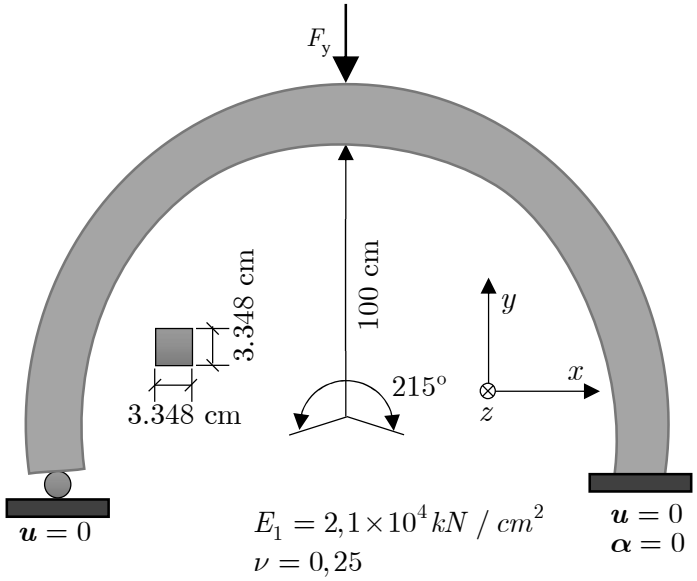

Source: Author

The problem was investigated several times in the literature. It shows a snap through behavior as at a certain point the system loses its stiffness. An arc-length method is used in this case to follow the equilibrium path. In case of this paper the arc-length method implemented in AceFEM was used, as in Stanić, Brank and Korelc (2016) [63]. The results are presented in Figure 34 and some typical states of the deformation are shown in Figure 35. The solution is able to cover the snap through behavior reported from the literature.

Figure 34: Clamped/Hinged arc problem, load displacement curve.

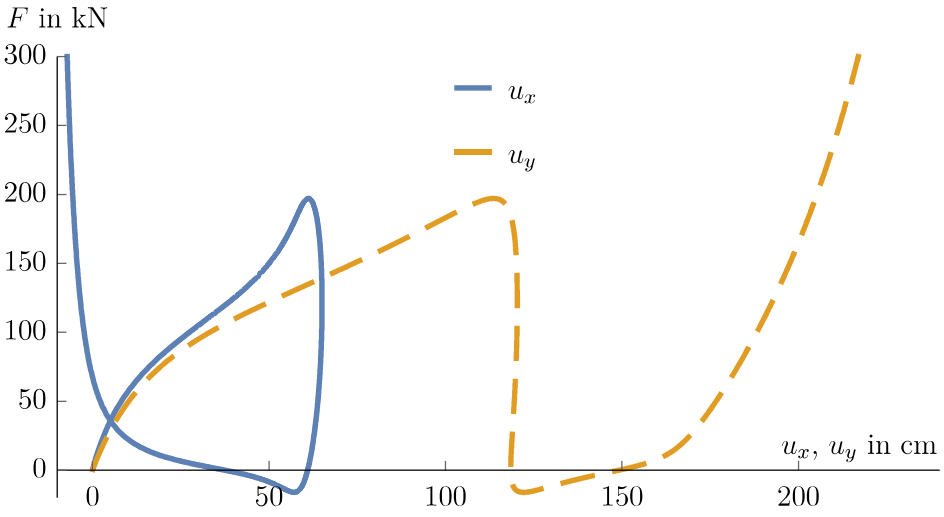

Source: Author

Figure 35: Clamped/Hinged arc problem, deformed states.

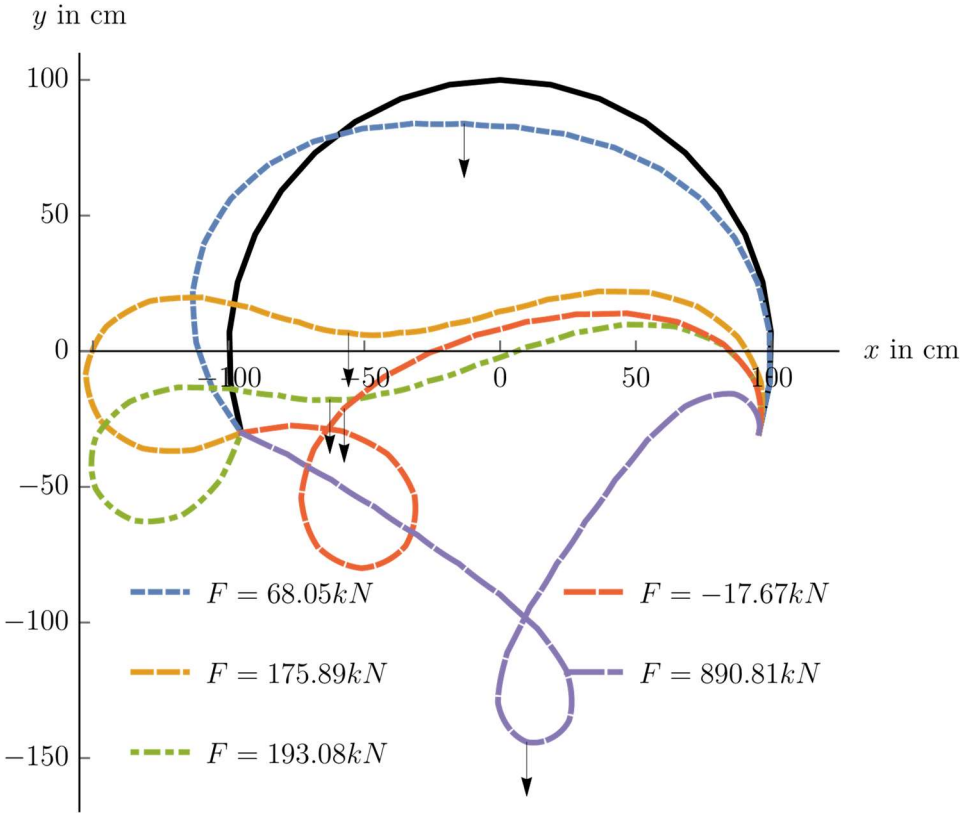

Source: Author

9.7. Deployment of an elastic ring

This numerical example represents a rather complex problem, computed to show the full capabilities of the theory at hand. It is completely three dimensional and presents large deformations and rotations. Therefore, it was investigated before as a benchmark for beam and rod models as, for example, in Romero 2004 [51] and Yoshiaki et al. (1992) [24]. A ring of elastic material is twisted by a moment and supported in a way such that is ends up with a full circle of one third the size of the initial one. A detailed visualization of the boundary value problem is given in Figure 36. The ring also shows snap through behavior and hence again the AceFEM arc-length procedure is applied in the simulation. To handle the non-straight reference configuration of the considered ring the same approach from the clamped/hinged arc was used. Some key states during the simulation are visualized in Figure 37.

It can be concluded that the final state of a full circle can be recovered. The displacement curves for point B and the rotation of the loaded point C is visualized in Figure 38 for comparison with

the results reported by the literature. The results show good comparison with those from the literature.

Figure 36: Elastic ring boundary value problem.

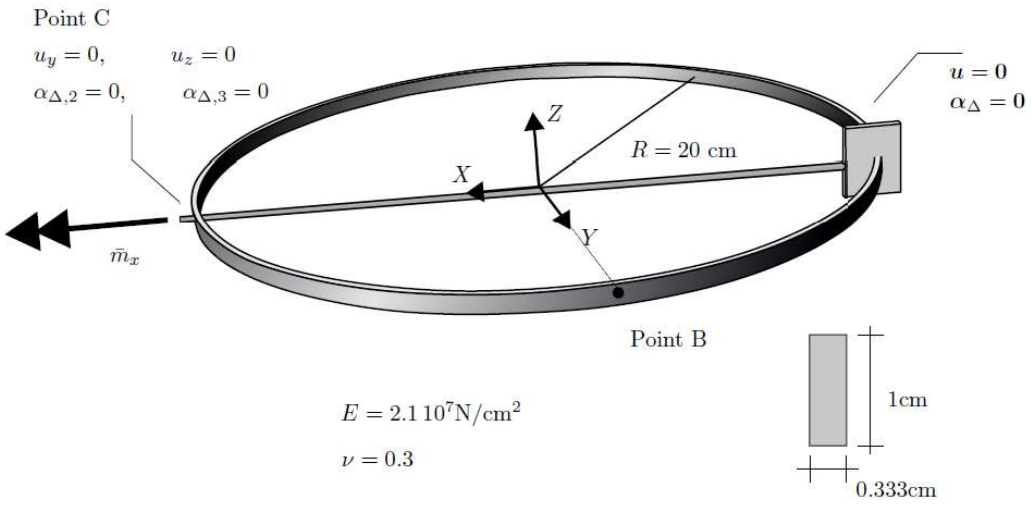

Source: Author

Figure 37: ring shapes.

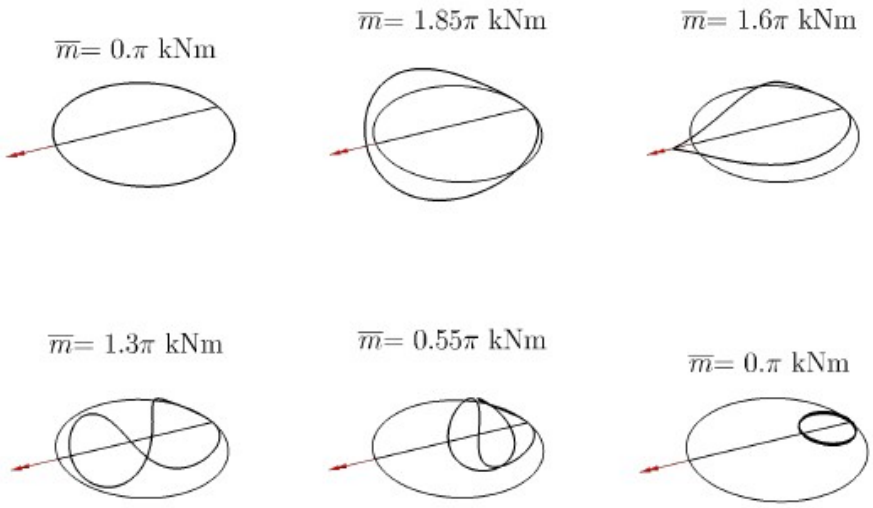

Source: Author

Figure 38: displacements and rotation curves.

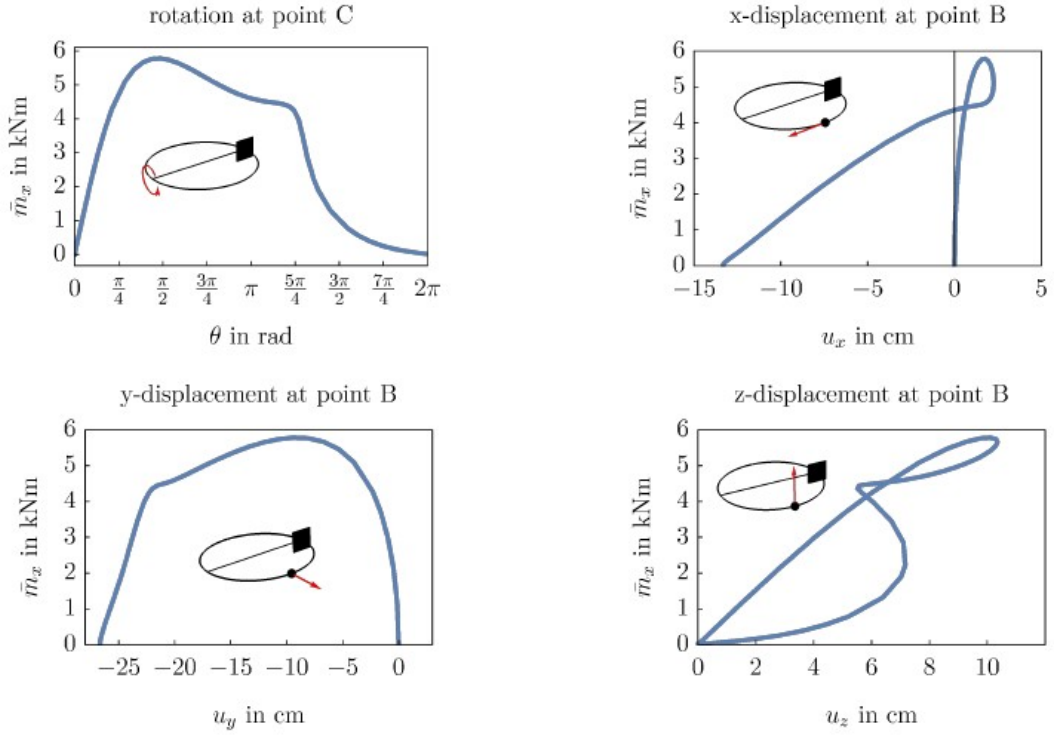

Source: Author

9.8. Buckling of a coil spring under compression load

One more application of the theory is shown in this example. A helicoidal spring is set under compression and after a critical load is reached the spring buckles. Coil springs are made up of a wire coiled in the form of a helix. On such springs the wire is subjected only to torsion. The major stresses are shear stresses due to twisting. The load applied is parallel to the axis of the spring. In Figure 39 one can see the scheme of the spring considered. The pitch angle is $\arctan\left[\frac{p}{\pi D}\right] = 17.657$ where D = 100 mm is the mean diameter of the cylinder and p = 48 mm is the pitch at free length. The spring wire diameter is 25 mm, and its free length (height) is 720 mm. The Young's modulus and Poisson's ratio are E = 210 GPa and $\nu = 0.3$, respectively. The number of turns on the coil is 15.

Figure 39: Coil parameters

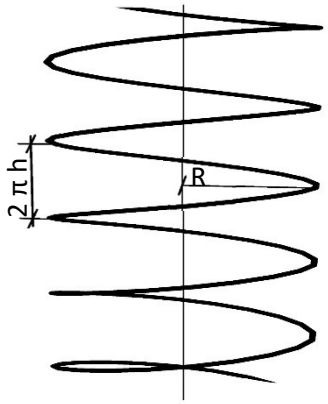

Source: Author

The only degree of freedom on the point of the application of the force that is free is the displacement in the direction of the applied force. At the opposite side of the force, the spring is clamped. Figure 41 shows the deformed state of the spring after it buckles. And Figure 40 shows the load displacement curve and the critical force can be observed.

Figure 40: Coil's displacement curves.

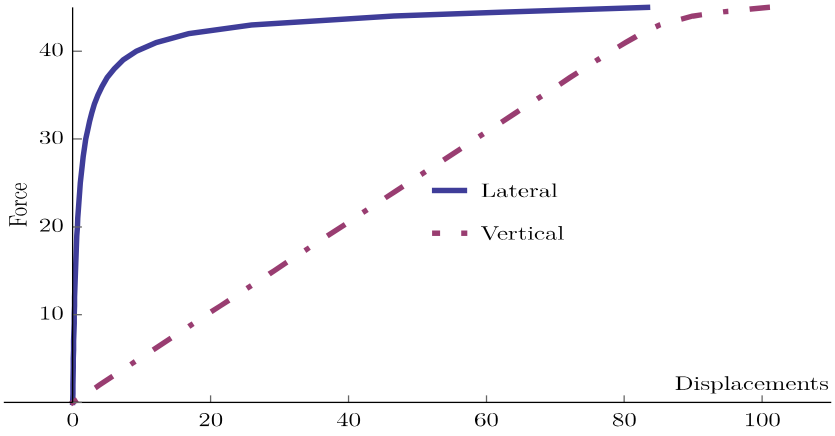

Source: Author

Figure 41: Coil's deformed state.

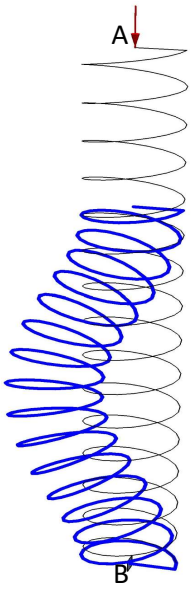

Source: Author

9.9. Pinched Cylinder

This example is shown to demonstrate that the connection between shells can be accomplished by using φ_Δ instead of the angle between normal vectors of neighboring elements β. A Lagrange multiplier approaches was implemented. This is a benchmark problem that can be seen in Campello Pimenta and Wriggers (2003) [11] and in Pimenta, Campello and Wriggers (2004) [47] for shear deformable theory. It is also shown in Ivannikov, Tiago and Pimenta (2015) [33] and Viebahn, Pimenta and Schröder (2016) [65] for the shear rigid theory. Figure 42 shows the boundary value problem which is similar to a finger-pinched beer can. The cylinder was modelled with shell elements with rigid end-diaphragms in its ends, which under large loads shows extremely nonlinear behavior. The isotropic cylindrical shell has the geometrical properties presented in Figure 42, while the material parameters are: Young's modulus $E = 3 \times 10^4\, N/mm^2$ and Poisson ratio $\nu = 0.3$. The final load applied is $F = 5.4 \times 10^4 N$. The displacements curves are shown in Figure 43, only one curve is shown because all the implementations leaded to the same results. The deformed configuration in true scale at the maximum load is depicted in Figure 44. It can be assured by the final deformation state that the element with both connection schemes behaves very well with large deformations and curvatures.

Figure 42: Pinched Cylinder – Boundary value problem.

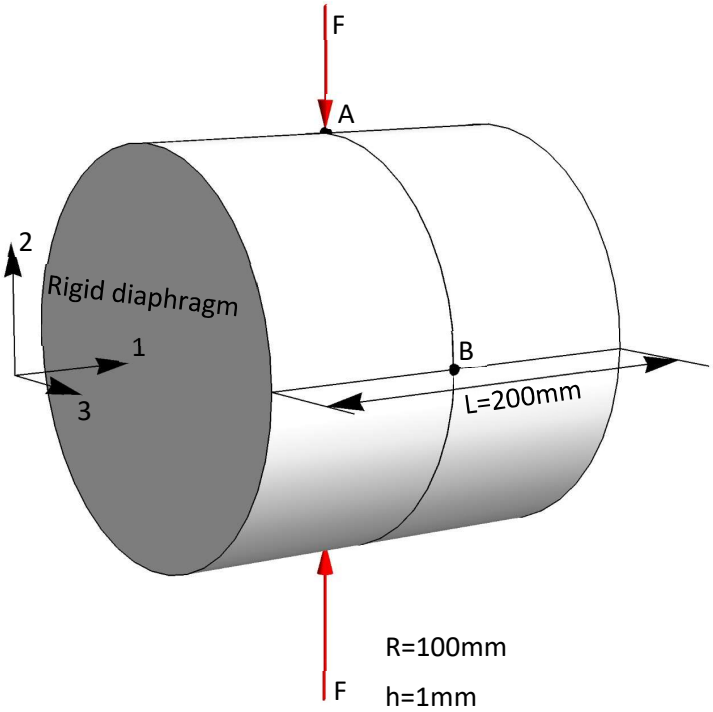

Source: Author

Figure 43: Pinched Cylinder – Analysis results.

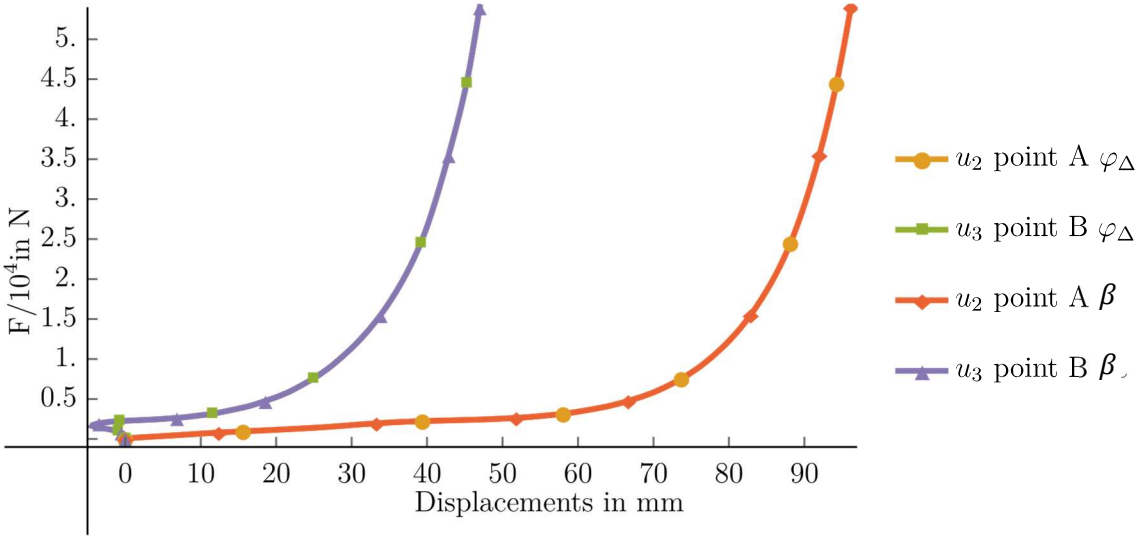

Source: Author

Figure 44: Pinched Cylinder – Deformed State at final load. (unscaled)

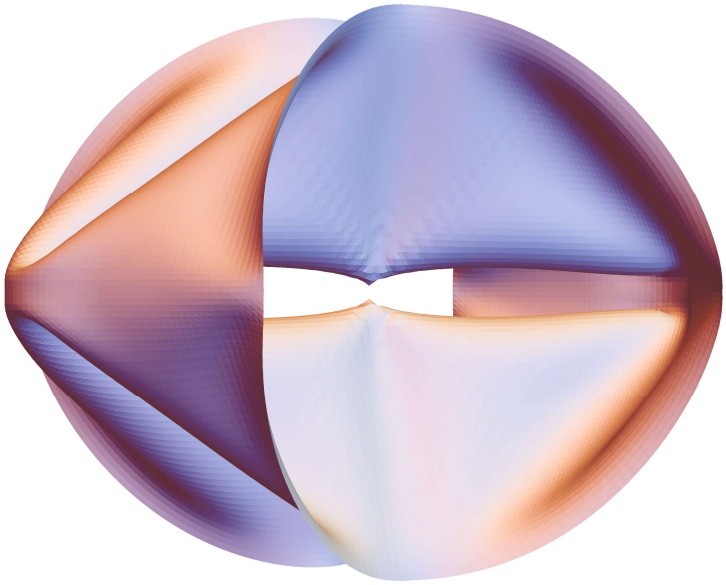

Source: Author

9.10. Simply supported square plate with diagonal stiffeners.

A simple supported square plate with diagonal stiffeners, with beam and shell elements for the stiffeners, is analyzed. In Viebahn, Pimenta and Schröder (2016) [65] this example was performed only with shells, now the results of the rod elements as stiffeners are compared to the shell elements.

The deflection of the square plates, which are loaded by a uniform distributed pressure p, are compared for three different stiffening conditions, the geometrical properties are shown in Figure 45 and Figure 46. The material parameters are E = 117.25 GPa for the Young's modulus, $\nu = 0.3$ for the Poisson's ratio. The plate is meshed by $8 \times 8 \times 2$ elements, whereas the flange is discretized by 2, respectively. One element over the thickness for the eccentric and concentric stiffening. In order to demonstrate the stiffening effects, the out of plane displacements in the center of the plate are compared in Figure 48. The obtained results are in very close agreement compared to the results from Viebahn, Pimenta and Schröder (2016) [65].

Figure 45: Reference configuration for the plates.

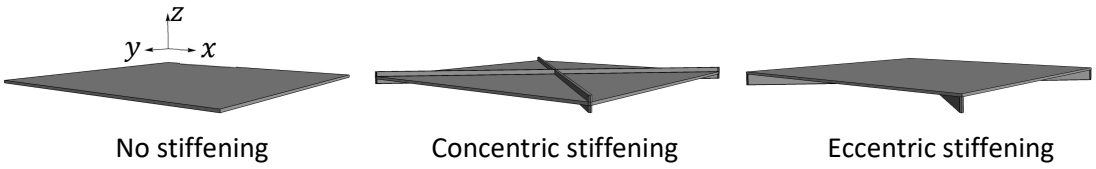

Source: Author

Figure 46: Square plate with diagonal stiffeners (in mm).

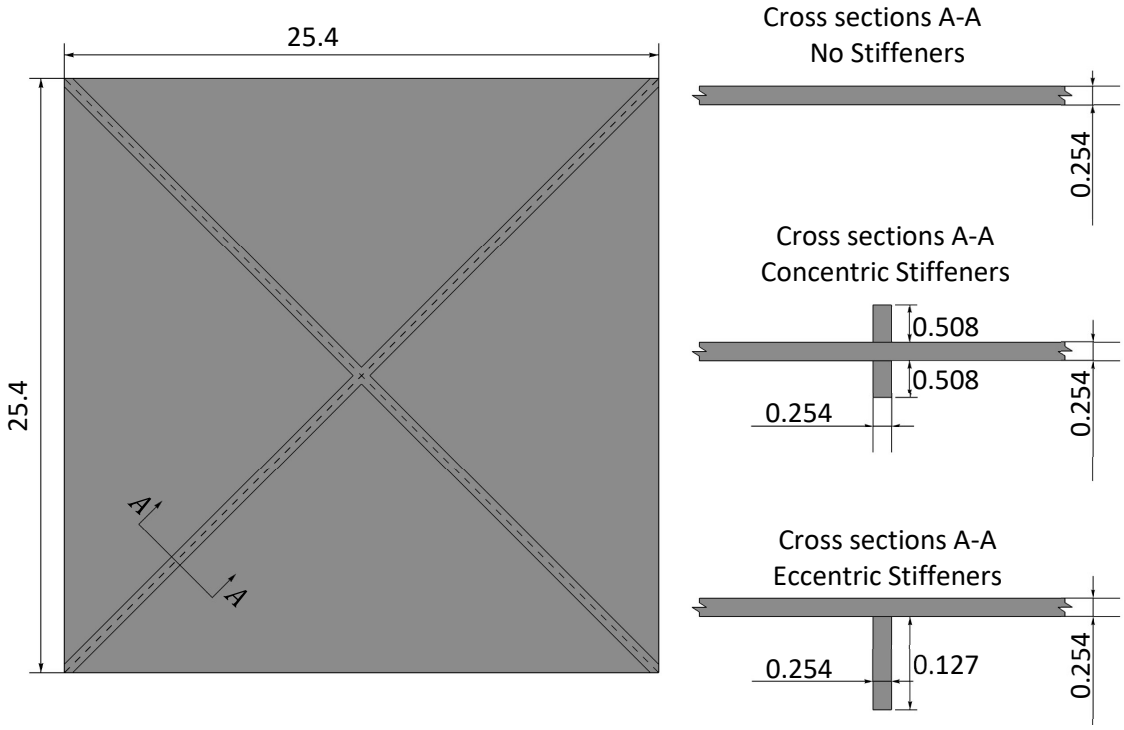

Source: Author

Figure 47: Eccentric Stiffened Plate deformed configuration scaled (by factor 10).

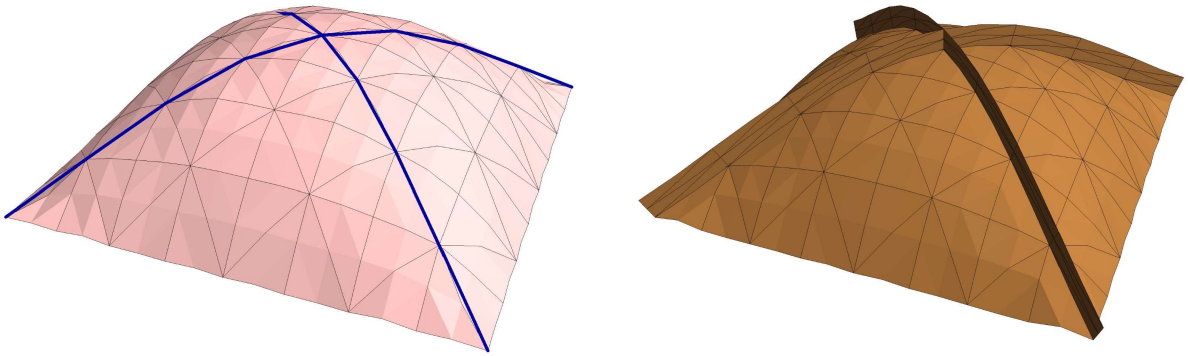

Source: Author

Figure 48 : Load–displacement plot for different stiffeners.

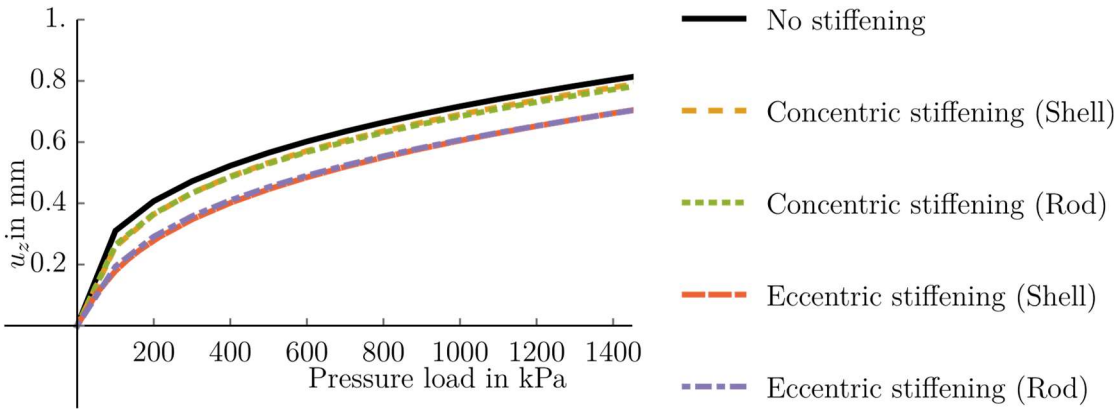

Source: Author

Conclusions

Shear rigid geometrically-exact rod and shell theories were presented. Within the theory new formulas to represent the Rodrigues vector were developed. These formulas made it possible to originate simple finite elements for shells and rods. New interpolation polynomials were also applied and compared for the rod theory. Since all the polynomials show similar response, one can select the best for each case. An important example is the connections with compatible elements. As in Pimenta and Yojo (1993) [41] , our approach has defined energetically conjugated generalized cross section stress and strains based on the concept of a cross section. Besides their practical importance, cross section quantities make the derivation of equilibrium equations easy, as well as the achievement of the corresponding tangent bilinear form, which is always symmetric for hyper-elastic materials and conservative loadings, even far from an equilibrium state. A straight/flat reference configuration was assumed for the rod/shell. Some examples were computed to show the capabilities of the formulation presented. As exposed throughout this work some benchmark problems were compared and presented satisfying results.

The cantilever investigations are simple and make it easy to show some basic capabilities of the formulation for problems undergoing large rotations or deformations. Different load cases for the cantilever are explored, first there is pure bending and the cantilever reaches a final state at full circle, and the follower load that also shows large displacements and rotations as it deforms. Some stability problems are presented as well, first the lateral buckling of a cantilever. It is also shown that cross section with different shapes can be applied to the formulation and the connection between shell and rods can be accomplished. Then there is a L-shaped frame that has change of the directions of the axis, this example shows some capabilities of the rod and shell theories, as well as their connection. For the shells one can see by the example of the pinched cylinder that the theory has no problem with large displacements and rotation and its continuity can be performed by the continuity of the rotation scalar originated by the Rodrigues vector. The connection between rod and shell elements is also verified by the simply supported plate with diagonal stiffeners. All examples demonstrate similar results when compared to the literature cited in this work

This work is relevant to structural analysis because there are many practical cases that need rods, shells and shells coupled with rods. These rod and shell theories can be used for very flexible structures, like thin shells and slender rods.

Appendix A – Tensor Properties

For $\boldsymbol{\kappa} = \text{axial}(\boldsymbol{K})$ and $\boldsymbol{m}$ a vertor, the following property is valid

$$\boldsymbol{Km} = \boldsymbol{\kappa} \times \boldsymbol{m} \tag{236}$$

If **B** and **C** are skew-symmetric tensors with their b and c axial vectors, respectively then,

$$\boldsymbol{BC} = \boldsymbol{c} \otimes \boldsymbol{b} - (\boldsymbol{b} \cdot \boldsymbol{c})\boldsymbol{I} \tag{237}$$

Considering **A** to be a skew-symmetric tensor the following applies,

$$\begin{aligned} \boldsymbol{A}^3 &= -\alpha^2 \boldsymbol{A} \\ \boldsymbol{A}^4 &= -\alpha^2 \boldsymbol{A}^2 \end{aligned} \tag{238}$$

Let **A**, **B** and **C** be skew-symmetric tensors and a, b and c their respective axial vectors. Then it is possible to write,

$$\boldsymbol{C} = \boldsymbol{AB} - \boldsymbol{BA} \Leftrightarrow \boldsymbol{c} = \boldsymbol{a} \times \boldsymbol{b} \tag{239}$$

The cross product of the vector $\boldsymbol{a}$ and the vector $\boldsymbol{b}$ with θ denoting the angle between them is not commutative and has the following properties

$$\|\boldsymbol{a} \times \boldsymbol{b}\| = \|\boldsymbol{a}\|\|\boldsymbol{b}\| \sin\theta \tag{240}$$

$$\boldsymbol{a} \times \boldsymbol{b} = -\boldsymbol{b} \times \boldsymbol{a} \tag{241}$$

Let ν be a scalar, then

$$(\nu \boldsymbol{a}) \times \boldsymbol{b} = \boldsymbol{a} \times (\nu \boldsymbol{b}) = \nu(\boldsymbol{a} \times \boldsymbol{b}) \tag{242}$$

Let c be another vector, where

$$\boldsymbol{c} \cdot (\boldsymbol{a} \times \boldsymbol{b}) = \boldsymbol{a} \cdot (\boldsymbol{b} \times \boldsymbol{c}) = \boldsymbol{b} \cdot (\boldsymbol{c} \times \boldsymbol{a}) \tag{243}$$

$$\boldsymbol{c} \times (\boldsymbol{a} + \boldsymbol{b}) = (\boldsymbol{c} \times \boldsymbol{a}) + (\boldsymbol{c} \times \boldsymbol{b}) \tag{244}$$

There is the Lagrange's identity

$$(\boldsymbol{a} \times \boldsymbol{b}) \cdot (\boldsymbol{c} \times \boldsymbol{d}) = (\boldsymbol{a} \cdot \boldsymbol{c})(\boldsymbol{b} \cdot \boldsymbol{d}) - (\boldsymbol{a} \cdot \boldsymbol{d})(\boldsymbol{b} \cdot \boldsymbol{c}) \tag{245}$$

There is the vector triple product rule

$$\boldsymbol{a} \times (\boldsymbol{b} \times \boldsymbol{c}) = \boldsymbol{b}(\boldsymbol{a} \cdot \boldsymbol{c}) - \boldsymbol{c}(\boldsymbol{a} \cdot \boldsymbol{b}) \tag{246}$$

$$(\boldsymbol{a} \cdot \boldsymbol{b})\boldsymbol{c} = (\boldsymbol{c} \otimes \boldsymbol{a})\boldsymbol{b} \tag{247}$$

Appendix B – Euler Rodrigues Parameters

For the complete understanding of the Rodrigues parameterization used it is shown in this appendix how to get the rotation tensor just thinking about vector properties and trigonometric relationships.

When there is a rigid body motion of a vector $\boldsymbol{a}$ to $\boldsymbol{b}$ this motion can be expressed by finding a rotation axis designated by the versor $\boldsymbol{e}$ and an intensity angle designated by θ in a way that there is $\boldsymbol{\theta} = \theta\boldsymbol{e}$ with this parameterization there is $0 \leq \theta \leq 2\pi$, and as it is seen in Figure 49 one has,

$$\boldsymbol{b} = \boldsymbol{Q}\boldsymbol{a} \tag{248}$$

The objective here is to find $\boldsymbol{Q}$, if one looks at Figure 49 one can draw the following conclusions.

Figure 49: Rotation on 3D space for the Euler-Rodrigues parameterization.

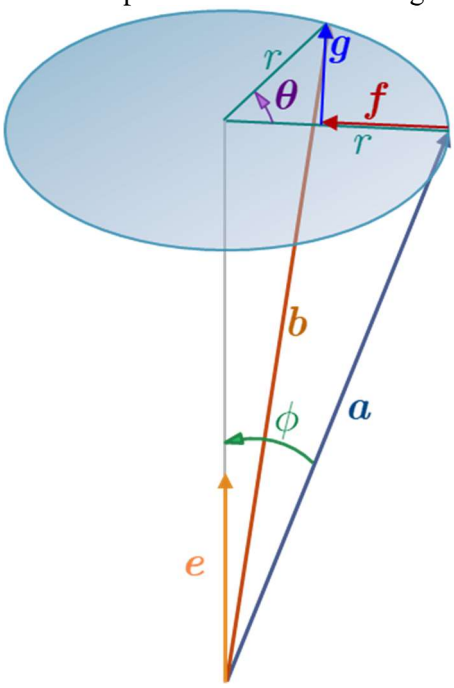

Source: Author

Considering a basic vector property, there is

$$\|\boldsymbol{e}\times\boldsymbol{a}\| = \|\boldsymbol{e}\|\|\boldsymbol{a}\|\sin\phi = \|\boldsymbol{a}\|\sin\phi = \|\boldsymbol{r}\| \tag{249}$$

Looking at Figure 49 and using (249) there is

$$\begin{aligned}\|\boldsymbol{g}\| &= \sin\theta\|\boldsymbol{r}\| = \sin\theta\|\boldsymbol{e}\times\boldsymbol{a}\|\\ \|\boldsymbol{f}\| &= (1-\cos\theta)\|\boldsymbol{r}\| = (1-\cos\theta)\|\boldsymbol{e}\times\boldsymbol{a}\|\end{aligned} \tag{250}$$

Considering that $\boldsymbol{g}$ is orthogonal to $\boldsymbol{e}$ and $\boldsymbol{a}$ one has

$$\boldsymbol{g} = \sin\theta(\boldsymbol{e}\times\boldsymbol{a}) \tag{251}$$

$\boldsymbol{f}$ is orthogonal to **g** and **e**,

$$\boldsymbol{f} = (1-\cos\theta)\|\boldsymbol{e}\times\boldsymbol{a}\|\frac{(\boldsymbol{e}\times\boldsymbol{g})}{\|\boldsymbol{e}\times\boldsymbol{g}\|} \tag{252}$$

Considering the vector property

$$\|\boldsymbol{e}\times\boldsymbol{g}\| = \|\boldsymbol{g}\|\|\boldsymbol{e}\|\sin 90° = \|\boldsymbol{g}\| \tag{253}$$

and $(250)_1$ one has

$$\boldsymbol{f} = (1-\cos\theta)\boldsymbol{e}\times(\boldsymbol{e}\times\boldsymbol{a})\varphi_{\Delta}^{S} = \varphi_{\Delta\mathrm{e}}^{S} \tag{254}$$

Considering

$$\boldsymbol{b} = \boldsymbol{a} + \boldsymbol{f} + \boldsymbol{g} \tag{255}$$

one gets,

$$\boldsymbol{b} = \boldsymbol{a} + (1-\cos\theta)\boldsymbol{e}\times(\boldsymbol{e}\times\boldsymbol{a}) + \sin\theta(\boldsymbol{e}\times\boldsymbol{a}) \tag{256}$$

Using $\boldsymbol{E} = \mathrm{Skew}(\boldsymbol{e})$ one gets

$$\boldsymbol{b} = \boldsymbol{a} + (1-\cos\theta)\boldsymbol{E}^2\boldsymbol{a} + \sin\theta\boldsymbol{E}\boldsymbol{a} \tag{257}$$

Hence,

$$\boldsymbol{Q} = \boldsymbol{I} + \sin\theta\boldsymbol{E} + (1-\cos\theta)\boldsymbol{E}^2 \tag{258}$$

That is a well-known formula for the Euler-Rodrigues rotation tensor

If one considers an α instead of θ with $\alpha = 2\tan\frac{\theta}{2}$ one has a computationally simpler parameterization, with this parameterization one has $0 \leq \theta \leq \pi$, the singularity can be avoided when needed by implementing the rotation incrementally.

Figure 50: Rotation on 3D space for the Rodrigues parameterization.

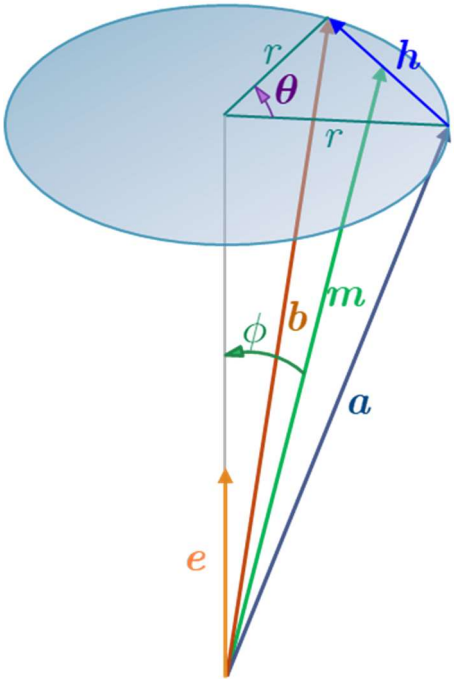

Source: Author

Considering a basic vector property, one has

$$\|\boldsymbol{e} \times \boldsymbol{m}\| = \|\boldsymbol{e}\|\|\boldsymbol{m}\|\sin\phi = \|\boldsymbol{m}\|\sin\phi \tag{259}$$

Looking at Figure 50 and using (259) one has

$$\tan\frac{\theta}{2} = \frac{\left\|\boldsymbol{h}/2\right\|}{\|\boldsymbol{m}\|\sin\phi} = \frac{\|\boldsymbol{h}\|}{2\|\boldsymbol{e} \times \boldsymbol{m}\|} \tag{260}$$

Since $\boldsymbol{h}$ is orthogonal to $\boldsymbol{m}$ and $\boldsymbol{e}$ one has

$$\boldsymbol{h} = \frac{(\boldsymbol{e} \times \boldsymbol{m})}{\|\boldsymbol{e} \times \boldsymbol{m}\|} \|\boldsymbol{h}\| \tag{261}$$

And

$$\boldsymbol{h} = \frac{(\boldsymbol{e} \times \boldsymbol{m})}{\|\boldsymbol{e} \times \boldsymbol{m}\|} 2\tan\frac{\theta}{2} \|\boldsymbol{e} \times \boldsymbol{m}\| = \alpha(\boldsymbol{e} \times \boldsymbol{m}) \tag{262}$$

Considering (262) and

$$\boldsymbol{h} = \boldsymbol{b} - \boldsymbol{a} \tag{263}$$

$$\boldsymbol{m} = \frac{1}{2}(\boldsymbol{a} + \boldsymbol{b}) \tag{264}$$

one has

$$\boldsymbol{b} - \boldsymbol{a} = \alpha\left(\boldsymbol{e} \times \frac{1}{2}(\boldsymbol{a} + \boldsymbol{b})\right). \tag{265}$$

Since $\boldsymbol{\alpha} = \alpha\boldsymbol{e}$

$$\boldsymbol{b} - \boldsymbol{a} = \boldsymbol{\alpha} \times \frac{1}{2}(\boldsymbol{a} + \boldsymbol{b}). \tag{266}$$

Using $\boldsymbol{A} = \text{Skew}(\boldsymbol{\alpha})$

$$\begin{aligned} \boldsymbol{b} - \frac{\boldsymbol{A}}{2}\boldsymbol{b} &= \frac{\boldsymbol{A}}{2}\boldsymbol{a} + \boldsymbol{a} \\ \left(\boldsymbol{I} - \frac{\boldsymbol{A}}{2}\right)\boldsymbol{b} &= \left(\boldsymbol{I} + \frac{\boldsymbol{A}}{2}\right)\boldsymbol{a} \\ \boldsymbol{b} &= \left(\boldsymbol{I} - \frac{\boldsymbol{A}}{2}\right)^{-1}\left(\boldsymbol{I} + \frac{\boldsymbol{A}}{2}\right)\boldsymbol{a} \end{aligned} \tag{267}$$

Hence,

$$\boldsymbol{Q} = \left(\boldsymbol{I} - \frac{\boldsymbol{A}}{2}\right)^{-1}\left(\boldsymbol{I} + \frac{\boldsymbol{A}}{2}\right) \tag{268}$$

From (258) considering $\alpha = 2\tan\frac{\theta}{2}$ a rotation tensor that is equivalent to (268) is achieved and demonstrated ahead using trigonometric properties.

If on considers

$$\tan\frac{\theta}{2}=\frac{1-\cos\theta}{\sin\theta}=\frac{\sin\theta}{1+\cos\theta} \tag{269}$$

Then one has,

$$\begin{aligned}\boldsymbol{Q}&=\boldsymbol{I}+\frac{\sin\theta}{1+\cos\theta}(1+\cos\theta)\boldsymbol{E}+\frac{1-\cos\theta}{\sin\theta}\sin\theta\boldsymbol{E}^2\\&=\boldsymbol{I}+\tan\frac{\theta}{2}(1+\cos\theta)\boldsymbol{E}+\tan\frac{\theta}{2}\sin\theta\boldsymbol{E}^2\end{aligned} \tag{270}$$

And,

$$\boldsymbol{Q}=\boldsymbol{I}+\frac{\alpha}{2}(1+\cos\theta)\boldsymbol{E}+\frac{\alpha}{2}\sin\theta\boldsymbol{E}^2 \tag{271}$$

Considering

$$\begin{aligned}&\frac{1+\cos\theta}{2}=\cos^2\frac{\theta}{2}=\frac{1}{1+\tan^2\frac{\theta}{2}}=\frac{4}{4+\left(2\tan\frac{\theta}{2}\right)^2}=\frac{4}{4+\alpha^2}\text{ and}\\&\frac{\sin\theta}{2}=\sin\frac{\theta}{2}\cos\frac{\theta}{2}=\frac{\sin\frac{\theta}{2}}{\cos\frac{\theta}{2}}\cos^2\frac{\theta}{2}=\frac{\tan\frac{\theta}{2}}{1+\tan^2\frac{\theta}{2}}=\frac{4\left(2\tan\frac{\theta}{2}\right)}{4+\left(2\tan\frac{\theta}{2}\right)^2}\frac{1}{2}=\frac{4\alpha}{4+\alpha^2}\frac{1}{2}.\end{aligned} \tag{272}$$

(273)a, is equivalent to (268).

$$\begin{gathered}\boldsymbol{Q}=\boldsymbol{I}+\frac{4}{4+\alpha^2}\alpha\boldsymbol{E}+\frac{4}{4+\alpha^2}\frac{1}{2}\alpha^2\boldsymbol{E}^2\\\text{and}\\\boldsymbol{Q}=\boldsymbol{I}+\frac{4}{4+\alpha^2}\left(\boldsymbol{A}+\frac{1}{2}\boldsymbol{A}^2\right)\end{gathered} \tag{273}$$

Appendix C – Relationship between $\boldsymbol{\omega}$ and $\dot{\boldsymbol{\alpha}}$ - Operator $\boldsymbol{\Xi}$

Herein the math work on the achievement of $\boldsymbol{\Xi}$ is demonstrated. Knowing that $\boldsymbol{\Omega} = \dot{\boldsymbol{Q}}\boldsymbol{Q}^T$. The objective here is to find the relationship between $\boldsymbol{\omega}$ and $\dot{\boldsymbol{\alpha}}$.

First there is the need for the time derivative of $\boldsymbol{Q}$ which is

$$\dot{\boldsymbol{Q}} = \frac{4}{4+\alpha^2}\left[\dot{\boldsymbol{A}} - \frac{2\boldsymbol{\alpha}\cdot\dot{\boldsymbol{\alpha}}}{4+\alpha^2}\left(\boldsymbol{A} + \frac{\boldsymbol{A}^2}{2}\right) + \frac{1}{2}(\dot{\boldsymbol{A}}\boldsymbol{A} + \boldsymbol{A}\dot{\boldsymbol{A}})\right] \tag{274}$$

There is also the need for $\boldsymbol{Q}^T$

$$\boldsymbol{Q}^T = \boldsymbol{I} + \frac{4}{4+\alpha^2}\left(-\boldsymbol{A} + \frac{\boldsymbol{A}^2}{2}\right) \tag{275}$$

Now $\boldsymbol{\Omega} = \dot{\boldsymbol{Q}}\boldsymbol{Q}^T$ is developed

$$\begin{aligned}\dot{\boldsymbol{Q}}\boldsymbol{Q}^T = {} & \frac{4}{4+\alpha^2}\left[\dot{\boldsymbol{A}} - \frac{2\boldsymbol{\alpha}\cdot\dot{\boldsymbol{\alpha}}}{4+\alpha^2}\left(\boldsymbol{A} + \frac{\boldsymbol{A}^2}{2}\right) + \frac{1}{2}(\dot{\boldsymbol{A}}\boldsymbol{A} + \boldsymbol{A}\dot{\boldsymbol{A}}) - \frac{4}{4+\alpha^2}\dot{\boldsymbol{A}}\boldsymbol{A} + \right] + \\ & + \frac{4}{4+\alpha^2}\left[\frac{8\boldsymbol{\alpha}\cdot\dot{\boldsymbol{\alpha}}}{(4+\alpha^2)^2}\left(\boldsymbol{A}^2 + \frac{\boldsymbol{A}^3}{2}\right) - \frac{2}{4+\alpha^2}(\dot{\boldsymbol{A}}\boldsymbol{A}^2 + \boldsymbol{A}\dot{\boldsymbol{A}}\boldsymbol{A}) + \frac{2\dot{\boldsymbol{A}}\boldsymbol{A}^2}{4+\alpha^2}\right] + \\ & + \frac{4}{4+\alpha^2}\left[-\frac{4\boldsymbol{\alpha}\cdot\dot{\boldsymbol{\alpha}}}{(4+\alpha^2)^2}\left(\boldsymbol{A}^3 + \frac{\boldsymbol{A}^4}{2}\right) + \frac{1}{4+\alpha^2}(\dot{\boldsymbol{A}}\boldsymbol{A}^3 + \boldsymbol{A}\dot{\boldsymbol{A}}\boldsymbol{A}^2)\right]\end{aligned} \tag{276}$$

Considering the following operations, (237) and (238) properties

$$\begin{aligned}&(\boldsymbol{A}\dot{\boldsymbol{A}})\boldsymbol{A} = [\dot{\boldsymbol{\alpha}}\otimes\boldsymbol{\alpha} - (\boldsymbol{\alpha}\cdot\dot{\boldsymbol{\alpha}})\boldsymbol{I}]\boldsymbol{A} = \dot{\boldsymbol{\alpha}}\otimes\boldsymbol{A}^T\boldsymbol{\alpha} - (\boldsymbol{\alpha}\cdot\dot{\boldsymbol{\alpha}})\boldsymbol{A} = \\ &= -\dot{\boldsymbol{\alpha}}\otimes(\boldsymbol{A}\boldsymbol{\alpha}) - (\boldsymbol{\alpha}\cdot\dot{\boldsymbol{\alpha}})\boldsymbol{A} = -\dot{\boldsymbol{\alpha}}\otimes(\boldsymbol{\alpha}\times\boldsymbol{\alpha}) - (\boldsymbol{\alpha}\cdot\dot{\boldsymbol{\alpha}})\boldsymbol{A} = -(\boldsymbol{\alpha}\cdot\dot{\boldsymbol{\alpha}})\boldsymbol{A}\end{aligned} \tag{277}$$

one gets,

$$\begin{aligned}\dot{\boldsymbol{Q}}\boldsymbol{Q}^T = {} & \frac{4}{4+\alpha^2}\left[\dot{\boldsymbol{A}} - \frac{2\boldsymbol{\alpha}\cdot\dot{\boldsymbol{\alpha}}}{4+\alpha^2}\left(\boldsymbol{A} + \frac{\boldsymbol{A}^2}{2}\right) + \frac{1}{2}(\dot{\boldsymbol{A}}\boldsymbol{A} + \boldsymbol{A}\dot{\boldsymbol{A}}) - \frac{4}{4+\alpha^2}\dot{\boldsymbol{A}}\boldsymbol{A}\right] + \\ & + \frac{4}{4+\alpha^2}\left[+\frac{8\boldsymbol{\alpha}\cdot\dot{\boldsymbol{\alpha}}}{(4+\alpha^2)^2}\left(\boldsymbol{A}^2 + \frac{-\boldsymbol{\alpha}^2\boldsymbol{A}}{2}\right) - \frac{2}{4+\alpha^2}(\dot{\boldsymbol{A}}\boldsymbol{A}^2 + \boldsymbol{A}\dot{\boldsymbol{A}}\boldsymbol{A}) + \frac{2}{4+\alpha^2}\dot{\boldsymbol{A}}\boldsymbol{A}^2\right] + \\ & + \frac{4}{4+\alpha^2}\left[-\frac{4\boldsymbol{\alpha}\cdot\dot{\boldsymbol{\alpha}}}{(4+\alpha^2)^2}\left(-\boldsymbol{\alpha}^2\boldsymbol{A} + \frac{-\boldsymbol{\alpha}^2\boldsymbol{A}^2}{2}\right) + \frac{1}{4+\alpha^2}(-\boldsymbol{\alpha}^2\dot{\boldsymbol{A}}\boldsymbol{A} + \boldsymbol{A}\dot{\boldsymbol{A}}\boldsymbol{A}^2)\right]\end{aligned} \tag{278}$$

Then with the following operations

$$\begin{aligned}\frac{4+\alpha^2}{4}\dot{\boldsymbol{Q}}\boldsymbol{Q}^T &= \dot{\boldsymbol{A}} - \frac{2\boldsymbol{\alpha}\cdot\dot{\boldsymbol{\alpha}}}{4+\alpha^2}\boldsymbol{A} - \frac{\boldsymbol{\alpha}\cdot\dot{\boldsymbol{\alpha}}}{4+\alpha^2}\boldsymbol{A}^2 + \frac{1}{2}(\dot{\boldsymbol{A}}\boldsymbol{A} + \boldsymbol{A}\dot{\boldsymbol{A}}) - \\ &+ \frac{4}{4+\alpha^2}\dot{\boldsymbol{A}}\boldsymbol{A} + \frac{8\boldsymbol{\alpha}\cdot\dot{\boldsymbol{\alpha}}}{(4+\alpha^2)^2}\boldsymbol{A}^2 - \frac{4\boldsymbol{\alpha}\cdot\dot{\boldsymbol{\alpha}}}{(4+\alpha^2)^2}\alpha^2\boldsymbol{A} - \frac{2}{4+\alpha^2}\dot{\boldsymbol{A}}\boldsymbol{A}^2 - \\ &+ \frac{2}{4+\alpha^2}\boldsymbol{A}\dot{\boldsymbol{A}}\boldsymbol{A} + \frac{2}{4+\alpha^2}\dot{\boldsymbol{A}}\boldsymbol{A}^2 + \frac{4\boldsymbol{\alpha}\cdot\dot{\boldsymbol{\alpha}}}{(4+\alpha^2)^2}\alpha^2\boldsymbol{A} + \\ &+ \frac{2\boldsymbol{\alpha}\cdot\dot{\boldsymbol{\alpha}}}{(4+\alpha^2)^2}\alpha^2\boldsymbol{A}^2 - \frac{\alpha^2}{4+\alpha^2}\dot{\boldsymbol{A}}\boldsymbol{A} + \frac{1}{4+\alpha^2}\boldsymbol{A}\dot{\boldsymbol{A}}\boldsymbol{A}^2\end{aligned} \tag{279}$$

$$\begin{aligned}\frac{4+\alpha^2}{4}\dot{\boldsymbol{Q}}\boldsymbol{Q}^T &= \dot{\boldsymbol{A}} - \frac{2\boldsymbol{\alpha}\cdot\dot{\boldsymbol{\alpha}}}{4+\alpha^2}\boldsymbol{A}^2 + \left(\frac{1}{2} - \frac{4+\boldsymbol{\alpha}^2}{4+\boldsymbol{\alpha}^2}\right)\dot{\boldsymbol{A}}\boldsymbol{A} + \\ &+ \frac{1}{2}\boldsymbol{A}\dot{\boldsymbol{A}} + \left(\frac{8\boldsymbol{\alpha}\cdot\dot{\boldsymbol{\alpha}}}{(4+\alpha^2)^2} + \frac{2\boldsymbol{\alpha}\cdot\dot{\boldsymbol{\alpha}}}{(4+\alpha^2)^2}\alpha^2\right)\boldsymbol{A}^2\end{aligned} \tag{280}$$

$$\begin{aligned}\frac{4+\alpha^2}{4}\dot{\boldsymbol{Q}}\boldsymbol{Q}^T &= \dot{\boldsymbol{A}} + \left(-\frac{1}{2}\right)\dot{\boldsymbol{A}}\boldsymbol{A} + \frac{1}{2}\boldsymbol{A}\dot{\boldsymbol{A}} + \\ &+ \left(\frac{8\boldsymbol{\alpha}\cdot\dot{\boldsymbol{\alpha}}}{(4+\alpha^2)^2} + \frac{2\boldsymbol{\alpha}\cdot\dot{\boldsymbol{\alpha}}}{(4+\alpha^2)^2}\alpha^2 - \frac{2\boldsymbol{\alpha}\cdot\dot{\boldsymbol{\alpha}}}{4+\alpha^2}\right)\boldsymbol{A}^2\end{aligned} \tag{281}$$

$$\frac{4+\alpha^2}{4}\dot{\boldsymbol{Q}}\boldsymbol{Q}^T = \dot{\boldsymbol{A}} + \frac{1}{2}(\boldsymbol{A}\dot{\boldsymbol{A}} - \dot{\boldsymbol{A}}\boldsymbol{A}) + \left(2(\boldsymbol{\alpha}\cdot\dot{\boldsymbol{\alpha}})\left(\frac{4+\alpha^2}{(4+\alpha^2)^2} - \frac{1}{4+\alpha^2}\right)\right)\boldsymbol{A}^2 \tag{282}$$

$$\frac{4+\alpha^2}{4}\dot{\boldsymbol{Q}}\boldsymbol{Q}^T = \dot{\boldsymbol{A}} + \frac{1}{2}(\boldsymbol{A}\dot{\boldsymbol{A}} - \dot{\boldsymbol{A}}\boldsymbol{A}) \tag{283}$$

$$\dot{\boldsymbol{Q}}\boldsymbol{Q}^T = \frac{4}{4+\alpha^2}\left[\dot{\boldsymbol{A}} + \frac{1}{2}(\boldsymbol{A}\dot{\boldsymbol{A}} - \dot{\boldsymbol{A}}\boldsymbol{A})\right] = \boldsymbol{\Omega} \tag{284}$$

Finally, applying $\boldsymbol{\omega} = \text{axial}(\boldsymbol{\Omega})$there is,

$$\boldsymbol{\omega} = \text{axial}\left(\frac{4}{4+\alpha^2}\left[\dot{\boldsymbol{A}} + \frac{1}{2}(\boldsymbol{A}\dot{\boldsymbol{A}} - \dot{\boldsymbol{A}}\boldsymbol{A})\right]\right) \tag{285}$$

With use of the property $\boldsymbol{C} = \boldsymbol{A}\boldsymbol{B} - \boldsymbol{B}\boldsymbol{A} \Leftrightarrow \boldsymbol{c} = \boldsymbol{a} \times \boldsymbol{b}$ one has

$$\boldsymbol{\omega} = \left(\frac{4}{4+\alpha^2}\left[\dot{\boldsymbol{\alpha}} + \frac{1}{2}(\boldsymbol{\alpha} \times \dot{\boldsymbol{\alpha}})\right]\right) = \frac{4}{4+\alpha^2}\left(\boldsymbol{I} + \frac{1}{2}\boldsymbol{A}\right)\dot{\boldsymbol{\alpha}} \tag{286}$$

From $\boldsymbol{\omega} = \boldsymbol{\Xi}\dot{\boldsymbol{\alpha}}$ one reaches the conclusion

$$\boldsymbol{\Xi} = \frac{4}{4+\alpha^2}\left(\boldsymbol{I} + \frac{1}{2}\boldsymbol{A}\right) \tag{287}$$

which agrees with Pimenta and Campello (2001) [40].

That is an important result because many authors believed that the spin vector was directly related to the time derivative of the rotation vector and it is not. The spin vector comes from second order tensors, so this relation doesn't necessarily have to be equal, $\boldsymbol{\Xi}$ tends to the identity for small rotation vectors.

References

1. ANTMAN, STUART S. **Kirchhoff's problem for nonlinearly elastic rods.** Quarterly of Applied Mathematics, vol. 32, no. 3, 1974, pp. 221–240. JSTOR, www.jstor.org/stable/43636681. Accessed 10 Feb. 2020.

2. ARGYRIS, J.h.; SYMEONIDIS, Sp.. **Nonlinear finite element analysis of elastic systems under nonconservative loading-natural formulation. part I. Quasistatic problems.** Computer Methods In Applied Mechanics And Engineering, [s.l.], v. 26, n. 1, p.75-123, abr. 1981. Elsevier BV. http://dx.doi.org/10.1016/0045-7825(81)90131-6.

3. ARGYRIS, John. **"An excursion into large rotations."** Computer Methods In Applied Mechanics And Engineering, [s.l.], v. 32, n. 1-3, p.85-155, set. 1982. Elsevier BV. http://dx.doi.org/10.1016/0045-7825(82)90069-x.]

4. ARMERO, F.; VALVERDE, J.. **"Invariant Hermitian finite elements for thin Kirchhoff rods. I: The linear plane case.**" Computer Methods In Applied Mechanics And Engineering, [s.l.], v. 213-216, p.427-457, mar. 2012. Elsevier BV. http://dx.doi.org/10.1016/j.cma.2011.05.009.

5. AURICCHIO, F.; CAROTENUTO, P.; REALI, A. **"On the geometrically exact beam model: A consistent, effective and simple derivation from three-dimensional finite-elasticity."** International Journal Of Solids And Structures, [s.l.], v. 45, n. 17, p.4766-4781, ago. 2008. Elsevier BV. http://dx.doi.org/10.1016/j.ijsolstr.2008.04.015.

6. BAşAR, Yavuz; DING, Yunhe. **"Finite-rotation shell elements for the analysis of finite-rotation shell problems."** International Journal For Numerical Methods In Engineering, [s.l.], v. 34, n. 1, p.165-169, 15 mar. 1992. Wiley. http://dx.doi.org/10.1002/nme.1620340109.

7. BAUER, A.m. et al. "**Nonlinear isogeometric spatial Bernoulli beam.**" Computer Methods In Applied Mechanics And Engineering, [s.l.], v. 303, p.101-127, maio 2016. Elsevier BV. http://dx.doi.org/10.1016/j.cma.2015.12.027.

8. BOYER, Frédéric et al**. Geometrically Exact Kirchhoff Beam Theory: Application to Cable Dynamics**. Journal Of Computational And Nonlinear Dynamics, [s.l.], v. 6, n. 4, p.1-1, 5 abr. 2011. ASME International. http://dx.doi.org/10.1115/1.4003625.

9. BOYER, Frédéric; PRIMAULT, Dominique. **"Finite element of slender beams in finite transformations: a geometrically exact approach."** International Journal For Numerical Methods In Engineering, [s.l.], v. 59, n. 5, p.669-702, 17 dez. 2003. Wiley. http://dx.doi.org/10.1002/nme.879.

10. BUFLER, H.. **Conservative systems, potential operators and tangent stiffness: reconsideration and generalization**. Archive Of Applied Mechanics, [s.l.], v. 63, n. 1,

p.51-58, 1993. Springer Science and Business Media LLC. http://dx.doi.org/10.1007/bf00787909.

11. CAMPELLO, E. M. B.; PIMENTA, P. M.; WRIGGERS, P.. **A triangular finite shell element based on a fully nonlinear shell formulation.** Computational Mechanics, [s.l.], v. 31, n. 6, p.505-518, 1 ago. 2003. Springer Science and Business Media LLC. http://dx.doi.org/10.1007/s00466-003-0458-8.

12. CAMPELLO, E. M. B.; PIMENTA, P. M.; WRIGGERS, P.. **An exact conserving algorithm for nonlinear dynamics with rotational DOFs and general hyperelasticity. Part 2: shells**. Computational Mechanics, [s.l.], v. 48, n. 2, p.195-211, 30 mar. 2011. Springer Science and Business Media LLC. http://dx.doi.org/10.1007/s00466-011-0584-7 .

13. CAMPELLO, Eduardo M.b.; LAGO, Leonardo B**.. Effect of higher order constitutive terms on the elastic buckling of thin-walled rods**. Thin-walled Structures, [s.l.], v. 77, p.8-16, abr. 2014. Elsevier BV. http://dx.doi.org/10.1016/j.tws.2013.11.001 .

14. CAMPELLO, Eduardo**. "Análise não-linear de perfis metálicos conformados a frio."** 106 f. Dissertação (Mestrado) - Curso de Engenharia Civil, Estruturas, Escola Politécnica da Universidade de São Paulo, São Paulo, 2000.

15. CARDONA, A.; GERADIN, M.. **A beam finite element non-linear theory with finite rotations.** International Journal For Numerical Methods In Engineering, [s.l.], v. 26, n. 11, p.2403-2438, nov. 1988. Wiley. http://dx.doi.org/10.1002/nme.1620261105.

16. CRISFIELD, M. A. Non-linear finite element analysis of solids and structures. England, UK: John Wiley & Sons Ltd. 2000. p360.

17. CHENG, Hui; GUPTA, K. C.. **An Historical Note on Finite Rotations.** Journal Of Applied Mechanics, [s.l.], v. 56, n. 1, p.139-145, 1 mar. 1989. ASME International. http://dx.doi.org/10.1115/1.3176034.

18. BORST, René de et al. **Non-Linear Finite Element Analysis of Solids and Structures**. [s.l.], 17 ago. 2012. John Wiley & Sons, Ltd. http://dx.doi.org/10.1002/9781118375938.

19. DASAMBIAGIO, E. **Um modelo geometricamente exato de barras com grandes deformações, que considera a distorção e o empenamento geral da seção transversal, e sua discretização pelo método dos elementos finitos**. 93 p. Dissertação (Mestrado em Engenharia Civil) – Universidade de São Paulo, São Paulo, 2008.

20. DASAMBIAGIO, E.R., CAMPELLO, E.M.B. and PIMENTA, P.M. **A finite strain rod model that incorporates general cross section deformation and its implementation by Finite Element Method.** In Heraldo S. da Costa Mattos and Marcilio Alves, editors, Solid Mechanics in Brazil, 2009, volume 2 ABCM Symposium Series in Solid Mechanics, pages, 145-168. ABCM, Rio de Janeiro, 2009.

21. EBERLEIN, R.; WRIGGERS, P.. **Finite element concepts for finite elastoplastic strains and isotropic stress response in shells: theoretical and computational analysis.** Computer Methods In Applied Mechanics And Engineering, [s.l.], v. 171, n. 3-4, p.243-279, abr. 1999. Elsevier BV. http://dx.doi.org/10.1016/s0045-7825(98)00212-6.

22. ERICKSEN, J. L.; TRUESDELL, C**.. Exact theory of stress and strain in rods and shells.** Archive For Rational Mechanics And Analysis, [s.l.], v. 1, n. 1, p.295-323, jan. 1957. Springer Science and Business Media LLC. http://dx.doi.org/10.1007/bf00298012.

23. GONÇALVES, Rodrigo; RITTO-CORRÊA, Manuel; CAMOTIM, Dinar. **A large displacement and finite rotation thin-walled beam formulation including cross-section deformation**. Computer Methods In Applied Mechanics And Engineering, [s.l.], v. 199, n. 23-24, p.1627-1643, abr. 2010. Elsevier BV. http://dx.doi.org/10.1016/j.cma.2010.01.006.

24. YOSHIAKI, Goto et al. **Elastic buckling phenomenon applicable to deployable rings.** International Journal Of Solids And Structures, [s.l.], v. 29, n. 7, p.893-909, 1992. Elsevier BV. http://dx.doi.org/10.1016/0020-7683(92)90024-n.

25. GRECO, L.; CUOMO, M.. **B-Spline interpolation of Kirchhoff-Love space rods**. Computer Methods In Applied Mechanics And Engineering, [s.l.], v. 256, p.251-269, abr. 2013. Elsevier BV. http://dx.doi.org/10.1016/j.cma.2012.11.017.

26. GRECO, L.; CUOMO, M.. **An isogeometric implicit G1 mixed finite element for Kirchhoff space rods**. Computer Methods In Applied Mechanics And Engineering, [s.l.], v. 298, p.325-349, jan. 2016. Elsevier BV. http://dx.doi.org/10.1016/j.cma.2015.06.014.

27. GRECO, L.; CUOMO, M.; CONTRAFATTO, L.. **Two new triangular G1-conforming finite elements with cubic edge rotation for the analysis of Kirchhoff plates.** Computer Methods In Applied Mechanics And Engineering, [s.l.], v. 356, p.354-386, nov. 2019. Elsevier BV. http://dx.doi.org/10.1016/j.cma.2019.07.026.

28. GRUTTMANN, F. et al. **A nonlinear composite shell element with continuous interlaminar shear stresses**. Computational Mechanics, [s.l.], v. 13, n. 3, p.175-188, dez. 1993. Springer Science and Business Media LLC. http://dx.doi.org/10.1007/bf00370134.

29. GRUTTMANN, F.; SAUER, R.; WAGNER, W.. **A geometrical nonlinear eccentric 3D-beam element with arbitrary cross-sections**. Computer Methods In Applied Mechanics And Engineering, [s.l.], v. 160, n. 3-4, p.383-400, jul. 1998. Elsevier BV. http://dx.doi.org/10.1016/s0045-7825(97)00305-8.

30. GRUTTMANN, F.; SAUER, R.; WAGNER, W.. **Shear stresses in prismatic beams with arbitrary cross-sections**. International Journal For Numerical Methods In Engineering, [s.l.], v. 45, n. 7, p.865-889, 10 jul. 1999. Wiley. http://dx.doi.org/10.1002/(sici)1097-0207(19990710)45:73.0.co;2-3.

31. GRUTTMANN, F.; SAUER, R.; WAGNER, W.. **Theory and numerics of three-dimensional beams with elastoplastic material behaviour.** International Journal For Numerical Methods In Engineering, [s.l.], v. 48, n. 12, p.1675-1702, 2000. Wiley. http://dx.doi.org/10.1002/1097-0207(20000830)48:123.0.co;2-6.

32. HUGHES, Thomas J.r.; LIU, Wing Kam. **Nonlinear finite element analysis of shells: Part I. three-dimensional shells. Computer Methods In Applied Mechanics And Engineering**, [s.l.], v. 26, n. 3, p.331-362, jun. 1981. Elsevier BV. http://dx.doi.org/10.1016/0045-7825(81)90121-3.

33. IVANNIKOV, V.; TIAGO, C.; PIMENTA, P.M.. **Generalization of the C1 TUBA plate finite elements to the geometrically exact Kirchhoff–Love shell model**. Computer Methods In Applied Mechanics And Engineering, [s.l.], v. 294, p.210-244, set. 2015. Elsevier BV. http://dx.doi.org/10.1016/j.cma.2015.05.018.

34. KORELC, Jože; WRIGGERS, Peter. **Automation of Finite Element Methods**. [s.l.], 2016. Springer International Publishing. http://dx.doi.org/10.1007/978-3-319-39005-5.

35. JELENIC, G.; SAJE, M.. **A kinematically exact space finite strain beam model — finite element formulation by generalized virtual work principle.** Computer Methods In Applied Mechanics And Engineering, [s.l.], v. 120, n. 1-2, p.131-161, jan. 1995. Elsevier BV. http://dx.doi.org/10.1016/0045-7825(94)00056-s.

36. KIENDL, Josef et al. **Isogeometric Kirchhoff–Love shell formulations for general hyperelastic materials**. Computer Methods In Applied Mechanics And Engineering, [s.l.], v. 291, p.280-303, jul. 2015. Elsevier BV. http://dx.doi.org/10.1016/j.cma.2015.03.010.

37. MEIER, Christoph et al. **Geometrically exact beam elements and smooth contact schemes for the modeling of fiber-based materials and structures.** International Journal Of Solids And Structures, [s.l.], v. 154, p.124-146, dez. 2018. Elsevier BV. http://dx.doi.org/10.1016/j.ijsolstr.2017.07.020.

38. MEIER, Christoph; POPP, Alexander; WALL, Wolfgang A.. **An objective 3D large deformation finite element formulation for geometrically exact curved Kirchhoff rods**. Computer Methods In Applied Mechanics And Engineering, [s.l.], v. 278, p.445-478, ago. 2014. Elsevier BV. http://dx.doi.org/10.1016/j.cma.2014.05.017.

39. MEIER, Christoph; POPP, Alexander; WALL, Wolfgang A.. **Geometrically Exact Finite Element Formulations for Slender Beams: Kirchhoff–Love Theory Versus Simo–Reissner Theory**. Archives Of Computational Methods In Engineering, [s.l.], v. 26, n. 1, p.163-243, 3 jul. 2017. Springer Science and Business Media LLC. http://dx.doi.org/10.1007/s11831-017-9232-5.

40. PIMENTA P. M. and CAMPELLO E. M. B., "**Geometrically nonlinear analysis of thin-walled space frames**", Proceedings of the Second European Conference on Computational Mechanics, II ECCM, Cracow, Poland, 2001.

41. PIMENTA, Paulo M.; YOJO, Takashi. **Geometrically Exact Analysis of Spatial Frames**. Applied Mechanics Reviews, [s.l.], v. 46, n. 11, p.118-128, 1 nov. 1993. ASME International. http://dx.doi.org/10.1115/1.3122626.

42. PIMENTA, Paulo M., "**Geometrically-Exact Analysis of Initially Curved Rods**", in: Advances in Computational Techniques for Structural Engineering, Edinburgh, U.K., v.1, 99-108, Civil-Comp Press, Edinburgh,1996.

43. PIMENTA, P. M.; CAMPELLO, E. M. B.. **Shell curvature as an initial deformation: A geometrically exact finite element approach**. International Journal For Numerical Methods In Engineering, [s.l.], v. 78, n. 9, p.1094-1112, 28 maio 2009. Wiley. http://dx.doi.org/10.1002/nme.

44. PIMENTA, Paulo M.; ALMEIDA NETO, Edgard S.; CAMPELLO, Eduardo M. B.. **A Fully Nonlinear Thin Shell Model of Kirchhoff-Love Type**. New Trends In Thin Structures: Formulation, Optimization and Coupled Problems, [s.l.], p.29-58, 2010. Springer Vienna. http://dx.doi.org/10.1007/978-3-7091-0231-2_2.

45. PIMENTA, P. M.; CAMPELLO, E. M. B.; WRIGGERS, P.. **A fully nonlinear multi-parameter shell model with thickness variation and a triangular shell finite element**. Computational Mechanics, [s.l.], v. 34, n. 3, p.181-193, 13 jul. 2004. Springer Science and Business Media LLC. http://dx.doi.org/10.1007/s00466-004-0564-2.

46. PIMENTA, P. M.; CAMPELLO, E. M. B.. **A fully nonlinear multi-parameter rod model incorporating general cross-section in-plane changes and out-of-plane warping**. Latin-American Journal of Solids and Structures, 1 (1), 119-140, 2003.

47. PIMENTA, P. M.; CAMPELLO, E. M. B.; WRIGGERS, P.. **A fully nonlinear multi-parameter shell model with thickness variation and a triangular shell finite element.** Computational Mechanics, [s.l.], v. 34, n. 3, p.1-1, 13 jul. 2004. Springer Science and Business Media LLC. http://dx.doi.org/10.1007/s00466-004-0564-2.

48. REISSNER, E.. **On finite deformations of space-curved beams**. Journal of Applied Mathematics and Physics, [s.l.], v. 32, n. 6, p.734-744, 1981. Springer Science and Business Media LLC. http://dx.doi.org/10.1007/bf00946983.

49. REISSNER, Eric. **On one-dimensional finite-strain beam theory: The plane problem.** Journal of Applied Mathematics and Physics, [s.l.], v. 23, n. 5, p.795-804, set. 1972. Springer Science and Business Media LLC. http://dx.doi.org/10.1007/bf01602645.

50. REISSNER, E.. **On One-Dimensional Large-Displacement Finite-Strain Beam Theory**. Studies In Applied Mathematics, [s.l.], v. 52, n. 2, p.87-95, jun. 1973. Wiley. http://dx.doi.org/10.1002/sapm197352287.

51. ROMERO, Ignacio. **The interpolation of rotations and its application to finite element models of geometrically exact rods.** Computational Mechanics, [s.l.], v. 34, n. 2, 5 abr.

2004. Springer Science and Business Media LLC. http://dx.doi.org/10.1007/s00466-004-0559-z.

52. SILVA, Cátia da Costa; MAASSEN, Sascha Florian; PIMENTA, Paulo de Mattos; SCHODER, Jörg. **A simple finite element for the geometrically exact analysis of Bernoulli–Euler rods**. Computational Mechanics, [s.l.], p.1-1, 12 dez. 2019. Springer Science and Business Media LLC. http://dx.doi.org/10.1007/s00466-019-01800-5.

53. SIMO, J.C.. **A finite strain beam formulation. The three-dimensional dynamic problem. Part I**. Computer Methods In Applied Mechanics And Engineering, [s.l.], v. 49, n. 1, p.55-70, maio 1985. Elsevier BV. http://dx.doi.org/10.1016/0045-7825(85)90050-7.

54. SIMO, J.C.. **The (symmetric) Hessian for geometrically nonlinear models in solid mechanics: Intrinsic definition and geometric interpretation**. Computer Methods In Applied Mechanics And Engineering, [s.l.], v. 96, n. 2, p.189-200, abr. 1992. Elsevier BV. http://dx.doi.org/10.1016/0045-7825(92)90131-3.

55. SIMO, J.C.; FOX, D.D.; HUGHES, T.J.R.. **Formulations of finite elasticity with independent rotations.** Computer Methods In Applied Mechanics And Engineering, [s.l.], v. 95, n. 2, p.277-288, mar. 1992. Elsevier BV. http://dx.doi.org/10.1016/0045-7825(92)90144-9.

56. SIMO, J.C.; FOX, D.D.. **On a stress resultant geometrically exact shell model. Part I: Formulation and optimal parametrization**. Computer Methods In Applied Mechanics And Engineering, [s.l.], v. 72, n. 3, p.267-304, mar. 1989. Elsevier BV. http://dx.doi.org/10.1016/0045-7825(89)90002-9.

57. SIMO, J.c.; VU-QUOC, L.. **A Geometrically-exact rod model incorporating shear and torsion-warping deformation**. International Journal Of Solids And Structures, [s.l.], v. 27, n. 3, p.371-393, 1991. Elsevier BV. http://dx.doi.org/10.1016/0020-7683(91)90089-x.

58. SIMO, , J.C.; FOX, D.D.; RIFAI, M.S.. **On a stress resultant geometrically exact shell model. Part III: Computational aspects of the nonlinear theory.** Computer Methods In Applied Mechanics And Engineering, [s.l.], v. 79, n. 1, p.21-70, mar. 1990. Elsevier BV. http://dx.doi.org/10.1016/0045-7825(90)90094-3.

59. SIMO, J.C.; HUGHES, T. J. R.. **Computational Inelasticity**. New York: Springer-verlag, 1998. 392 p. (7).

60. SIMO, J.c.; VU-QUOC, L.. **A three-dimensional finite-strain rod model. part II: Computational aspects**. Computer Methods In Applied Mechanics And Engineering, [s.l.], v. 58, n. 1, p.79-116, out. 1986. Elsevier BV. http://dx.doi.org/10.1016/0045-7825(86)90079-4.

61. SMOLENSKI, W. Marek. **Statically and kinematically exact nonlinear theory of rods and its numerical verification**. Computer Methods In Applied Mechanics And

Engineering, [s.l.], v. 178, n. 1-2, p.89-113, jul. 1999. Elsevier BV. http://dx.doi.org/10.1016/s0045-7825(99)00006-7.

62. SOKOLOV, I.; KRYLOV, S.; HARARI, I.. **Extension of non-linear beam models with deformable cross sections**. Computational Mechanics, [s.l.], v. 56, n. 6, p.999-1021, 16 nov. 2015. Springer Science and Business Media LLC. http://dx.doi.org/10.1007/s00466-015-1215-5..

63. STANIć, Andjelka; BRANK, Boštjan; KORELC, Jože. **On path-following methods for structural failure problems**. Computational Mechanics, [s.l.], v. 58, n. 2, p.281-306, 29 abr. 2016. Springer Science and Business Media LLC. http://dx.doi.org/10.1007/s00466-016-1294-y.

64. TIMOSHENKO, S.P. "**History of Strength of Materials: With a brief account of the history of theory of elasticity and theory of structures**.", New York: McGraw-Hill, 1953. 452 p.

65. VIEBAHN, Nils; PIMENTA, Paulo M.; SCHRÖDER, Jörg. **A simple triangular finite element for nonlinear thin shells: statics, dynamics and anisotropy.** Computational Mechanics, [s.l.], v. 59, n. 2, p.281-297, 8 nov. 2016. Springer Science and Business Media LLC. http://dx.doi.org/10.1007/s00466-016-1343-6.

66. WACKERFUß, J.; GRUTTMANN, F.. **A mixed hybrid finite beam element with an interface to arbitrary three-dimensional material models**. Computer Methods In Applied Mechanics And Engineering, [s.l.], v. 198, n. 27-29, p.2053-2066, maio 2009. Elsevier BV. http://dx.doi.org/10.1016/j.cma.2009.01.020.

67. WACKERFUß, J.; GRUTTMANN, F.. **A nonlinear Hu–Washizu variational formulation and related finite-element implementation for spatial beams with arbitrary moderate thick cross-sections.** Computer Methods In Applied Mechanics And Engineering, [s.l.], v. 200, n. 17-20, p.1671-1690, abr. 2011. Elsevier BV. http://dx.doi.org/10.1016/j.cma.2011.01.006.

68. WHITMAN, A. B.; DESILVA, C. N.. **An exact solution in a nonlinear theory of rods**. Journal Of Elasticity, [s.l.], v. 4, n. 4, p.265-280, dez. 1974. Springer Science and Business Media LLC. http://dx.doi.org/10.1007/bf00048610.

69. WRIGGERS, Peter. **Nonlinear Finite Element Methods**. p566.. Berlin: Springer. 2008.